The EGS Collab Project: Outcomes and Lessons Learned from Hydraulic Fracture Stimulations in Crystalline Rock at 1.25 and 1.5 km Depth

Tim Kneafsey[a], Pat Dobson[a], Doug Blankenship[b], Paul Schwering[b], Mark White[c], Joseph Morris[d], Lianjie Huang[e], Tim Johnson[c], Jeff Burghardt[c], Earl Mattson[f, g], Ghanashyam Neupane[f], Chris Strickland[c], Hunter Knox[c], Vince Vermuel[c], Jonathan Ajo-Franklin[a,h], Pengcheng Fu[d], Bill Roggenthen[i], Tom Doe[j], Martin Schoenball[a,k], Chet Hopp[a], Verónica Rodríguez Tribaldos[a,l], Mathew Ingraham[b], Yves Guglielmi[a], Craig Ulrich[a], Todd Wood[a], Luke Frash[e], Tatiana Pyatina[m], George Vandine[n], Megan Smith[d], Roland Horne[o], Mark McClure[p], Ankush Singh[o,q], Jon Weers[r], Michelle Robertson[a], and the EGS Collab Team*

Keywords
Enhanced Geothermal Systems, EGS Collab, stimulation, crystalline rock, Sanford Underground Research Facility, coupled process modeling, experimental, field test, flow test

Highlights
Three multi-test stimulation and flow experiments were performed in crystalline rock.
Stimulation occurred by hydraulic fracturing, but flow required hydropropping.
Shear stimulation did not occur because of low shear-to-normal force ratio.
Shear stimulation was also impacted by healed fractures having low permeability.
Lessons learned are presented.

Abstract

With the goal of better understanding stimulation in crystalline rock for improving enhanced geothermal systems (EGS), the EGS Collab Project performed a series of stimulations and flow tests at 1.25 and 1.5 km depths. The tests were performed in two well-instrumented testbeds in the Sanford Underground Research Facility in Lead, South Dakota, United States. The testbed for Experiment 1 at 1.5 km depth contained two open wells for injection and production and six instrumented monitoring wells surrounding the targeted stimulation zone. Four multi-step stimulation tests targeting hydraulic fracturing and nearly year-long ambient temperature and chilled water flow tests were performed in Experiment 1. The testbed for Experiments 2 and 3 was at 1.25 km depth and contained five open wells in an outwardly fanning five-spot pattern and two fans of well-instrumented monitoring wells surrounding the targeted stimulation zone. Experiment 2 targeted shear stimulation, and Experiment 3 targeted low-flow, high-flow,

and oscillating pressure stimulation strategies. Hydraulic fracturing was successful in Experiments 1 and 3 in generating a connected system wherein injected water could be collected. However, the resulting flow was distributed dynamically, and not entirely collected at the anticipated production well. Thermal breakthrough was not observed in the production well, but that could have been masked by the Joule-Thomson effect. Shear stimulation in Experiment 2 did not occur – despite attempting to pressurize the fractures most likely to shear – because of the inability to inject water into a mostly-healed fracture, and the low shear-to-normal stress ratio. The EGS Collab experiments are described to provide a background for lessons learned on topics including induced seismicity, the correlation between seismicity and permeability, distributed and dynamic flow systems, thermoelastic and pressure effects, shear stimulation, local geology, thermal breakthrough, monitoring stimulation, grouting boreholes, modeling, and system management.

1.0 Introduction

Enhanced or engineered geothermal systems (EGS) offer tremendous potential as an energy resource supporting the energy security of the United States, with implementation being considered worldwide. Estimates exceed 500 gigawatt electrical (GWe) for the western United States, surpassing the resource base hosted by conventional hydrothermal systems [*Williams et al.*, 2008], and up to an order of magnitude larger when including the entire United States [*Augustine*, 2016]. Implementation of an EGS will typically require stimulation to generate appropriate hydraulic communication between injection and production wells to allow effective mining of the heat. Although there are decades of experience with hydraulic fracturing in the oil and gas industries, drillback studies have only recently been performed providing some elucidation of subsurface behavior during hydraulic fracturing, and unexpected behaviors (e.g., fracture swarming) have been observed [*Elliott and Gale*, 2018; *Gale et al.*, 2018; *Gale et al.*, 2021; *Raterman et al.*, 2018]. Stimulation for EGS is different from fracturing in the oil and gas industry. In oil and gas applications, porous media is typically fractured to allow resources to flow towards a well, and typically attempts to avoid creating fractures that connect wells (frac hits). In EGS, crystalline rock is generally the fracturing target, and indirect connections between wells are needed to collect injected fluid and harvest heat from the formation. To implement EGS, appropriate stimulation requires greater understanding including stimulated reservoir creation, distribution of flow in a created reservoir, and responses to stimuli such as the injection of water out of chemical equilibrium with the rock. Additionally, implementing EGS requires knowledge of and managing associated seismicity, developing technologies to control fast-flow paths within the reservoir to reduce early thermal breakthrough, improving imaging and monitoring techniques for permeability enhancement and evolution, improving technologies for zonal isolation for

multistage stimulations under elevated temperatures, and developing scientifically-based long-term EGS reservoir sustainability and management techniques. Another critical aspect of EGS reservoir creation is better understanding the interaction between preexisting fractures and new fractures created via hydraulic stimulation.

To investigate stimulation and flow in crystalline rock with a focus applicable to EGS, field tests have been performed at several mine and underground research laboratory sites globally including the Bedretto Underground Laboratory for *Geosciences and Geoenergies (BULGG, Switzerland), the Grimsel Test Site (Switzerland), the* Äspö Hard Rock Laboratory (Sweden), Northparkes Mine (Australia), and Reiche Zeche (Germany) [*Amann et al.*, 2018; *Boese et al.*, 2022; *Dutler et al.*, 2019; *Gischig et al.*, 2020; *Jeffrey et al.*, 2009; *Kaiser et al.*, 2013; *Reinhard*, 2013; *Zimmermann et al.*, 2019]. Each of these projects/laboratories contributes differently towards understanding EGS issues. At Northparkes Mine, hydraulic fracturing tests were performed in a mine at about 580 m deep resulting in subhorizontal fractures. Proppants were used and the resulting fractures were investigated by mining back [*Jeffrey et al.*, 2009]. At *the* Äspö Hard Rock Laboratory, Zang and colleagues examined attempted to propagate parallel hydraulic fractures in stimulation of crystalline rock at 410 m depth in a rock mass of about 30 x 30 x 30 cubic meters, also investigating fatigue fracturing [*Zang et al.*, 2017]. At Reiche Zeche the STIMTEC project targeted a volume of about 60 x 30 x 30 meters of strongly foliated metamorphic gneiss at a depth of about 130 m [*Renner et al.*, 2021] with mineback used to examine resulting fractures. The total injected volume per interval was 15 to 25 liters during the combined frac and refrac stages and up to 500 liters during the subsequent steprate tests and periodic-pumping (with periods of 60 to 800 seconds), amounting to about 10 m^3 of injected fluid volume in total. At the Grimsel Test Site, decameter hydraulic stimulation experiments were performed in granodiorites and granites at about 450 m depth. The overall objective of this work was to conduct fundamental research enhancing process understanding of hydraulic stimulations. Both shear stimulation and hydraulic fracturing were investigated. Guiding questions included the hydromechanical response of fractures during stimulation, the pressure propagation away from the injection boreholes, rock mass deformation and stress interaction, the transition from aseismic to seismic slip and its relative importance, the interaction of hydraulic fractures with pre-existing structures, as well as the spatial and temporal variability of induced seismicity. These experiments showed the variability in stimulation outcomes even for the comparably small target rock volume, and hypothesized that flow is strongly channelized. Very importantly, complex rock deformation and fracturing processes were observed [*Gischig et al.*, 2020]. BULGG is the largest of the existing underground laboratories (100 m scale) and hosts a variety of experiments such as “Validating of technologies for reservoir engineering” (VALTER), the EU funded project “Soft stimulation

treatments of geothermal reservoirs" (DESTRESS), and the EU funded project "Zonal isolation, drilling and exploitation of EGS projects" (ZoDrEx) [*Hertrich and team*, 2021]. The experiments at BULGG are a step closer towards real EGS because of the larger size, depth (1000-1200 m), and anticipated large injected water volume. Although the conditions and spatial scales of these field tests are different from geothermal reservoirs, much can be learned and applied to understanding EGS reservoirs. At the reservoir scale, the Frontier Observatory for Research in Geothermal Energy (FORGE) project near Milford Utah (USA) is a full-scale EGS laboratory dedicated to understanding EGS science and engineering issues [*Moore et al.*, 2019].

1.1 The EGS Collab Project

The EGS Collab Project goals were to establish a collaborative experiment and model comparison project to compare and validate reservoir model predictions with ~10 m-scale field experiment data. These comparisons would be based on in-depth fracture characterization through well-performed, well-monitored experiments that collected high-quality data using comprehensive instrumentation. We also sought to elucidate the basic relationship between permeability enhancement and stress, seismicity, and other parameters, and to improve field, lab, and modeling tools and process understanding for FORGE and EGS.

The approach of the EGS Collab project was to refine our understanding of rock mass response to stimulation using accessible deep rock. We performed 10-m scale experiments under stresses relevant to EGS (at 1.25 and 1.5 km depth) in crystalline rock. Our tests and analyses were performed to support validation of thermal-hydrological-mechanical-chemical (THMC) modeling approaches (e.g., [*Sonnenthal et al.*, 2018; *White et al.*, 2019; *Winterfeld et al.*, 2019; *Wu et al.*, 2019c; *Wu et al.*, 2020c; *Wu et al.*, 2019e]). In addition, the EGS Collab project tested and improved novel and conventional field monitoring tools (e.g., *Feng et al.* [2024]; *Guglielmi et al.* [2021a]; *Guglielmi et al.* [2021b]; *Guglielmi et al.* [2023]; *Johnson et al.* [2022]; *Johnson et al.* [2021]; *Johnson et al.* [2024]; *Johnson et al.* [2019b]; *Li et al.* [2024]; *Qin et al.* [2024]). Project observations and interpretations provide additional understanding towards creating sustained and distributed permeability for heat extraction in an EGS reservoir by generating new fractures that complement existing fractures.

In spite of our thrust being EGS, we performed our experiments in accessible, deep, cool rock at the Sanford Underground Research Facility because of its excellent accessibility and infrastructure. Our assumption was that the physics of stimulation of cool deep crystalline rock are similar to the physics of stimulation of the hotter rock that would be targeted for EGS. By doing this, we were able to perform tests nearby and closely monitor them at much higher resolution from shorter boreholes that surround our testbed providing

high quality monitoring data. Very long and expensive boreholes would be required if we used a deep hotter testbed, causing either extremely complex equipment deployments or deployment of much less monitoring equipment. Our approach also allowed using monitoring equipment that would be difficult to deploy at geothermal temperatures.

The EGS Collab Project was successful at stimulating crystalline rock and monitoring the stimulations and resulting flow fields at two deep testbeds having different fracture distributions and stress conditions. We collected high quality data from both the testbed characterizations and individual tests stimulation and flow tests. We analyzed a subset of the data and compared it to numerical models. Specific results from the EGS Collab project have been presented in numerous conference and journal publications indexed at https://scholar.google.com/citations?hl=en&authuser=3&user=h-rd4hkAAAAJ, and Project data are freely available at https://gdr.openei.org/egs_collab. In addition to the conference and journal publications, more detail can be found in project reports ([*Kneafsey et al.*, 2019a; *Kneafsey et al.*, 2024; *Kneafsey et al.*, 2021c; *Roggenthen et al.*, 2024]). To the extent possible, this paper provides a guide to many of these writings.

In this paper, after a brief description of the project, we summarize results and lessons learned from the EGS Collab Experiments 1 - 3. A large number of tests were performed, extensive, high-quality data were collected, and many observations have been noted. A partial data set is presented for one stimulation to provide an example of data collected and available and to provide context for Project learnings. In addition, a summary of Project learnings is presented on topics including induced seismicity, the correlation between seismicity and permeability, distributed and dynamic flow systems, thermoelastic and pressure effects, shear stimulation, local geology, thermal breakthrough, monitoring stimulation, grouting boreholes, modeling, and system management. We hope these are informative to those interested in EGS, but acknowledge that they are not limited specifically to EGS.

1.2 Project description

The EGS Collab Project consisted of three multi-test experiments to increase understanding of 1) hydraulic fracturing (Experiment 1 - E1), 2) shear stimulation (Experiment 2 – E2), and 3) other stimulation methods (Experiment 3 - E3). Modeling was key in supporting experiment design and observation interpretation. Post-test modeling and analysis were performed to examine the effectiveness of modeling and monitoring tools and approaches to allow building confidence in and improving the array of modeling and monitoring tools and approaches.

The EGS Collab experiments were conducted at the Sanford Underground Research Facility (SURF) in Lead, South Dakota [*Heise*, 2015]. SURF maintains and upgrades underground facilities remaining from the former

Homestake gold mine at multiple depths in a variety of rock types for scientific investigations. SURF hosts a number of scientific projects ranging from collection and analysis of rock and water samples for biological investigation, to enormous infrastructure-intensive multibillion dollar physics experiments. E1 (Section 2 below) was performed at 1.5 km depth (the 4850-foot depth level, Figure 1 and Figure 2 top) hosted in the Poorman phyllite formation [*Caddey et al.*, 1991]. E1 tests established a fracture network connecting an injection well and a production well using hydraulic fracturing ([*Kneafsey et al.*, 2021a; *Kneafsey et al.*, 2021b; *Kneafsey et al.*, 2021e; *Morris et al.*, 2018a] and references therein). Four stimulations were performed in stages and the injection and production boreholes were connected [*White et al.*, 2019]. Flow tests using ambient-temperature water and chilled water (as an analog to EGS) were conducted over the course of a year [*Kneafsey et al.*, 2021b], and tracer tests were intermittently performed to understand flow conditions [*Mattson et al.*, 2019a; *Mattson et al.*, 2019b; *Neupane et al.*, 2020; *Wu et al.*, 2019a; *Wu et al.*, 2019c]. E2 (Section 3 below) and E3 (Section 4 below) were performed in a testbed at 1.25 km depth (4100-foot depth, Figure 2), hosted in the Yates amphibolite, a blocky, low permeability rock, with subsurface stress conditions different from those of E1 [*Caddey et al.*, 1991; *Ingraham et al.*, 2020]. Hydraulic shear stimulation was attempted in E2. In E3, variations on hydraulic fracturing were performed, including slow stimulation, fast stimulation, and cyclic pressure stimulation.

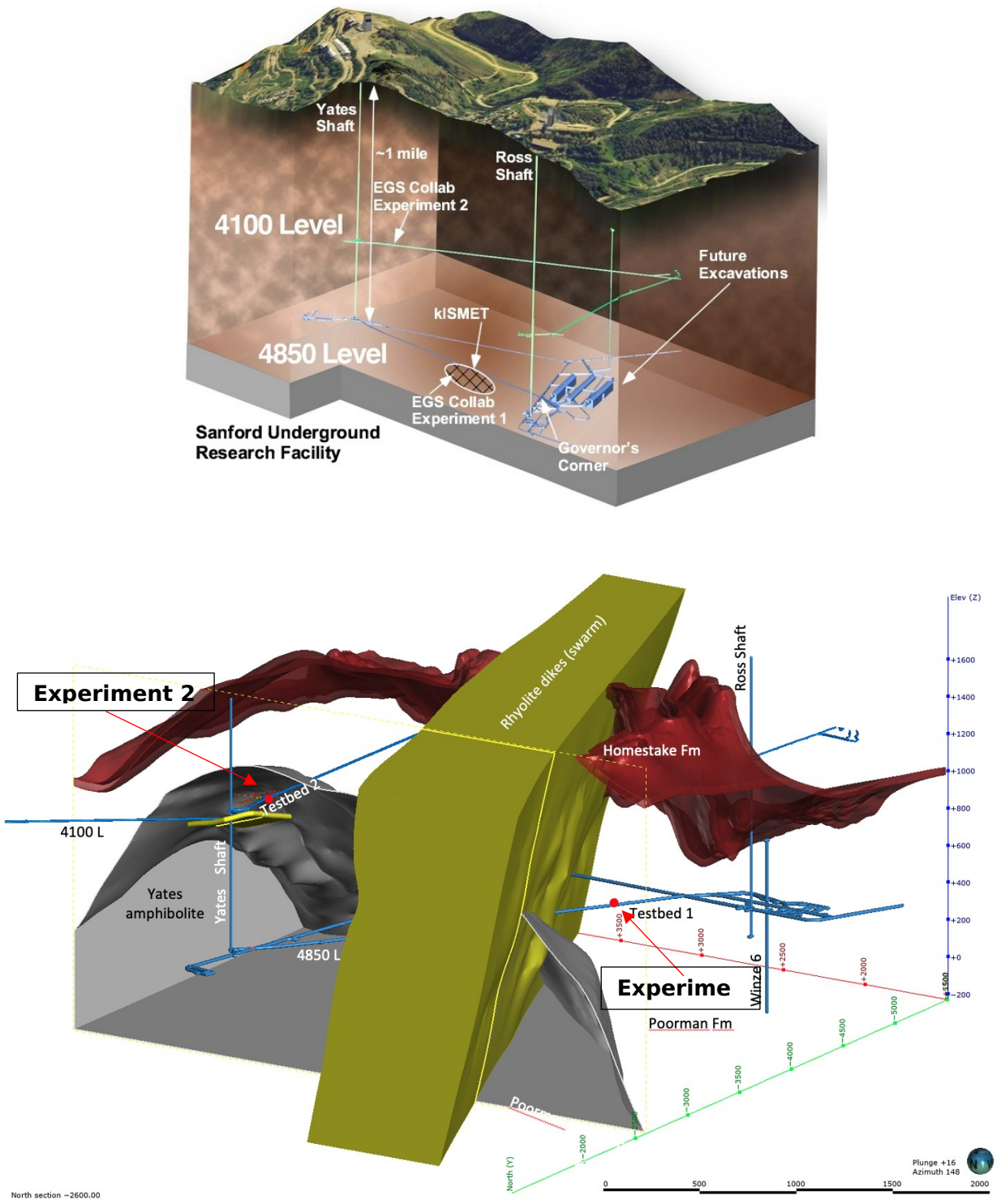

Figure 1. Top - Schematic view of the Sanford Underground Research Facility (SURF), depicting a small fraction of the underground facilities including the Yates (left) and Ross (right) shafts, the 4850 and 4100 levels, and testbeds for Experiments 1 and 2, 3. Bottom - Geologic model showing testbed locations.

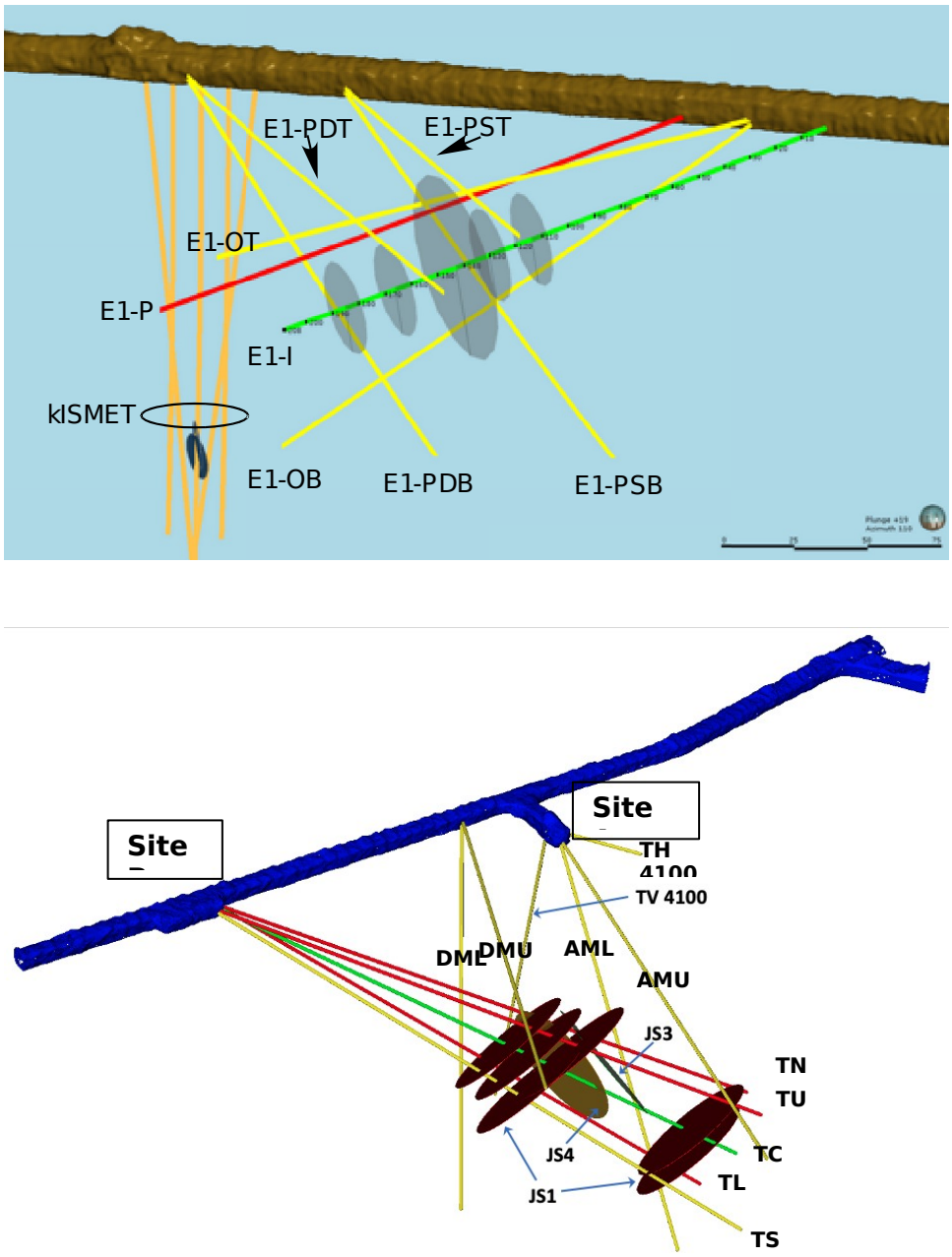

Figure 2 Top - Schematic of wells for Experiment 1 along the West Access Drift on the 4850 level. The green line represents the stimulation (injection) well (E1-I), the red line represents the production well (E1-P), yellow lines represent monitoring wells, and orange lines represent kISMET (permeability (k) and Induced Seismicity Management for Energy Technologies) Project wells. Orientation of stimulation and production boreholes is approximately parallel to S_{hmin} and the gray disks indicate nominal hydraulic fractures. Bottom - Oblique view of borehole orientations for Experiments 2 and 3. The thick blue object represents the drift (mine tunnel), the green line represents the injection well, red lines represent production wells, and yellow lines represent monitoring wells. Other than the vertical well TV4100, all wells are subhorizontal. Disks

indicate nominal fractures oriented parallel to natural fracture sets that connect the injection and production wells and hotter colors indicate greater slip tendency. JS1 has a higher slip tendency than other fracture set orientations.

1.2 Modeling and Validation

A focus of the project was model validation. It seems conceptually simple to challenge thermal-hydrological-mechanical-chemical (THMC) modeling approaches with field data. The model validation is initiated by devising a conceptual model. Then, on the experiment side, the steps would be to build a testbed, quantify as many properties as possible, and perform a well-designed and monitored test while quantifying results. On the numerical modeling side, the steps would be to convert the conceptual model into a numerical model, parameterize it using quantified properties, and perform a parallel experiment (digital twin) using a well-developed modeling platform. The two sets of results could then be compared and conclusions could be drawn. Unfortunately, these steps are inadequate for real-world field experimentation and modeling because they presume that the originally-devised conceptual model behaves identically to the physical system. This assumption requires that all key features of the natural physical system can be characterized and captured in the numerical model, which is rarely possible.

Two examples illustrate this limitation: 1) the necessity to include stress gradients in modeling fracture extension (especially those created by the initial temperature field surrounding the drift), and 2) the necessity to include Joule-Thomson effects for sharp pressure drops at fracture-borehole intersections. The change in temperature in the rock in E1 caused by drift ventilation was relatively small. The normal rock temperature at the E1 depth was about 35℃, and the temperature of the drift wall was about 20℃ (Figure 3). Our preliminary conceptual model and test design did not consider the effect of this temperature gradient on stress. After modeling and measuring the temperature gradient, the effect on rock stress was computed and was found to be significant. This temperature-induced stress gradient is thought to have resulted in hydraulic fractures propagating primarily towards the cooler drift where stresses were lower. This was recognized prior to the field test, and our models did predict that fracture propagation would propagate toward the drift. We also failed to include Joule-Thomson effects in our initial conceptual model and testbed design. The Joule-Thomson coefficient for water at our temperatures and pressures is about -0.2176 (℃/MPa) (-0.0027 ℉/psia)[*Lemmon et al.*] with the negative sign indicating that water will increase in temperature upon lowering of pressure under constant enthalpy conditions. Numerical modeling did identify this problem [*Zhang et al.*, 2018a] as this behavior is built into the TOUGH code that was used. When the experiment was performed, water entering the production borehole was observed to jet into the hole (Figure 4)

indicating a large depressurization at that location and, consequently, inducing a water temperature not matching the host rock at that location. Because the flowrates into the boreholes were relatively low, we assume that the water temperature in the rock near the borehole is in rough equilibrium with local rock. This is justified by the very local temperature increase over about 1 meter at a flowing fracture location where we claim a Joule-Thomson effect (Figure 9). Outside of that warmed region the temperature is largely unchanged. The temperature gradient in a location where a 1 degree C increase was measured is about 0.05 to 0.1 C/m (Figure 3). If the temperature change were caused by warmed water flowing to the inlet location, water would have to flow 10 – 20 meters without changing temperature. This is unlikely.

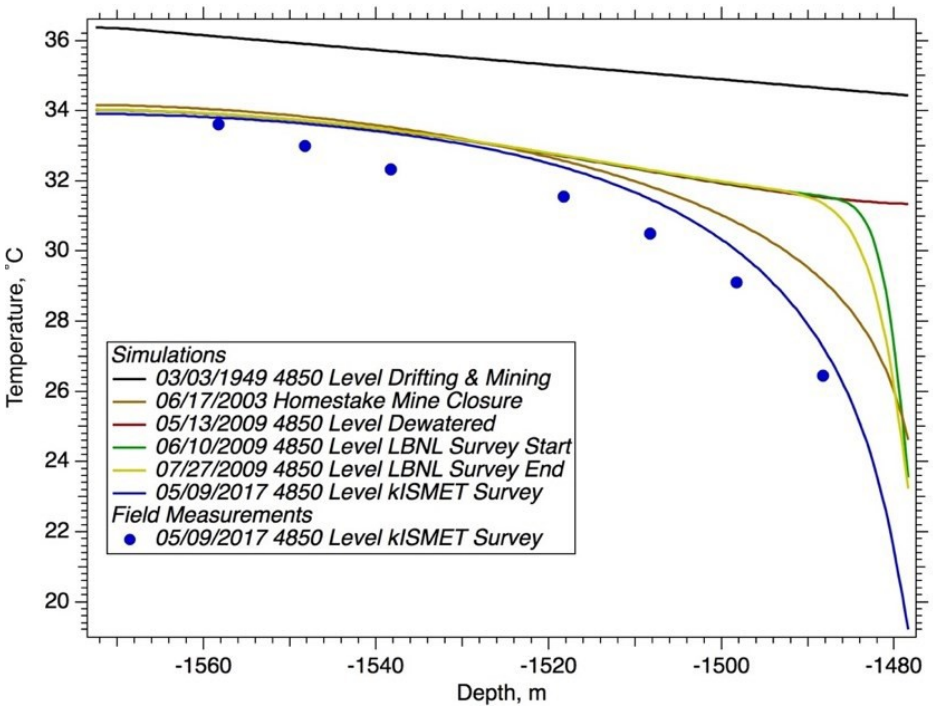

a.

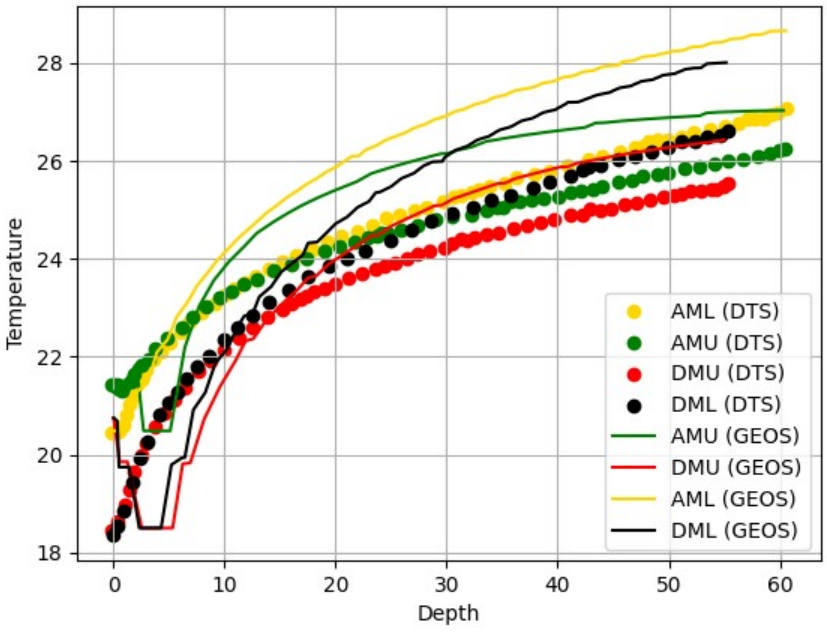

b.

Figure 3. a. Measured and modeled temperature gradients for Experiment 1 (left) [*Fu et al.*, 2018b] and b. Experiments 2 and 3 [*Cusini et al.*, 2023].

Figure 4. E1. Water jetting into borehole E1-P (see arrows).

Designing our testbeds and optimally placing instruments required many simulations to be performed [*Chen et al.*, 2018; 2019a; *Gao et al.*, 2018; *Huang et al.*, 2017; *Morris et al.*, 2018a; *Morris et al.*, 2018b; *White et al.*, 2017; *White et al.*, 2018]. Quality characterization of the testbeds was done through use of preexisting site observations, extensive field and laboratory measurements, complemented with every reasonable assessment tool useful in modeling. With field complexities and heterogeneities, interpretation of these experimental results often required simulation [*White et al.*, 2019]. In spite of the exceptional quality of the characterization, it was still inadequate to appropriately parameterize the numerical models with currently expected data densities. In addition, typically model validation is performed by completing an experiment and providing the data to the modelers to model and compare. In the EGS Collab Project, the tests were designed collaboratively. Because of this collaboration, modeling within the EGS Collab project was performed in lock-step with the experimentation. Modelers (a different kind of experimentalist) and experimentalists (a different kind of modeler) designed, performed, and analyzed tests together. For testbed and test design, modelers and experimentalists worked together to create effective field tests with the highest chance of testing the models and modeling platforms [*Fu et al.*, 2021a; *Fu et al.*, 2021b; *White et al.*, 2017; *White et al.*, 2018]. As the tests were performed, models were tested and corrected in parallel with the experimental efforts, and learnings were incorporated to further support interpretation. As such, the EGS Collab Project did not identify a “validated” modeling platform, but rather improved conceptual and numerical models throughout the project, and provided an understanding of the value and limitations of modeling in the field project [*White et al.*, 2019]. The modeling efforts were one of the key contributions to understanding what happened in the experiments. Appendix A lists Project modeling and analysis papers.

2.0 Experiment 1 (Test Bed 1, 4850 Level)

Experiment 1 (Figure 2 top) was intended to establish a fracture network connecting an injection well and a production well pair using hydraulic fracturing [*Morris et al.*, 2018b]. E1 was performed at about 1.5 km depth [*Kneafsey et al.*, 2019a; *Kneafsey et al.*, 2020]. The testbed for E1 was entirely within the Poorman Formation, a metasedimentary rock consisting of sericite-carbonate-quartz phyllite (the dominant rock type), biotite-quartz-carbonate phyllite, and graphitic quartz-sericite phyllite [*Caddey et al.*, 1991]. The rock is highly deformed and contains carbonate, quartz veins/boudinage, pyrrhotite, and minor pyrite. Initial characterization included mapping fractures and features observed at the drift wall. Boreholes for E1 are all subhorizontal, nominally 60 meters long and 10 cm diameter, and were continuously cored (near 100% recovery). The injection and production boreholes (green and red lines in Figure 2) are approximately parallel to the minimum principal stress direction determined from kISMET (permeability (k) and Induced Seismicity Management for Energy Technologies) Project tests (orange boreholes in Figure 2) [*Dobson et al.*, 2018; *Oldenburg et al.*, 2017; *Ulrich et al.*, 2018; *Wang et al.*, 2017], so that hydraulic fractures would tend to propagate orthogonally to the injection well. Values of the maximum, minimum, and intermediate principal stresses are approximately 41.8 MPa (6062 psi) vertical, 21.7 MPa (3147 psi), and 34.0 MPa (4931 psi) respectively [*Dobson et al.*, 2018]. Boreholes were typically characterized using optical and acoustic televiewers, full waveform sonic, electrical resistivity, natural gamma, and temperature/conductivity logs, as well as through detailed mapping of the recovered core samples. Of the eight boreholes, two were left open for injection and production, and monitoring instrumentation was grouted in the remaining six monitoring wells.

The E1 test block was characterized using seismic tomography, electrical resistivity tomography (ERT), and extended hydrologic characterization including tracer tests (for details and references see *Kneafsey et al.* [2020] and *Kneafsey et al.* [2019a]; *Roggenthen and Doe* [2018]; *Roggenthen et al.* [2022]). While natural existing flow paths might be celebrated and included in a geothermal system design, our hydraulic characterization guided us as we attempted to avoid these features to focus on stimulation, however they still impacted the stimulation and flow in the system. A number of methods were used to monitor flow and stimulation tests including: 1) Passive seismic monitoring (e.g. [*Qin et al.*, 2024; *Schoenball et al.*, 2019]), 2) continuous active source seismic monitoring (CASSM) [*Daley et al.*, 2013; *Daley et al.*, 2007; *Feng et al.*, 2024], 3) dynamic ERT imaging using high contrast fluids [*Johnson et al.*, 2022; *Johnson et al.*, 2019a; *Johnson et al.*, 2021; *Johnson et al.*, 2024], 4) acoustic emissions, 5) fiber optic cables for distributed acoustic sensing (DAS) [*Li et al.*, 2024], distributed temperature sensing (DTS), distributed strain sensing (DSS) [*Hopp*, 2023a; *Rodríguez Tribaldos et al.*, 2024 (in press); *Rodríguez Tribaldos et al.*, 2021], and 6) tracer tests

[*Mattson et al.*, 2019a; *Mattson et al.*, 2023; *Mattson et al.*, 2021; *Neupane et al.*, 2020; *Wu et al.*, 2019c; *Wu et al.*, 2020b]. Sensor location optimization to allow appropriate coverage of all implemented systems was performed [*Chen et al.*, 2019a]. During stimulation, fracture aperture strain monitoring in the borehole was performed using the Step-rate Injection Method for Fracture In-situ Properties (SIMFIP) tool [*Guglielmi et al.*, 2015; *Guglielmi et al.*, 2013; *Guglielmi et al.*, 2021a]. Laboratory investigations of core samples provided additional rock behavior understanding [*Condon et al.*, 2020; *Condon et al.*, 2019; *Frash et al.*, 2019c; *Ye et al.*, 2020; *Ye et al.*, 2019; *Yildirim et al.*, 2018]. Following stimulation and flow tests, acoustic televiewer and fluid conductivity logs were collected in the open boreholes to assess and orient generated fractures in the injection well(s) and fracture(s) interception within the production well(s). Recovered cores were laid out and carefully examined, particularly open fractures, and correlated to the borehole measurements and borehole DAS ambient noise [*Li et al.*, 2024]. Detailed measurements were also performed on a subsection of the core including computed tomography (CT) scanning, magnetic susceptibility, P-wave velocity, gamma density, and X-ray fluorescence spectrometry [*Paronish et al.*, 2022].

2.1 Stimulation

Four stimulation tests were carried out [*White et al.*, 2019] and short-term and long-term ambient temperature and chilled water flow tests were performed [*Kneafsey et al.*, 2019b; *Mattson et al.*, 2019a], resulting in numerous data sets and analyses [*Chen et al.*, 2019b; *Feng et al.*, 2024; *Frash et al.*, 2019a; *Fu et al.*, 2021a; *Fu et al.*, 2019; *Guglielmi et al.*, 2023; *Huang et al.*, 2019; *Johnson et al.*, 2019a; *Johnson et al.*, 2021; *Li et al.*, 2024; *Lu and Ghassemi*, 2019; *Mattson et al.*, 2019b; *Pan et al.*, 2019; *Qin et al.*, 2024; *Schoenball et al.*, 2019; *Schoenball et al.*, 2020a; *Schoenball et al.*, 2021; *Templeton et al.*, 2019; *Weers and Huggins*, 2019; *White et al.*, 2019; *Winterfeld et al.*, 2019; *Wu et al.*, 2019a; *Wu et al.*, 2021b; *Wu et al.*, 2019b; *Wu et al.*, 2021c; *Ye et al.*, 2019]. Data are available at https://gdr.openei.org/egs_collab. Table SI-1 provides more imformation on the stimulatons.

In the injection borehole E1-I, notches were scribed at three locations (39, 43, and 50 m ~ 128, 142, and 164 ft from the well collar at the drift wall) to initiate fractures propagating perpendicular to the wellbore axis. Fracture initiation at the notch tip cannot be observed comparing the pre- and post-stimulation optical and acoustic televiewers, thus their effectiveness is unclear. The first stimulation was performed at the 43 m (142 ft) Notch. The packer interval (approximately 1.65 m ~ 65 in. long) long including the SIMFIP tool) straddled a large apparently-healed natural fracture. The stimulation was planned to occur in 3 steps. The initial stimulation was designed such that it might create an ideal 1.5 m radius penny-shaped fracture prior to being shut in for the night to monitor pressure decay. The

second step would extend the fracture to 5 m radius followed by being shut in for the night, and the third step would extend the fracture to the production borehole approximately 10 m away. A hydraulic fracture was created with a breakdown pressure of 31 MPa (4500 psi) - significantly above the minimum principal stress of 21.7 MPa (3147 psi), probably intersecting an observed natural fracture and leading to water flow returning up the borehole. Since shear stimulation was not intended in this test and the results indicated that we might be pumping into the natural fracture, the stimulation was terminated and the packer set was moved to the 50 m (164 ft) Notch.

The stimulation at the 50 m (164 ft) Notch was carried out in three steps over three days with shut-in periods between each step. In the first step, 2.1 L of water was injected at 200 mL/min. The propagation pressure was 25.43 MPa (3688 psi) and the instantaneous shut-in pressure (ISIP) was 25.37 MPa (3679 psi). In the second step, 23.5 L of water was injected at 400 mL/min resulting in slightly higher propagation pressure and ISIP (25.95 and 25.82 MPa respectively, 3763 and 3744 psi). The pressure decay following this step indicated that the hydraulic fracture may have intersected a natural fracture. The third step was performed at 5L/min and had an injection volume of 80.6 L, with a propagation pressure and ISIP of 26.88 and 25.31 MPa (3898 psi and 3670 psi), respectively. This stimulation resulted in water being produced at the production well (E1-P, Figure 4). In addition to intersecting E1-P, this stimulation intersected monitoring well E1-OT (located between the injection and production boreholes), as indicated by seismic sensors. A temperature increase was indicated by the DTS at the location the fracture intersected the well, and eventually water leaked out from the top of the grouted E1-OT well. The temperature increase is the result of the Joule-Thomson effect where depressurizing water at constant enthalpy increases in temperature. These temperature increases are useful in identifying fracture hit timing and location. This intersection and leakage from this well were problematic and required remediation including pressure grouting with epoxy and application of a custom well cap with wire feedthroughs that was backfilled with epoxy. The third stimulation was conducted at the 39 m (128 ft) Notch, attempting to avoid a fracture that connects wells E1-OT and E1-P while still connecting the injection and production wells. In this test, flow bypassed the top injection packer through fractures, and resulted in a hydraulic fracture connecting to E1-OT, but not E1-P.

After this stimulation, a medium-term set of hydraulic characterization tests was conducted at the 50 m (164 ft) Notch. Following that, a second stimulation experiment was completed at the 43 m (142 ft) Notch by carefully placing the straddle packer interval over the target region. This hydraulic stimulation involved higher flow rates and pressures, extended at least one hydraulic fracture to E1-OB and E1-P, and also connected to all other wells except for E1-PDB according to DTS evidence. For stimulations at both the 50 m (164 ft) and 43 m (142 ft) notches, micro-seismic event

locations consistently indicated that the fracture zone extended preferentially toward the drift (Figure 5) [*Schoenball et al.*, 2019]. This was predicted by earlier modeling of fracture growth under the stress gradient induced by cooling of the rock by decades of drift ventilation [*Fu et al.*, 2018b; *White et al.*, 2018].

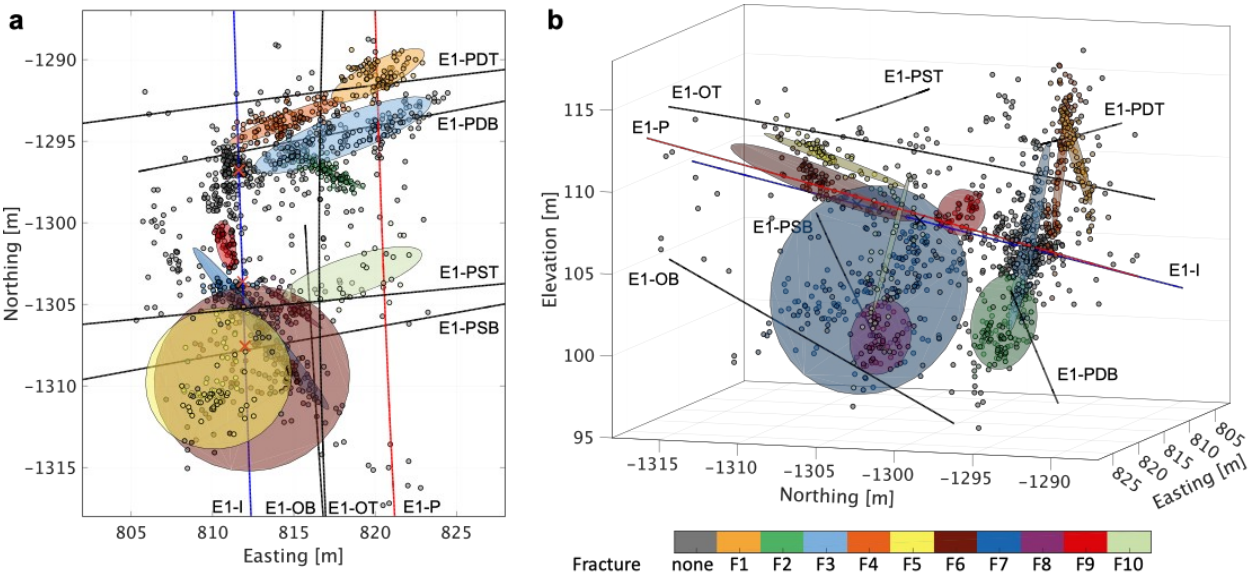

Figure 5. E1. Two views of fracture planes identified from microearthquake (MEQ) locations. Stimulation locations are indicated by red crosses with the shallowest (43 m, 128 ft) located lowest on the figure. The drift, which has an orientation of ~N30E, is located to the right in a, to the left in b.

2.2 Flow Tests

Long-term ambient temperature and chilled water flow tests were performed for about 10 months. The chilled water flow test was performed to quantify thermal breakthrough, which was not conclusively observed. In these tests, water was introduced into the injection well E1-I at the 50 m (164 ft) Notch interval, typically at 0.4 L/m. This rate, although lower than desired, did not result in microseismicity, indicating that the stimulated system is seismically stable. During the first part of the flow test, ambient temperature “mine” water (tap water quality) was injected into the system. After a month of ambient temperature water, chilled mine water injection was initiated.

During the flow test, the pressure required to inject the mine water at 0.4 L/min was significantly higher than the ISIP (ISIP ~ 25.5 MPa (3700 psi), injection ~34.5 MPa (5,000 psi)). The pressure required to inject 0.4 L/min rose constantly under constant flow conditions. Pump shutdowns occurred for various reasons over the 10 months of injection. When restarting to flow at the same rate, the injection pressure was typically significantly lower than prior to shutdown regardless of the shutdown duration. This behavior could be attributed to poroelasticity, geochemical dissolution and precipitation,

and/or biofouling, but the cause was not identified [*Kneafsey et al.*, 2020]. This trend did *not* occur in E3.

Upon changing to chilled water injection at the same rate, a decrease in injection pressure was observed prior to pressure increasing. This decrease was likely caused by thermal contraction of the rock in the region of the injection well and concomitant increase in the fracture aperture, followed by the aforementioned processes driving increases in injection pressure over time.

Water was collected at the production well, as well as at other wells and drift wall surfaces. Volumetric recovery of the injected water increased over the duration of the test [*Kneafsey et al.*, 2020] reaching nearly 95% recovery [*Kneafsey et al.*, 2020]. Over the duration of the flow tests the proportions of the water collected at various locations changed dynamically. These changes in location and rate were not necessarily related to applied system changes (flow, temperature, or outflow control change). The primary collection locations were two zones in the production well, called the production interval (between the straddle packers – E1-PI) where flow enters through natural fractures, and the region below the bottom packer (E1-PB) where flow enters the well through hydraulic fractures. Tracer and microbial analyses suggest that the recovered water is different from the injected water [*Mattson et al.*, 2021; *Neupane et al.*, 2020; *Zhang et al.*, 2020], indicating perhaps that the injected water is partially displacing native water in the system, or the water is altered in different ways along different flow paths.

3.0 Experiment 2 (Testbed 2, 4100 level)

E2 was intended to investigate shear stimulation [*Kneafsey et al.*, 2024]. Testbed 2 was constructed at 1.25 km depth (4100-foot) (Figure 2 bottom)) in the Yates amphibolite (a blocky low-permeability rock) having different stress conditions from E1 [*Ingraham et al.*, 2020]. Based on the best initial information, there was a reasonable probability that shear stimulation would occur along appropriately oriented, sufficiently weak fractures [*Burghardt et al.*, 2020; *Dobson et al.*, 2018; *Singh et al.*, 2019]. Initial characterization included mapping fractures and features observed at the drift wall, drilling a 10 m horizontal borehole (TH4100), and a 50 m vertical borehole (TV4100). TV4100 penetrated an unexpected ~10m thick rhyolite intrusion within the amphibolite, which is also exposed to the north near the Yates Shaft on this level. Based upon rhyolite intercepts in TV4100 and the exposure in the 4100 Level drift, this layer was expected to be continuous and present beneath our testbed. Eighteen stress tests were performed in TV4100, eight of which used the SIMFIP tool to quantify three-dimensional displacement during testing. These tests showed significant stress heterogeneity and lower than expected stress anisotropy [*Ingraham et al.*, 2020]. ISIPs in the lower amphibolite (below the rhyolite layer) were ~ 27.6 MPa (4000 psi), in the

rhyolite ~ 18.6 MPa (2700 psi), and in the upper amphibolite ~ 21.4 MPa (3100 psi) [*Kneafsey et al.*, 2021b]. Because of the lower stress in the rhyolite and the complexity that it introduced, the E2 testbed was designed to be entirely *above* the rhyolite layer. The most probable magnitude of the intermediate principal stress, which is subhorizontal, is between 30 and 40 MPa [*Burghardt et al.*, 2022]. Since the lithostatic stress at the 4100-level site is approximately 35 MPa, this places the stress state as transitional between a normal faulting and strike-slip regime. More detailed descriptions of the geology, testbed characterization, and evaluation of stresses are contained in *Burghardt et al.* [2022] and *Kneafsey et al.* [2022b].

3.1 Testbed 2

Testbed 2 consisted of nine ~10-cm-diameter continuously cored subhorizontal boreholes ranging from 55 to 80 m deep (Figure 2 bottom). Well TC for stimulation/injection was oriented to optimally intersect fractures that were interpreted to be best oriented for shear stimulation while also avoiding the gently dipping rhyolite zone below the drift [*Burghardt et al.*, 2022; *Kneafsey et al.*, 2022c]. Two pairs of monitoring wells containing grouted sensors fan out from Site A (AMU and AML) and Site C (DMU and DML). Well TC was surrounded by four open injection/production/monitoring wells (TU, TL, TN, TS shown in Figure 2 bottom as Site B) in an outward fanning five-spot pattern. Following the drilling of these wells, an extensive low pressure hydrologic characterization was performed. A detailed description of the E2 testbed is presented in *Roggenthen et al.* [2024] and *Kneafsey et al.* [2022c].

Testbed 2 instrumentation included active seismic sources and sensors for CASSM and passive seismic monitoring, a hybrid fiber-optic cable with single mode (strain – DSS, acoustic – DAS) and multi-mode fiber (temperature – DTS), electrodes for electrical resistivity tomography, and thermistors. These were deployed and grouted in boreholes AMU, AML, DMU, and DML (Figure 6). CASSM sources, an array of hydrophones, ERT electrodes and multi-mode fiber-optic cable for DTS were also deployed in TS but not grouted. Additionally, ERT and multi-mode fiber were deployed in TU, TL, and TN as allowed by experiment constraints. A low pressure Downhole Robotic Stress Analysis (DORSA) tool, conceptually similar to the SIMFIP tool, which measures borehole displacement in six degrees of freedom was also constructed and co-deployed with ERT sensors in well TN (Figure 6). Stimulations could be performed in any of the open wells emanating from Site B, with initial stimulations targeted for the central borehole TC. Initial stimulations used the SIMFIP tool to quantify multidirectional strain during stimulation, and subsequent stimulations were performed with other standard straddle packer sets.

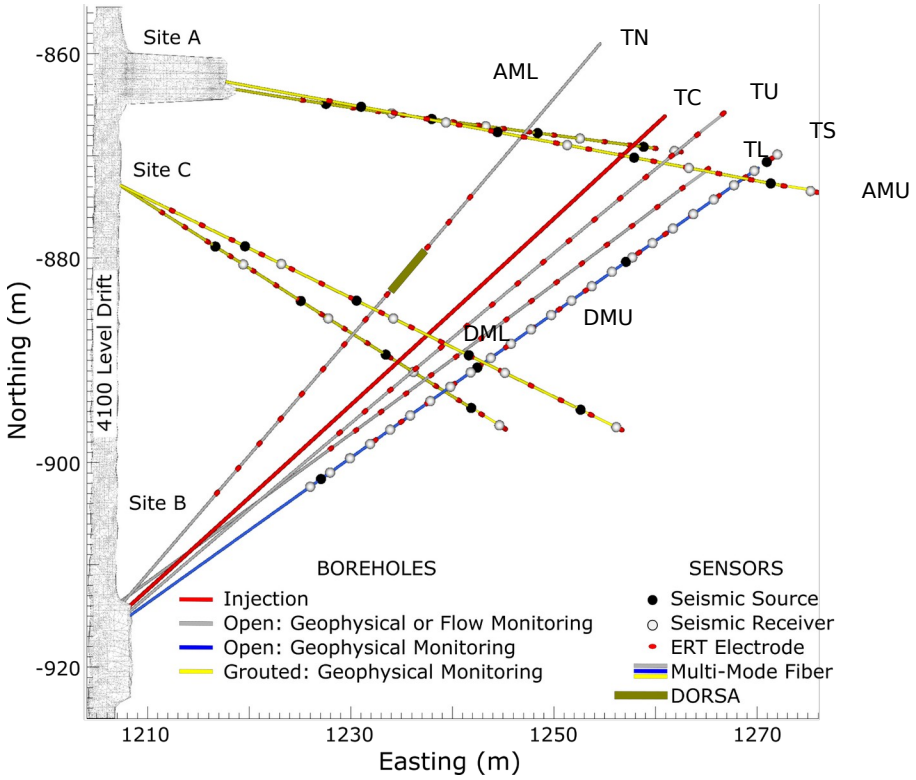

Figure 6. Plan view of geophysical monitoring borehole layout and sensor locations for E2. Coordinates are based on the Homestake coordinate grid system. Well names starting with AM and DM are monitoring wells with collars in the Alcove or Drift. Test well names from Site B begin with T. U is upper, L is lower, N is North, and S is South. (modified from *Johnson et al.* [2024]

3.2 Stimulation

Initial calculations indicated shearing would be likely in some fractures in the rock (Singh et al., 2019). As further information was collected during testbed construction, calculations indicated that shear stimulation was less likely, as the maximum shear-to-normal stress ratios were computed to be about 0.35, which is significantly less than the desired value of 0.6 (Figure 7, Figure SI-1) [*Burghardt et al.*, 2022; *Meng et al.*, 2021; *Meng et al.*, 2022]. *Meng et al.* [2022] conducted laboratory tests on core samples and found that most of the tested sealed fractures did not fail at in-situ shear conditions. Additionally, for shear stimulation to occur, the selected fracture set would need to be in flow and pressure communication with the well and able to take water at a rate adequate to pressurize a significant area of the fracture within the time-frame of the stimulation. The sealed fractures had very low permeability, thus were unable to take water at the necessary rate. Based on this updated information, shear stimulation was not expected.

The E2 stimulation was executed by first identifying the fracture most likely to shear and pressurizing it to 90% of the estimated minimum principal

stress. These conditions would maximize the possibility of shearing while precluding hydraulic fracturing. The test was performed using the SIMFIP in well TC at depths between 58.64 and 61.05m (192.4 and 200.3 ft) (Zone 7). The zone was pressurized to 16.13 MPa (2340 psi) for two weeks. Over this time, the rock and fractures took only tens of mL/day, which was insufficient to induce shear as predicted. Table SI-2 lists details of the attempted Experiment 2 stimulation. This test was concluded and E3 begun.

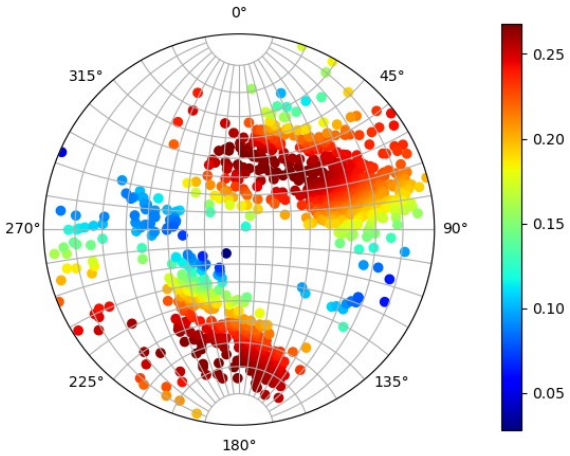

Figure 7. E2. Equal angle lower hemisphere projection of poles of identified fractures in E2-TC, colored according to the mean shear-to-normal stress ratio under the hypothesis that the principal stresses are rotated from vertical/horizontal. See also Figure SI-1. [*Burghardt et al.*, 2022].

4.0 Experiment 3 (Testbed 2, 4100 level)

The purpose of E3 was to investigate alternate methods of stimulation. In E3, stimulations were performed at pressures above the minimum principal stress in three intervals in well TC and one interval in well TU (Figure 8) [*Kneafsey et al.*, 2024]. E3 was performed in the same testbed as E2 using the same wells and same monitoring equipment. The first E3 stimulation was performed at the same location as the attempted E2 stimulation (Zone 7) at low flow rates ramping up from 3 mL/min to 400 mL/min with a total injected volume of 300 L. The stimulation was performed to ascertain whether a slow-growing hydraulic fracture might intersect fractures that could then shear. The next stimulation was performed by cycling the pressure about the minimum principal stress (40 L total volume, Zone 4). This was done to extend a hydraulic fracture in mini steps with short relaxation between steps. *Zang et al.* [2017] noted reduced seismicity for this type of stimulation. The next stimulations in TC Zone 1 and TU Zone 3 were performed by breaking the rock down at 1 L/min and extending the fracture at 5 L/min with a total injected volume of about 400 L (TC Zone 1) and 1200

L (TU Zone 3). These stimulations are described in greater depth in *Kneafsey et al.* [2022a] and selected observations from these stimulations are presented below. The first stimulation is described in greater detail than the others with more data presented to illustrate the collected and available data.

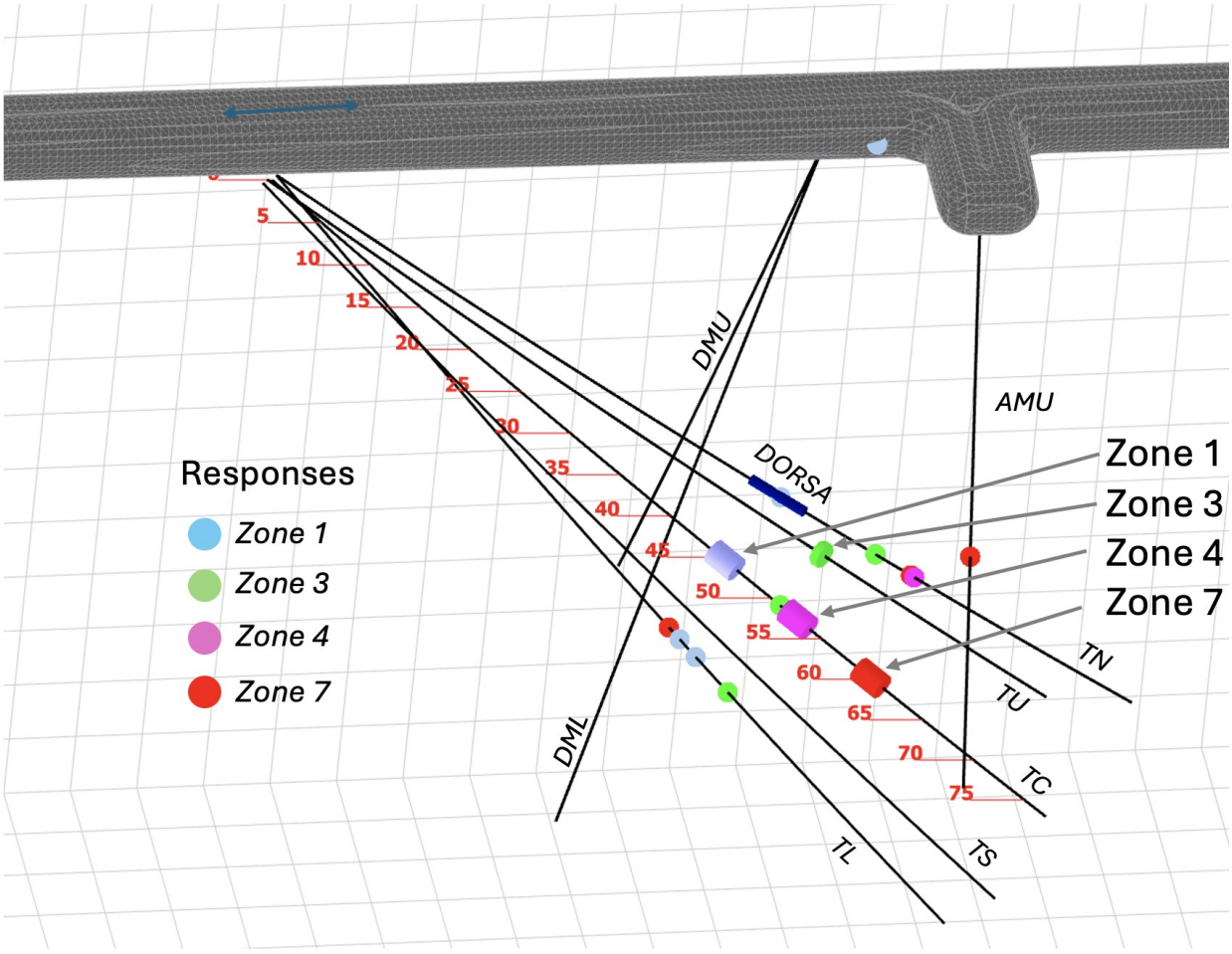

Figure 8. E3. Stimulation locations in TC and early fracture intersections indicated by colored dots. The grid spacing is 5 meters.

4.1 Stimulations

4.1.1 Stimulation 1 – TC Zone 7 (58.64 - 61.05m, 192.4-200.3 ft) – Slow Flow

For this stimulation, the SIMFIP tool was left at the location in TC where E2 was performed (see Figure SI-3, and Table SI-3). This stimulation initiated by pumping water at 3 mL/min into the packed interval. Following breakdown, the rate was increased stepwise every ~80 minutes or more until a maximum flow rate of 400 mL/min was attained. The rationale for this approach was to propagate the fracture with as low of a flow rate as was practical to maximize the potential for shear activation of natural fractures intersected by the hydraulic fracture. After several hours of pumping at 400

mL/min, breakthrough into the production wells (primarily TN with a drip observed from TS) was observed. Flows as high as 250 mL/min were recovered from TN (63% of the inflow rate). Spikes in strain were observed in the DAS monitoring system in AMU at the location where an elevated temperature spike in the DTS data occurred (Figure 9) but the strain began to increase 6 hours *before* the intersection (Figure 10). The initial strain signal was somewhat diffuse with a larger zone showing compressive strain just below the location of the fracture. The breakthrough is highlighted by a more defined extensional signal (Figure 10 center). A slow drip of water from the grouted AMU wellhead was also observed confirming the intersection. The ERT data are consistent with the strain and temperature data. Figure 11 shows a decrease in electrical conductivity near the injection site. This decrease is probably caused by pressure in the packers compressing water-filled conductive pores by the increased compressive stress adjacent to the borehole and fracture [*Johnson et al.*, 2021]. A decrease in conductivity is also observed near the breakthrough location in AMU. This may also be caused by compression of the rock prior to breakthrough also shown by the DAS strain data. Well AMU increased in conductivity because of the influx of water into this well. When it was determined that the fracture intersected the monitoring well, the injection was stopped, and outflows from production wells and E2-AMU decreased slowly with time.

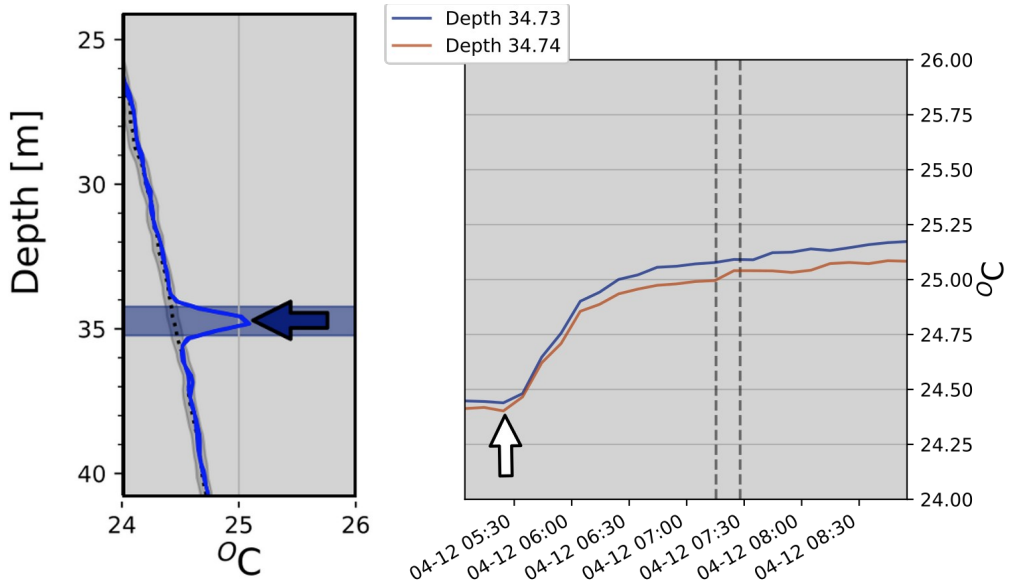

Figure 9. E3. Temperature signal from the downgoing DTS fiber in monitoring well AMU showing a peak at a depth of about 35 m (left) starting at about 5:30 UTC (white arrows, right). Red and blue lines are from the downgoing and upgoing fiber. See Figure SI-2 for additional detail.

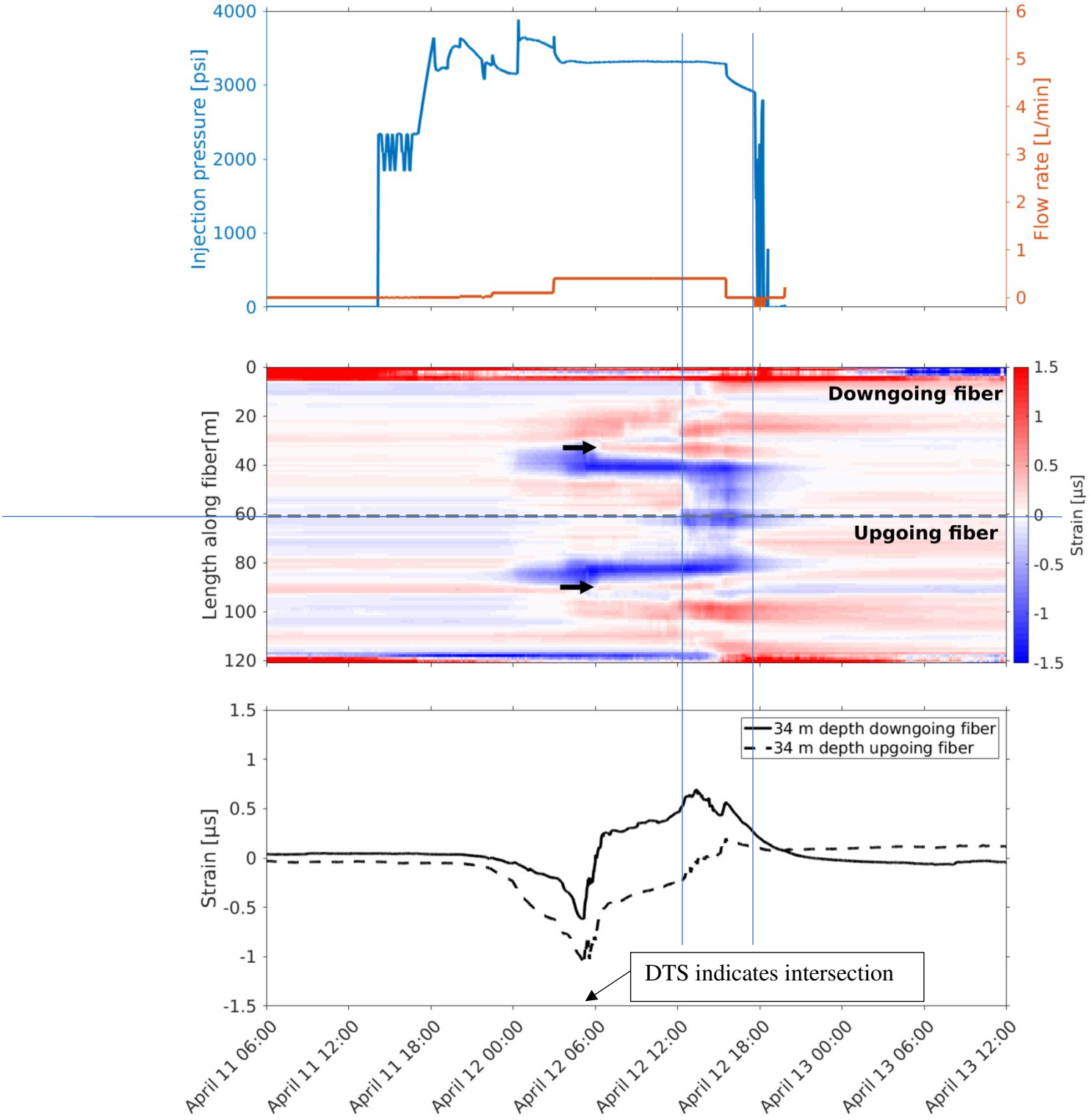

Figure 10. E3. Low-frequency DAS strain recorded along borehole AMU during Stimulation 1 in Zone 7. (Top) Injection pressure and flow rate Note: breakdown occurred with an injection flow rate of 3 mL/min.; (Center) Low-frequency DAS strain recorded along the length of the fiber

deployed in borehole AMU. Note symmetry with respect to the bottom of the well from downgoing and upgoing fiber lengths. Arrows indicate extensional signals indicating fracture hits at a depth of ~34 m, recorded on both sections of the fiber. (Bottom) Strain at ~34 m depth at the time of the observed DTS spike (5:23 am UTC) for both sections of the fiber. Vertical lines added as visual guides.

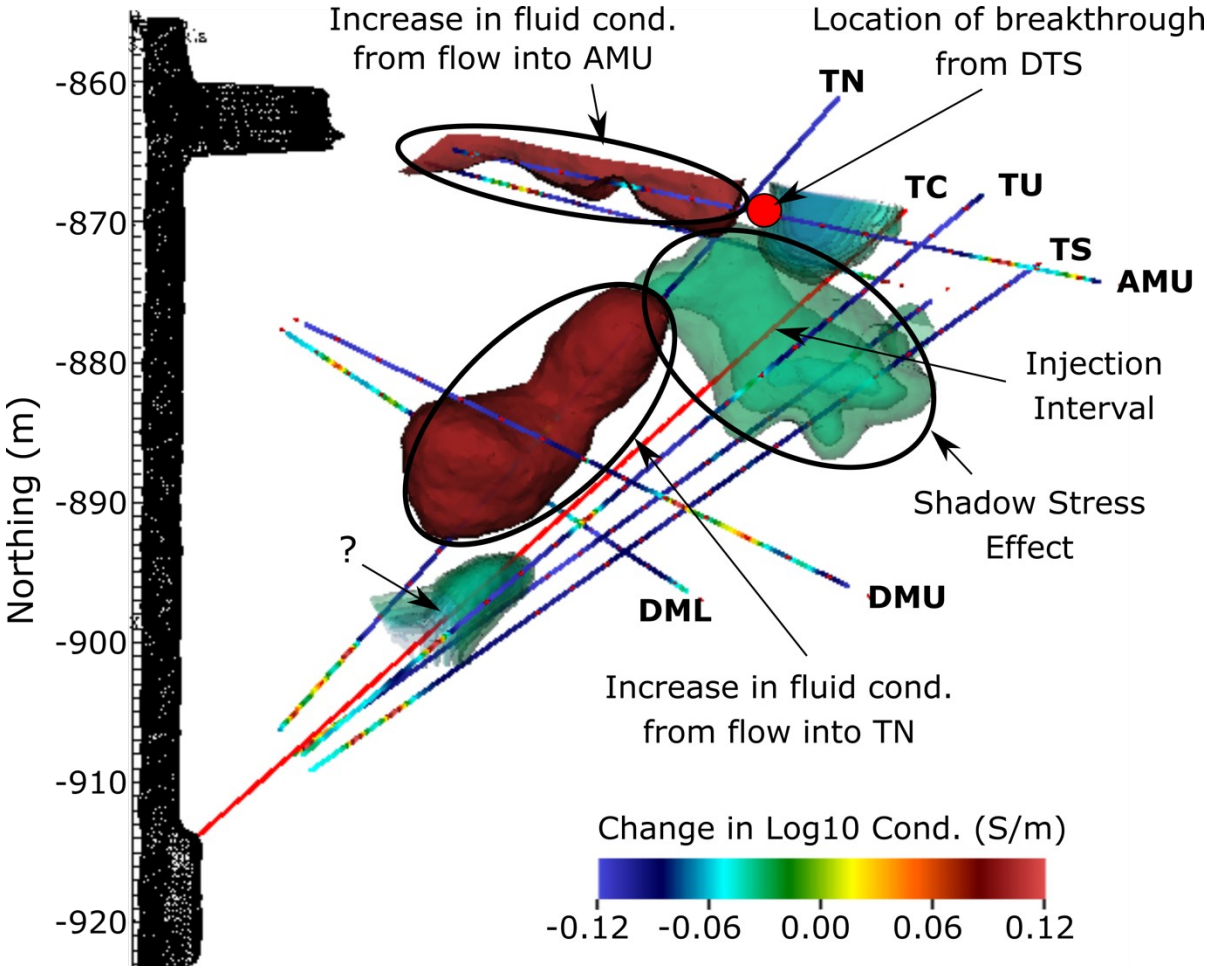

Figure 11. E3. Electrical resistivity tomography image of the testbed during Stimulation 1. Several features are notable: near the injection interval, a shadow stress feature is observed (green). Increases in conductivity are observed near well TN carrying produced water, and AMU, which the stimulated fracture penetrated.

Early during this stimulation while the flowrate was very low (3 mL/min), the SIMFIP tool measured a consistent, mostly vertically downward displacement in short steps of a few micrometers each, totaling about 20 micrometers starting at pressures between 17.23 – 20.68 MPa) (2500 – 3000 psi), which is well below the breakdown pressure of 25.16 MPa (~3650 psi) (Figure SI-3). At the breakdown (pressure of ~ 25.16 MPa - 3650 psi), an abrupt change in the directionality of the displacement of almost 90 degrees from mostly

vertical down to north and slightly upwards occurred totaling about 5 micrometers, which was accompanied by a drop in pressure (with flow kept at a constant flowrate of 3 mL/min). This displacement was subsequently partially reversed, however an irreversible component in the direction of the initial step-wise displacements remained (Figure SI-3). The pattern of the displacements observed in combination with the initial pressure build up and subsequent drop could be an indication of the activation of a pre-existing fracture in a stick-slip-like shear mode before fracture opening at the breakdown pressure and partial closing when pressure started to drop again. The same step-wise displacement was not observed during later stages of the test.

The initial strain of the rock during stimulation was not indicated by the DORSA probe located in the TN borehole several tens of meters away. However, after flow was increased to 400 ml/min, the DORSA started to exhibit a very linear but polyaxial contraction. This trend started to reverse after the injection was stopped (Figure SI-3). The contraction on the DORSA is in agreement with the negative strain measured by the DAS below the fracture intersection at 34m in AMU, indicating a compression of the rock mass. The DORSA was distant from where the fractures intersected TN, therefore only measuring secondary fracturing effects. Interestingly, the DORSA was ideally placed for the later stimulation of Zone 1 and clearly showed fracture opening of approximately 200 micrometers when the fracture intersected and passed borehole TN.

4.1.2 Stimulation 2 - TC Zone 4 (51.42 - 53.83m, 168.7-176.6 ft) - Cyclic Injection

Stimulation 2 was performed by cycling the injection pressure about the fracture opening pressure repeatedly in an effort to create a scalloped fracture [*Kneafsey et al.*, 2024]. The fracture initiation pressure on this zone was higher than the other zones. Because of that, pressures on the high and low part of the cyclic injection were gradually increased until it was evident that a fracture had been formed. The pressure continued to be cycled until a net volume of 40 L was injected. Cycling was performed by manually changing the injection flowrate. The initial cycles were injected at 0 or 1 L/m with durations of about one-half minute (one half minute flow, one half minute no flow), in the middle of the test, the injection flowrates were 0 or 1.5 L/m with durations about 2 minutes, and at the late stage, the injection flow rates were zero or 2 L/m with durations about 2.6 minutes. It should be noted that some backflow did occur during the “zero-flow” segments. During this time a small amount of effluent flow was observed from wells TN, TL, and TS, though the production rate from TS was considerably smaller than from the other two wells. No production was observed from well TU. This stimulation did not intersect any grouted monitoring wells or the drift, but the total injection volume was small compared to our other stimulations. Following this stimulation, the injection interval in the TC well was held at 16.13 MPa (2340 psi) for several days to observe flowback. Flowback tests

allow the evolution of the closure pressure to be observed [*Burghardt et al.*, 2020].

The displacement signal measured by the SIMFIP was masked by the effects from the rapid pressure cycles from the stimulation. The DORSA probe showed less than 10 micrometers extensional deformation in the area around 42.6 m (140 ft) in TN, without a clear fracture breakthrough event. The extension started to reverse into an axial contraction after the injections ended. While weak inflow could be observed in TN, likely from several locations between 42.6 and 54.9 m (140 and 180 ft), no flowing fracture or fracture network could be identified. The DTS shows an inflow of warmer water somewhere in the lower section of TN at the same time as the deformation is recorded on the DORSA. Faint, small magnitude strain signals were observed in monitoring boreholes AML, DMU and DML, although they are most likely related to poroelastic deformation being transferred through the volume being stimulated.

4.1.3 Stimulation 3 - TC Zone 1 (44.20 - 46.61 m, 145.0-152.9 ft) - High Flow

To compare with the low rate (Zone 7) and cyclical (Zone 4) injections, a higher-rate stimulation was performed in Zone 1 [*Kneafsey et al.*, 2024]. The fracture was initiated by injecting at 1 L/min for approximately 2 minutes, then the well was shut-in for approximately 1 hour. Following the shut-in, the well was flowed back at a controlled rate of 250 mL/min followed by shutting in the well when the pressure declined to atmospheric pressure. This shut-in resulted in a significant pressure increase in the packed off interval, indicating that pressurized water remained trapped in the fracture. The fracture was reopened by pumping at 1 L/min for approximately 2 minutes followed by a controlled flowback at 100 mL/min. This lower rate was selected to minimize the near-wellbore fracture pinching that might trap pressurized water inside the rock. Again, the pressure rebounded significantly but more slowly and to a lower magnitude. We opened the fracture again by injecting at 1 L/min, then propagated the fracture by injection at 5 L/min for about 72 minutes. A short time later breakthroughs into TN, TL, and the wall of the drift near Site A were observed. The peak production rate from the production wells was approximately 1.3 L/min. Typical flows from TL were ~0.640 L/min, TN ~0.55L/min, and TS was dripping. No production was observed from well TU. Although this stimulation did not intersect any grouted monitoring wells as no temperature spikes were observed in the DTS data, it did intersect the drift and appears to also result in low-rate water production from well TV4100 (collared in Alcove A). In spite of not indicating intersection of the fracture and any grouted monitoring wells, a significant strain signal was observed in DML at depths that correspond to DTS hits during later tests. This may indicate that fractures were created or opened, but flow was not achieved. Low magnitude strain signals were also observed in AML and DMU. This might suggest poroelastic deformation in the testbed. The intersection of the fracture with

TV4100 is hypothesized to occur through a path within or along the contact with the rhyolite dike that underlies the stimulation wells and connects to TV4100.

A flow test was performed while a sewer camera was deployed in TL and TN while injecting into TC to observe water entering the boreholes. Water jetted vigorously into TN at 48.5 m (148.9 ft) similar to Figure 4. After shut-in, the jetting declined. Reinitiating injection at 2 L/min resulted in a time lag of about 2 minutes for the jets to reappear. Jets were also observed at 47.1 m (154.5 ft) in TL, and another inflow point was observed in TL at 48.8 m (160 ft). DTS data from TN during this stimulation show a clear temperature signal from the inlet water at about the same location identified using the visual observations.

During the stimulation of Zone 1, the pressure control of the system anchoring the SIMFIP probe to the rock was overpowered by the rapid rise in zone pressure, resulting in a declamping of the tool and loss of data during the breakdown phase of the test. During later cycles of the test, clear and mostly reversible displacements of up to 200 micrometers (not corrected for potential tool-pressure effects) were observed. During the last cycle of this stimulation with flow increased to 5 L/min, the DORSA indicated a clear displacement of the rock in TN of several hundred micrometers at the DORSA location. This displacement is spatiotemporally synchronized with a peak in temperature observed on the DTS in TN, indicating a breakthrough of fluid right at the DORSA location. This was later confirmed with a downhole camera during a repeat-injection. Before the large displacement corresponding to the hydraulic TC-TN connection, the DORSA recorded a clear micrometer-scale signal. This rapid DORSA response is likely a poroelastic deformation prior to the fracture propagation to TN.

DAS data suggest strain responses in wells AMU, AML and DMU. Low-frequency (1Hz) DAS strain data recorded a strain peak in borehole DML at depths of ~15 m (49.2 ft) and ~43 m (141 ft) shortly after the flow rate was increased to 5 L/min. Interestingly, fracture intersections at these exact depths were observed in DTS measurements during flow tests conducted a month later. These observations could be linked to areas of pre-existing weakening that did not carry flow during this first round of tests but subsequently opened and conducted water into the monitoring boreholes after repeated stimulation. Minor strain signals were observed in boreholes AML and DMU at depths of 20-30 m (61.6-98.4 ft) and 25-35 m (82-114.8 ft), respectively. These less localized, smaller magnitude extensional signals are most likely related to poroelastic deformation transferred across the rock volume.

4.1.4 TU Stimulation 54.07 – 54.74 m (177.4 - 179.6 ft.) Interval

TU was targeted for stimulation to improve the connection to TC. TU has a number of wells below it to possibly cage flow potentially keeping it from reaching the rhyolite [*Frash et al.*, 2018b; *Frash et al.*, 2021a; *Frash et al.*,

2020]. The stimulation was performed at a depth approximately aligned with Zone 4 of TC. Injection commenced at 1 L/min until breakdown was observed approximately 1 min later (bottom panel of Figure SI-4). A peak pressure of ~37.92 MPa (5500 psi) was reached and flow was subsequently increased to 5 L/min and held for roughly 4 hrs. During this time, pressure approached a steady state value of 31.03 MPa (4500 psi). The resulting fracture intersected TC, TN, and TL and outflow from these boreholes totaled approximately 25% of the injected volume. Flow was stopped at the end of the day and injection resumed the following day at 5 L/min. While flowing into TU, the packer assembly installed in TC was repositioned slightly because it appeared that a fracture from TU was impinging on a packer element. Injection was then switched to TC at 2 L/min to identify whether flow from TC would be captured at TU. Outflow was measured from the packer intervals in TN and TU totaling ~35% of injection, representing a significant improvement in fluid recovery from previous TC injections.

During this phase of stimulation, no intersections were observed with the grouted monitoring boreholes via DTS. However, this phase of injection did produce the first detectable seismic events beginning with the restart of injection at 5 L/min on the second day (Figure SI-4). Because of the low signal-to-noise ratio of the seismic events, automatic processing during the entire experiment did not produce reliable locations. We manually revised all phase arrival picks, added S-wave arrivals (these were not included in the automatic workflow) and relocated the seismicity before interpreting the results. Figure SI-4 shows the timing and location of seismicity during this time period. Nine events were detected and they were located generally above and towards the drift from the injection point. This is consistent with the observations of flow at the grouted wells and drift during previous tests.

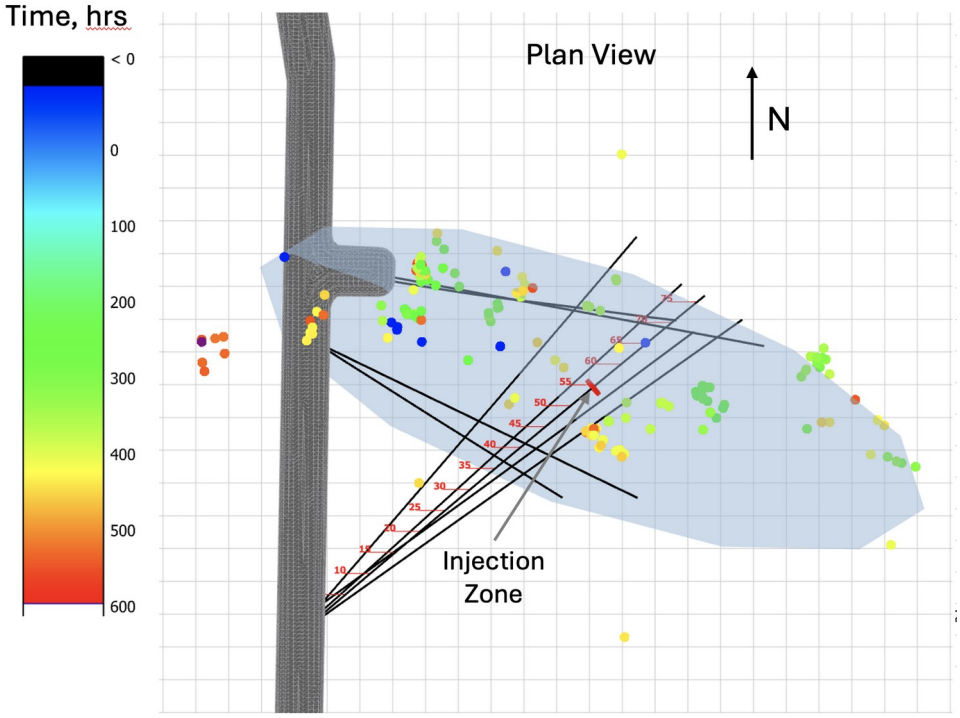

a.

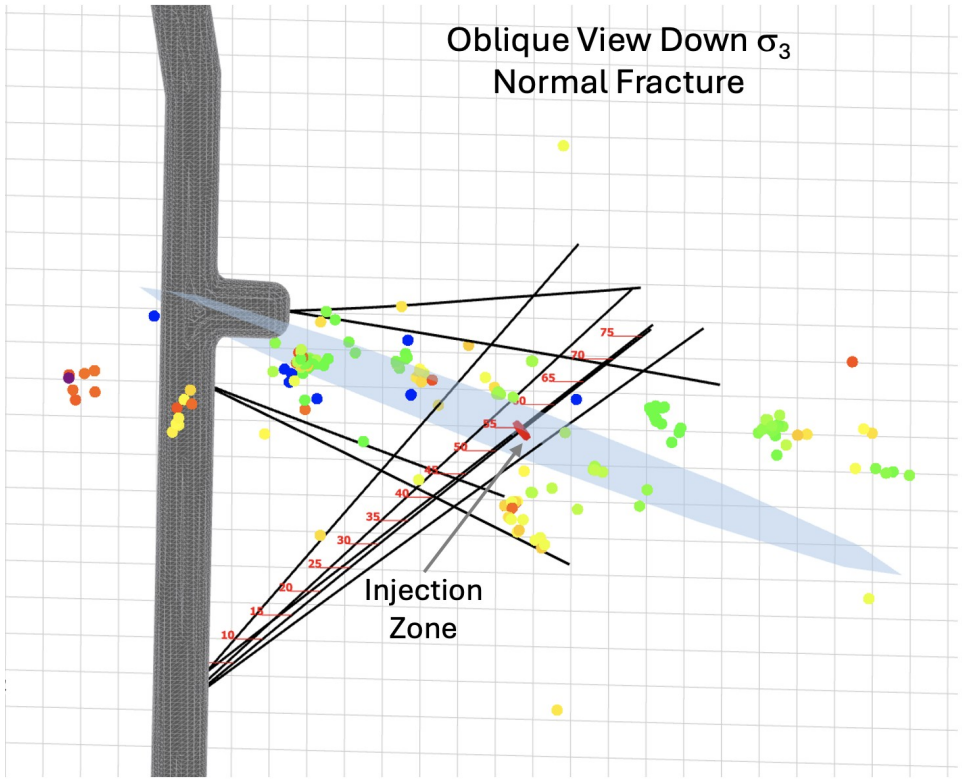

b.

Figure 12. E3. Microseismic events detected during flow testing into the 54.07 – 54.74 m (177.4 - 179.6 ft.) interval of TU. a. plan view of the MEQs, and b view parallel to the plane normal to the minimum principal stress

based on stress measurements in borehole TV4100. The grid is 5 meter spacing.

4.2 Flow Testing Well TU

The start of flow testing in TU at rates from 2, 3, and 3.4 L/min produced microseismic events up to 60 meters from the injection point both above and below the drift (Figure SI-5). Because water was injected at pressures exceeding the minimum principal stress (hydropropping), it is very possible that stimulation continued over the duration of the flow test. The lateral extent to which water pressure exceeded the minimum principal stress is not known. The flow also produced a complex pattern of fracture intersections with the grouted monitoring boreholes, as shown by temperature measured on the DTS system (Figure SI-6) and strains recorded on the DAS systems. Temperature increases indicate flowing fracture intersections and are most abundant in DML, which is consistent with a generally SSW dipping fracture trends. More seismicity was also recorded during the two-week flow test, however there was no apparent trend in distance between injection and located microseismic events over this time (Figure SI-5). Comparing sequential changes in electrical resistivity (Figure SI-7) shows a significant increase in conductivity relative to the baseline (just prior to injection on May 19 Figure SI-7) between the injection location and the drift indicating an increase in water in this region. These data are also consistent with observations of seeps in the drift (Figure SI-8). At the beginning of the flow test, seeps into the drift were primarily in the area near the Site A. In general, ceiling drips appear in groups of multiple dripping points within ~ 1 square meter (~10 square ft). As the test continued, seeps developed at locations south of the initial locations, and that trend continued over the duration of the flow test, indicating a dynamic testbed.

5.0 Discussion and Lessons Learned

The EGS Collab experiments directly address THMC challenges associated with EGS and provide critical insights at the fundamental science level. Predictions, and often assumptions of behavior going into these experiments were frequently defied during execution and had to be addressed through a continuous cycle of hypothesis, modeling, field trial, data analysis, interpretation of processes, and re-evaluation of understanding. This practice was constantly performed in a remote and challenging environment and is relevant for commercially viable EGS utilization. Full-scale EGS applications will similarly have to confront the realities of induced seismicity, stress/geologic heterogeneity, stimulated fracture propagation mechanics, the influence of natural fractures and geologic structure on stimulation, evolving permeability pathways due to physical and chemical effects over time, and optimization of thermal circulation/conductivity. These challenges were commonplace for the five-year duration of EGS Collab activities at SURF and it is reasonable to expect similar behavior of EGS reservoirs at the full

scale. This project provides new insights, crucial observations, valuable updates to models, and a suite of both novel and commonplace stimulation, circulation, characterization, and monitoring tools/techniques to reduce uncertainties and increase the probability of success for EGS applications. Researchers and practitioners are encouraged to build upon both the successes and the unsolved complexities that the EGS Collab Team illuminated within the underground mine workings at SURF. Here we share lessons learned on:

- Induced seismicity
- Correlation between seismicity and permeability
- Distributed and dynamic flow systems
- Thermoelastic and pressure effects
- Shear stimulation
- Local geology
- Thermal breakthrough
- Monitoring stimulation
- Grouting boreholes
- Modeling
- System management

5.1. Lessons learned at the scale of our experiments and lessons applicable to EGS at the full scale

5.1.1 Induced seismicity

Prior to initiating our tests in E1, we estimated seismicity associated with our stimulations. Our estimation considered low injection flow rates that flow test models indicated could give us a clear temperature change over a reasonable timeframe at our production well. At our experiment flowrates, we did not induce significant seismicity (no sensible ground motion, see equipment specifications in SI [*Hopp*, 2023b; *Schoenball et al.*, 2020a]), but we did not detect a temperature change at our production well either. In E2 and E3, we used the results of E1 to estimate that we would not induce seismicity in these experiments. Again, we injected at the lower flow rates, did not induce seismicity, and again did not detect a clear temperature change. Higher flowrates would probably helped to cause a temperature change, but would come with a greater risk of induced seismicity that might affect workers only tens of meters away. The ability to better predict and control induced seismicity related to injection actions is one key to future EGS development.

5.1.2 Correlation between seismicity and permeability

The correlation between seismicity and permeability remains elusive. One of the key challenges faced in developing EGS reservoirs is to create distributed permeability throughout the reservoir to facilitate efficient transfer of heat to

the circulating fluid (e.g., *Doe et al.* [2022]; *Grant* [2016]), so it is critical to understand where fluid is actually flowing. In E3, much of the seismicity that could be detected occurred in the upper regions of the testbed, even above the drift whereas all injection took place at elevations beneath the drift. Flow on the other hand apparently concentrated in the lower regions of the testbed and is predominantly thought to enter the drift from the floor [*Kneafsey et al.*, 2023; *Mattson et al.*, 2023]. In E1, seismicity identified opening along many planes that were confirmed to be hydraulically conductive. ERT data however showed that a large fraction of the flow occurred where little seismicity occurred (b.). In both E1 and E3, the fractures were hydropropped (injection pressure exceeding the minimum principal stress) at the borehole maintaining an open fracture at that location.

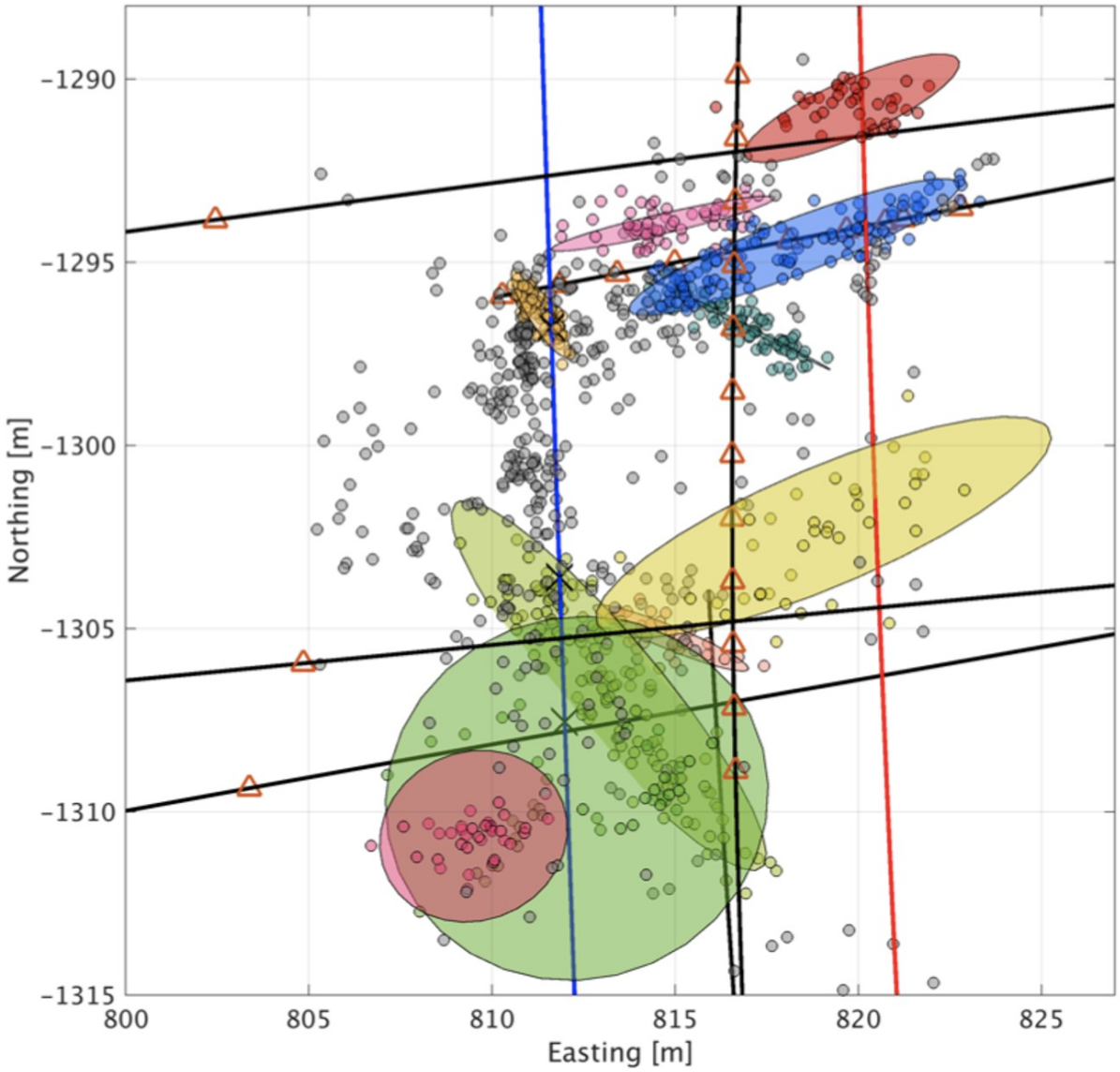
Northing [m]
−1290
−1295
−1300
−1305
−1310
−1315
800
805
810
815
820
825
Easting [m]

a.

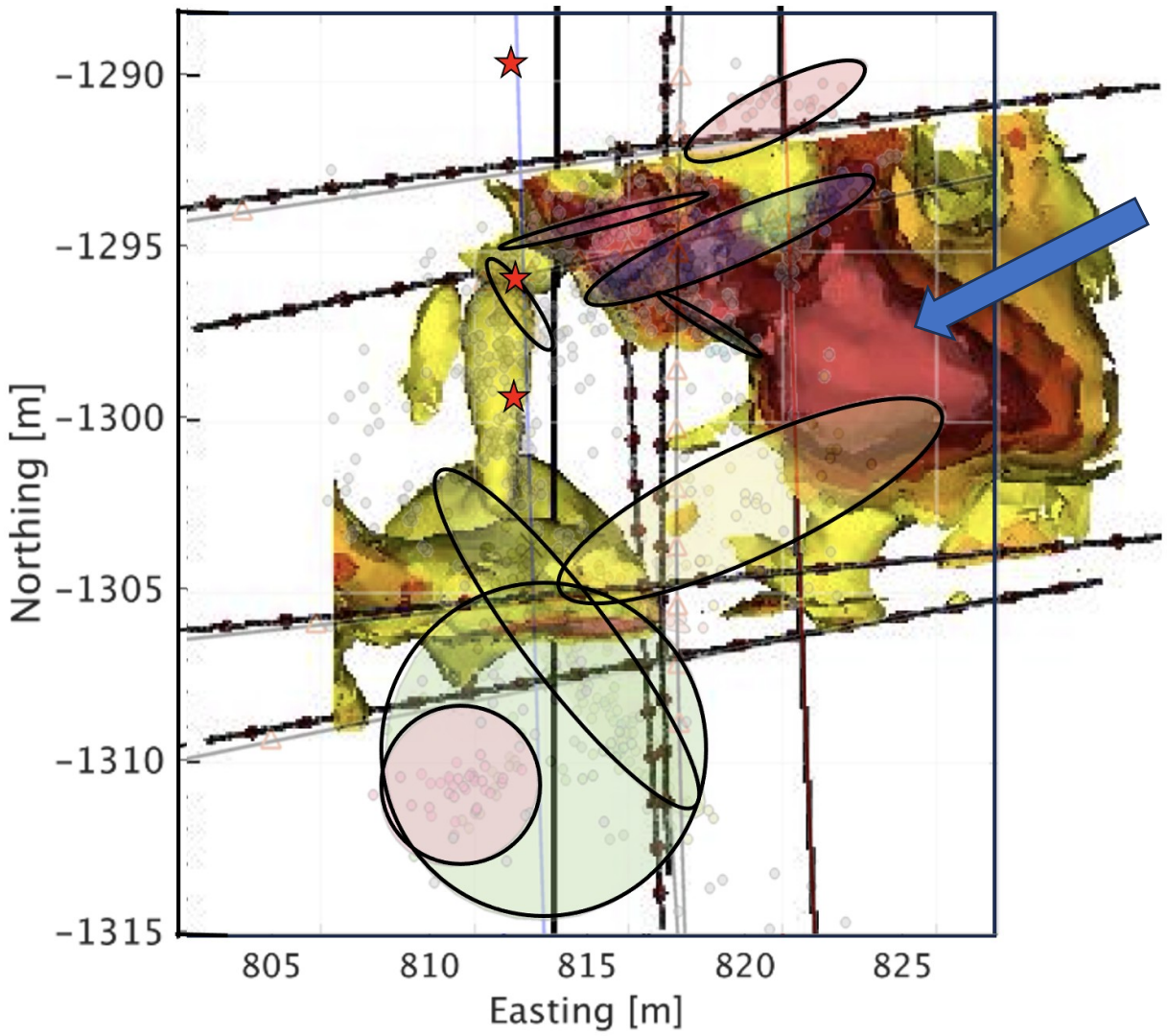

b.

Figure 13. a. Microearthquake-identified fracture planes (left) [*Schoenball et al.*, 2020a] and b. these planes overlapping and ERT image showing water flow (right) [*Johnson et al.*, 2019a]. Arrow shows region with large water saturation change thought to be hydraulically conductive where seismicity was minor.

Seismicity occurs when energy is released in the rock, for example from fracture tips or stick-slip friction from different sides of a fracture colliding with each other during shearing. The seismicity does not necessarily indicate that the pathways are large or viable for conveying fluid. Previously open pathways can take significant flow without the occurrence of new seismicity. Despite these challenges, microseismic data were shown to be highly valuable for confirming the stimulation of fractures, but that the absence of seismicity does not imply the absence of the ability to flow. Our data indicate that new fractures may be more prone to the generation of seismicity

whereas the ERT responded to larger flows in either the existing or new fractures. In practice, this suggests that investigations relying heavily on seismicity to delineate the fracture system should recognize that they may be missing important components of the flow and heat transfer system and may be highlighting mechanically active zones that are not necessarily providing significant flow.

5.1.3 Distributed, dynamic flow systems

The flow systems developed in our experiments were distributed and dynamic [*Mattson et al.*, 2023]. In both E1 and E3 we hydraulically fractured the rock and connected our injection and production wells. In addition, the stimulated flow system connected to many other locations beyond the intended testbed, resulting in reduced recovery rates at the production wells (e.g. Figure SI – 8). Whether connecting to an existing fracture network or creating new fractures, flow was observed and quantified at numerous locations away from where desired [*White et al.*, 2021]. Clearly, the flow pathway having least resistance is all flow paths together. Dynamic flow rates at the many collection locations changed over time, often without obvious reason.

There are many possible explanations for a dynamic system, and these may operate independently or together. These include geomechanical, geochemical, and biological processes [*Kneafsey et al.*, 2021d; *Kneafsey et al.*, 2020]. The geomechanical argument is that we injected water at pressures exceeding the minimum principal stress. Flow entering a fracture would exert a force on the rock blocks on both sides of the fracture impacting the overall stress distribution. This force could open fractures locally to an extent. When flow reached another intersecting fracture, the force balance and directions would change, altering system apertures and flow, and changing flow paths. It is not clear whether pressure exceeding the minimum principal stress is required for this since under proper conditions shear stimulation occurs below the minimum principal stress. The water jetting into the production borehole in E1 (Figure 4) indicates that the injected water was at high pressure in the fracture near the production well but that pressure was not quantified. Biological processes are unlikely but possible in geothermal systems if the injected water is cool enough. In the EGS Collab systems, microbes were present [*Zhang et al.*, 2020; *Zhang et al.*, 2022], and they could change flow paths through biofouling. Biofilms are documented at locations within SURF [*Osburn et al.*, 2014]. The presence and abundance of microorganisms will also change as a result of nutrient consumption, thus biofouling would likely change spatially and temporally. These flow path alterations would impact the pressures on rock blocks perhaps accentuating geomechanical processes. Geochemical processes include dissolution and precipitation of solid phases that will impact permeability. Dissolution could concentrate flow as apertures increase, and this process could be self-enhancing, and precipitation would decrease permeability. Again, this could impact the geomechanics of the system. It is

important to realize that for both biological and geochemical processes, there are immense numbers of kinds of microbes and mineral phases. Experimenting with or modeling a single phase or single organism systems can be informative but is extremely limiting and possibly misleading.

If these behaviors are general, they could be positive for EGS because they may increase the heat sweep area beyond the expected area improving heat sweep. *Grant* [2016] noted that the fraction of the reservoir volume where heat transfer occurs appears to be much lower than that observed for natural hydrothermal systems, which will impact how much thermal energy can be efficiently recovered from the system. Changes in flow paths could also direct injected water into hotter rock, and that would be beneficial for heat sweep. It is also possible that flow systems might become less dynamic and distributed over time [*Ameli et al.*, 2013; *Elkhoury et al.*, 2013; *Polak et al.*, 2004; *Polak et al.*, 2003; *Yasuhara et al.*, 2004]. Over time the factors causing short-term dynamic behavior may lose importance, and longer-term factors like thermoelastic and geochemical processes may focus flow into more limited flow pathways. These important behaviors should be monitored in current and future field tests and EGS implementations.

One aspect of this dynamic system is that for flow to occur, elevated injection fluid pressures were needed to maintain open fractures and fluid flow between injection and production wells (hydropropping). If this were to occur in an EGS reservoir, this would increase the energy required to operate the EGS and indicates issues with flow impedance. The use of proppants (which were not employed at the EGS Collab testbed because of difficulty injecting them with the equipment used) may help sustain an open fracture network at lower operating pressures and could result in a less dynamic and more predictable reservoir fracture network, or possibly result in unwanted fast-flow paths. The choice of proppant material will need to respect chemical compatibility with formation matrix and fluids to maintain long-term conductivity. These questions require further study.

5.1.4 Thermoelastic and pressure effects

The mine drifts in the EGS Collab testbeds impacted experiment outcomes. Decades of ventilation resulted in temperature and stress perturbations in the rock and pressure perturbations in the flow paths [*Fu et al.*, 2018a]. Stress gradients from temperature gradients in the rock likely impacted flow direction, probably toward the drift where pressure was atmospheric, and 25% - 90% of our injected water was recovered. In E1, resuming pumping after any stop typically resulted in a decrease in the injection pressure required to resume a constant rate of injection. In E3, halts in pumping appeared to cause an increase in the injection pressure to resume a constant flow rate. We don’t have an explanation for this behavior. Injection of chilled water during the E1 flow test initially resulted in an increase in permeability. Following this increase, the permeability decreased consistent with previous observations. This thermal effect should be expected at FORGE and in EGS

systems where cooler water will be injected into hot rock. Tracer studies at EGS Collab also indicated changes in flow paths over time and in response to stopping or changing the flow rate [*Mattson et al.*, 2019a; *Mattson et al.*, 2023; *Neupane et al.*, 2019a; *Neupane et al.*, 2020].

In considering our experiment results, we expect full-scale EGS will also have complications because of stress gradients occurring from injection, production, and temperature changes, and dynamic flow networks that will change over time and in response to varying injection and production rates and fouling processes in addition to the complications related to the injection and later degradation of proppants. The role of the uncertain and heterogeneous stress gradients should be carefully considered, especially with respect to the imperfect prediction of propagation direction of hydraulically stimulated fractures. The EGS Collab project highlighted the current inability to accurately predict the behavior of a planned EGS stimulation because of irreducible uncertainties and heterogeneity in the rock and local stress conditions. Although changes in the mechanical behavior of the rock mass may be due to stresses induced by pumping and draining, modeling shows that thermal gradients created by the presence of the access drifts can greatly affect the trajectories of induced fractures. In larger-scale EGS operations, temperature gradients from injecting and flowing cool water may impact flow and rock mechanical behavior, particularly in conjunction with infill drilling and refracturing.

5.1.5 Shear stimulation

We did not establish flow systems at pressures below the minimum principal stress in either testbed. This does not mean shear stimulation below the minimum principal stress is not possible, however. There were microseismic indications of shear stimulation between the injection and production wells in E1, but the extent of the shear was not quantifiable because it was between boreholes. Small amounts of shear were measured using the SIMFIP tool during stimulations (tens of microns, See Figure SI-3, *Guglielmi et al.* [2023]), however these were not significant in that they did not provide improved permeability. Effective shear stimulation requires displacement over a sizeable area and asperities that will keep the rock walls apart. In Testbed 2 healed or filled fractures would not open below the minimum principal stress and indeed can be stronger than the host rock [*Frash et al.*, 2019a; *Frash et al.*, 2019c; *Jahnke et al.*, 2022; *Meng et al.*, 2022]. The testbed lacked properly oriented naturally conductive fractures that might be shear stimulated. Naturally conductive fractures observed elsewhere at the 4100 level were avoided over concerns that they might produce excessive flow to the underground openings significantly reducing the ability to build pressure in the fracture. Other sites have investigated shear stimulation with large permeability increases [*Evans et al.*, 2005] or no indication of permeability change [*McLennan et al.*, 2023].

This indicates that when planning an EGS, the right conditions (high shear stress, properly oriented fractures, fractures that will take flow and will increase in pressure when stimulated) are required for shear stimulation. These may occur in the field of interest, may occur only in specific locations, or may not occur at all. Other stimulation methods will need to be used where shear stimulation will not work, and more development of stimulation methods is needed.

5.1.6 Local geology

Local geology was observed to affect stimulation and flow behavior. kISMET drilling (with near-vertical boreholes) showed few fractures [*Oldenburg et al.*, 2017]. Adjacent EGS Collab drilling (with subhorizontal boreholes) identified many fractures, particularly in the lower regions of the testbed. Full waveform seismic data and electrical resistance tomography data showed the geologic complexity was greater than anticipated [*Johnson et al.*, 2019a; *Roggenthen et al.*, 2022]. Analysis of campaign seismic data for E1 revealed that the rock is likely a horizontal transverse isotropic (HTI) medium [*Gao et al.*, 2020]. Variations in stress measurements from a vertical borehole at 1.25 km depth (on the 4100 level) highlight the effects of local geology as well, particularly the presence of a rhyolite body having a significantly lower minimum principal stress than the amphibolite strata above and below it [*Roggenthen et al.*, 2024]. Careful characterization is needed to understand the local geology and its effect on local stress and fluid flow.

The role of natural fractures on stimulation can be estimated a-priori if enough information including stress and fracture orientations can be determined by characterization [*Singh et al.*, 2019]. Good discrete fracture network models graphically summarize this information, making interpretation of stimulation behavior more tractable [*Schwering et al.*, 2020]. Such models require frequent updating to include newly found or inferred fractures.

5.1.7 Thermal breakthrough

We did not conclusively establish thermal breakthrough in either of our flow tests. For our experimental conditions modeling indicated that significant thermal breakthrough (1 ˚C) would require months to years [*Cusini et al.*, 2023; *White et al.*, 2019; *Wu et al.*, 2020a] in spite of the relatively small scale of the experiments. As flow was distributed and dynamic (Figure SI-8, *Mattson et al.* [2023]), it is possible that thermal breakthrough occurred at higher-flow weep locations where temperature could not readily be monitored. Additionally, we encountered Joule-Thomson effects which caused temperature increases as the water depressurized from the fractures to the wells. This effect would mask the breakthrough of chilled water and the lack of consistent flow made confident estimation unlikely. The moderate temperature contrast between the injected fluid and the reservoir rock, along with the relatively low water injection rates, also contributed to this outcome.

5.1.8 Monitoring Stimulation

The particular set concurrent multiple independent measurement technologies working together is unique to the EGS Collab project. Instead of having to take specific observations as circumstantial evidence, the EGS Collab Project produced several lines of evidence that support our observations. The many techniques used simultaneously during stimulation and flow tests allow for technique comparison, and results from one can be used corroborate others. For example, fracture hits indicated by the DTS system were used to corroborate MEQ locations [*Schoenball et al.*, 2020a]. Several methods of quantifying fracture opening and closure were demonstrated. Continuous active source seismic monitoring (CASSM) spatially imaged fracture opening in the monitored region in E1. These data have been compared with both passive seismic and DTS data [*Ajo-Franklin et al.*, 2018; *Chi et al.*, 2020; *Kneafsey et al.*, 2019b]. The SIMFIP tool was used to quantify rock motion across a fracture or fractured zone in a borehole during stimulations, and in a number of stress measurements in a vertical borehole on the 4100-level [*Guglielmi et al.*, 2021b; *Guglielmi et al.*, 2023; *Kneafsey et al.*, 2019b]. These high precision measurements show fracture opening and shear as well, however not to a level where shear became important. The DORSA tool also indicated changes in rock strain at a distance from the injection well. ERT results have been used to interpret geomechanical changes including fracture opening and closure [*Johnson et al.*, 2021], new flow in boreholes, and stress in the rock at locations distant from the borehole (Figure 11) [*Johnson et al.*, 2024]. DAS indicated strain and DTS indicated fracture hits. The combination of DAS and DTS anomalies show that strain was observed prior to temperature spikes indicating fracture hits. This may indicate that fractures can be created hours before significant flow occurs. The spatio-temporal relationship between strain, temperature, ERT anomalies and seismicity are also being visualized to understand observations. All of these quantifications provide key insights into stimulation.

5.1.9 Grout

EGS Collab tests were designed assuming that the grout used to fill boreholes with monitoring equipment would work well. Our needs were complex because we needed the grout to seal, have stiffness similar to the rock, and to have electrical properties allowing the ERT system to function properly. In E1, our grout was designed by researchers very familiar with grouting environmental boreholes, not exposed to high pressure. The grout we used in E1 contracted slightly and may have had too much water in it. This led to small pathways where water could and did flow. Repairing this so the monitoring equipment in a grouted borehole was functional required significant effort. For Testbed 2 we worked with researchers and designers familiar with oil and gas drilling and unique grout applications. This resulted in a custom grout with known properties that was deployed with custom

equipment and required custom wellheads [*Sollohub et al.*, 2022]. This resulted in far fewer problems and improved data and operation.

5.1.10 Modeling

Although not addressed here, modeling was a critical element in the EGS Collab project, used in experiment design, behavior prediction, analysis/interpretation, and model development was required at times. Modeling was also extremely useful in incorporating multiple data sources and providing output to support interpretations from other data sources. The major learnings regarding modeling were to start with well-developed platforms that have been validated to the extent possible. Create models that can be challenged, and use those models to help interpret field observations. Change the models and let them be simplified or made more complex in response to field observations. Use these growing models to determine what data are needed to further challenge the model. To paraphrase D.D. Eisenhower – Models are worthless, but modeling is everything.

5.1.11 System Management

The management of our simple systems was complex. It required exercising a number of models from conceptual to numerical that had to be changed routinely to adapt to new responses from known or unknown stimuli. Successful reservoir management at any scale must be an active process requiring attention to and integration of important data streams. When interpreting multiple data sources of various types, we found that it was valuable to employ a wide-range of data sources (https://gdr.openei.org/egs_collab), data analytics (e.g., inversion models [*Chen et al.*, 2018; *Feng et al.*, 2024; *Li et al.*, 2024; *Lia et al.*, 2023 Submitted; *Linneman et al.*, 2019; *Pan et al.*, 2019; *Pan et al.*, 2020; *Qin et al.*, 2021; *Qin et al.*, 2024], mapping [*Fu et al.*, 2020; *Jafarov et al.*, 2020; *Neupane et al.*, 2019b; *Schwering et al.*, 2020; *Ulrich et al.*, 2022; *Ulrich et al.*, 2018; *Wu et al.*, 2021c], data integration [*Burghardt et al.*, 2020; *Kneafsey et al.*, 2021c; *Schoenball et al.*, 2020b], machine learning methods [*Chai et al.*, 2022; *Chai et al.*, 2020; *Chakravarty et al.*, 2021; *Crowe et al.*, 2019; *Lia et al.*, 2023 Submitted]), visualization methods [*Johnson et al.*, 2021; *Neupane et al.*, 2019b; *Ulrich et al.*, 2022], and broad-spectrum subject matter expertise to best interpret this information. Using this process in an open forum enabled our team to obtain the most comprehensive understanding of what we were observing, the most likely causes of the observations, and potential solutions to remedy the problems that were encountered. It is recognized that long-term involvement of a large group of subject matter experts is infeasible, however access to such input may be important.

Many tools were used to characterize the site and to identify and quantify behaviors resulting in many data streams and types. Both operational and scientific data were collected. The most useful data were those that could be

and were analyzed as soon as possible. Data collected “to be modeled later” were less useful than those that were available ASAP. This drove the development of a centralized, cloud-based data repository accessible to all team members across multiple organizations [*Weers and Huggins*, 2019] and more rapid analysis tools, often requiring edge computing (i.e. some simplification prior to data transfer). An example of this was in locating MEQs [*Schoenball et al.*, 2020b] which were typically plotted within 30 seconds of the events, enabling effective use of this information in near real time for adaptive control of the experiments.

The limited permeability shown by many crystalline rock masses is well-represented by the rocks of the current testbeds. Division of the rock mass into separate reservoirs, often by high-angle fracture systems can result in different fluid pressures between those reservoirs (i.e., reservoir compartmentalization) depending upon the frequency of fracturing. Therefore, extrapolation of results from one of the separate reservoirs to an entire geothermal field should be done with care unless good reasons can be made to assume a sufficient number of fractures or fracture systems exist to allow communication.

Acknowledgments

This material was based upon work supported by the U.S. Department of Energy, Office of Energy Efficiency and Renewable Energy (EERE), Office of Technology Development, Geothermal Technologies Office, under Award Number DE-AC02-05CH11231 with LBNL and other awards to other national laboratories. The United States Government retains, and the publisher, by accepting the article for publication, acknowledges that the United States Government retains a non-exclusive, paid-up, irrevocable, world-wide license to publish or reproduce the published form of this manuscript, or allow others to do so, for United States Government purposes. This paper describes objective technical results and analysis. Any subjective views or opinions that might be expressed in the paper do not necessarily represent the views of the U.S. Department of Energy or the United States Government. Sandia National Laboratories is a multimission laboratory managed and operated by National Technology & Engineering Solutions of Sandia, LLC, a wholly owned subsidiary of Honeywell International Inc., for the U.S. Department of Energy’s National Nuclear Security Administration under contract DE-NA0003525. Portions of this work were performed under the auspices of the U.S. Department of Energy by Lawrence Livermore National Laboratory under Contract DE-AC52-07NA27344, and by the National Renewable Energy Laboratory (NREL), operated by Alliance for Sustainable Energy, LLC, for DOE under Contract No. DE-AC36-08GO28308. Idaho National Laboratory is a multi-program Federally Funded Research and Development Center (FFRDC) established under Federal Acquisition Regulation Part 35 and operated for U.S. Department of Energy by Battelle Energy Alliance, LLC. through the Contract No. DE-AC07-05ID14517.

The research supporting this work took place in whole or in part at the Sanford Underground Research Facility in Lead, South Dakota. The assistance of the Sanford Underground Research Facility and its personnel in providing physical access and general logistical and technical support is gratefully acknowledged. We thank the crew from RESPEC, who logged the core upon recovery from drilling, and also supported the wireline logging operations. We thank Daniel Bour of Danial Bour Consulting and Lance Sollohub of Cudd Energy Services for help in grout design and manufacture. The earth model output for this paper was generated using Leapfrog Software, copyright Seequent Limited. Leapfrog and all other Seequent Limited product or service names are registered trademarks or trademarks of Seequent Limited.

*EGS Collab Team - J. Ajo-Franklin, T. Baumgartner, K. Beckers, D. Blankenship, A. Bonneville, L. Boyd, S. Brown, J.A. Burghardt, C. Chai, A. Chakravarty, T. Chen, Y. Chen, B. Chi, K. Condon, P.J. Cook, D. Crandall, P.F. Dobson, T. Doe, C.A. Doughty, D. Elsworth, J. Feldman, Z. Feng, A. Foris, L.P. Frash, Z. Frone, P. Fu, K. Gao, A. Ghassemi, Y. Guglielmi, B. Haimson, A. Hawkins, J. Heise, C. Hopp, M. Horn, R.N. Horne, J. Horner, M. Hu, H. Huang, L. Huang, K.J. Im, M. Ingraham, E. Jafarov, R.S. Jayne, T.C. Johnson, S.E. Johnson, B. Johnston, S. Karra, K. Kim, D.K. King, T. Kneafsey, H. Knox, J. Knox, D. Kumar, K. Kutun, M. Lee, D. Li, J. Li, K. Li, Z. Li, M. Maceira, P. Mackey, N. Makedonska, C.J. Marone, E. Mattson, M.W. McClure, J. McLennan, T. McLing, C. Medler, R.J. Mellors, E. Metcalfe, J. Miskimins, J. Moore, C.E. Morency, J.P. Morris, T. Myers, S. Nakagawa, G. Neupane, G. Newman, A. Nieto, T. Paronish, R. Pawar, P. Petrov, B. Pietzyk, R. Podgorney, Y. Polsky, J. Pope, S. Porse, J.C. Primo, T. Pyatina, C. Reimers, B.Q. Roberts, M. Robertson, V. Rodríguez-Tribaldos, W. Roggenthen, J. Rutqvist, D. Rynders, M. Schoenball, P. Schwering, V. Sesetty, C.S. Sherman, A. Singh, M.M. Smith, H. Sone, E.L. Sonnenthal, F.A. Soom, D.P. Sprinkle, S. Sprinkle, C.E. Strickland, J. Su, D. Templeton, J.N. Thomle, C. Ulrich, N. Uzunlar, A. Vachaparampil, C.A. Valladao, W. Vandermeer, G. Vandine, D. Vardiman, V.R. Vermeul, J.L. Wagoner, H.F. Wang, J. Weers, N. Welch, J. White, M.D. White, P. Winterfeld, T. Wood, S. Workman, H. Wu, Y.S. Wu, E.C. Yildirim, Y. Zhang, Y.Q. Zhang, Q. Zhou, M.D. Zoback

References

Ajo-Franklin, J. B., M. Schoenball, T. Wood, M. Robertson, P. Petrov, L. Huang, . . . EGS Collab Team (2018), Imaging Hydraulic Fracture Propagation Using Semi-Permanent Continuous Active Seismic Source Monitoring: Results from the DOE EGS Collab Experiment, paper presented at American Geophysical Union Fall Meeting 2018, American Geophysical Union, Washington DC, December 12, 2018.

Amann, F., V. Gischig, K. Evans, J. Doetsch, R. Jalali, B. Valley, . . . D. Giardini (2018), The seismo-hydromechanical behavior during deep geothermal reservoir stimulations: open questions tackled in a decameter-scale in situ stimulation experiment, *Solid Earth*, *9*(1), 23, doi:10.5194/se-9-115-2018.

Ameli, P., J. E. Elkhoury, and R. L. Detwiler (2013), High-resolution fracture aperture mapping using optical profilometry, *Water Resources Research*, *49*(10), 7126-7132, doi:10.1002/wrcr.20501.

Augustine, C. (2016), Update to Enhanced Geothermal System Resource Potential Estimate, *GRC Transactions*, *40*, 6.

Boese, C. M., G. Kwiatek, T. Fischer, K. Plenkers, J. Starke, F. Blumle, . . . G. Dresen (2022), Seismic monitoring of the STIMTEC hydraulic stimulation experiment in anisotropic metamorphic gneiss, *Solid Earth}*, *13*(2), 24, doi:10.5194/se-13-323-2022.

Burghardt, J., T. Doe, M. Ingraham, P. Schwering, C. Ulrich, W. M. Roggenthen, . . . E. C. Team (2020), Integration of Shut-In Pressure Decline, Flow back, Hydraulic and Sleeve Re-Opening Tests to Infer In-Situ Stress, paper presented at 54th U.S. Rock Mechanics/Geomechanics Symposium.

Burghardt, J., H. A. Knox, T. Doe, D. Blankenship, P. C. Schwering, M. Ingraham, . . . W. Roggenthen (2022), EGS Stimulation Design with Uncertainty Quantification at the EGS Collab Site, paper presented at 56th U.S. Rock Mechanics/Geomechanics Symposium.

Caddey, S. W., R. L. Bachman, T. J. Campbell, R. R. Reid, and R. P. Otto (1991), The Homestake gold mine, an early Proterozoic iron-formation-hosted gold deposit, Lawrence County, South Dakota, *1857J*.

Chai, C., M. Maceira, and EGS Collab Team (2022), Machine Learning Enhanced Seismic Monitoring at 100 km and 10 m Scales, paper presented at 47th Workshop on Geothermal Reservoir Engineering, Stanford University, Stanford, CA, February 7-9, 2022.

Chai, C., M. Maceira, H. J. Santos-Villalobos, S. V. Venkatakrishnan, M. Schoenball, W. Zhu, . . . EGS Collab Team (2020), Using a Deep Neural Network and Transfer Learning to Bridge Scales for Seismic Phase Picking, *Geophysical Research Letters*, *47*(16), e2020GL088651, doi:10.1029/2020GL088651.

Chakravarty, A., C. Hopp, V. Rodriguez-Tribaldos, S. Misra, and T. Kneafsey (2021), Self-supervised Machine Learning from Hydraulic Fracturing Induced Seismicity Signatures: Case Study of the EGS Collab Experiment 1, paper presented at AGU Fall Meeting 2021, New Orleans, LA, 13-17 December 2021.

Chakravarty, A., and S. Misra (2022), Unsupervised learning from three-component accelerometer data to monitor the spatiotemporal evolution of meso-scale hydraulic fractures, *International Journal of Rock Mechanics and Mining Sciences*, *151*, 105046, doi:https://doi.org/10.1016/j.ijrmms.2022.105046.

Chen, Y., L. Huang, and EGS Collab Team (2018), Microearthquake Hypocenter-Location and Focal-Mechanism Inversions for the EGS Collab Project: A Synthetic Study, paper presented at 43rd Workshop on Geothermal Reservoir Engineering, Stanford University, Stanford, CA, February 12-14, 2018.

Chen, Y., L. Huang, and EGS Collab Team (2019a), Optimal design of 3D borehole seismic arrays for microearthquake monitoring in anisotropic media during stimulations in the EGS collab project, *Geothermics*, *79*, 61-66, doi:https://doi.org/10.1016/j.geothermics.2019.01.009.

Chen, Y., L. Huang, M. Schoenball, J. Ajo-Franklin, T. Kneafsey, and EGS Collab Team (2019b), Real-Time Microearthquake Event Detection and Location in Anisotropic Media Using a Multiscale Scanning Approach for EGS Collab Experiments, paper presented at 44th Workshop on Geothermal Reservoir Engineering, Stanford University, Stanford, California, February 11-13, 2019.

Chi, B., L. Huang, K. Gao, J. Ajo-Franklin, T. J. Kneafsey, J. Hampton, and EGS Collab Team (2020), Anisotropic Imaging of Created Fractures in EGS Collab Experiments Using CASSM Data, paper presented at 45th Workshop on Geothermal Reservoir Engineering, Stanford University, Stanford, California, February 10-12, 2020.

Condon, K. J., H. Sone, H. F. Wang, J. Ajo-Franklin, T. Baumgartner, K. Beckers, . . . EGS Collab Team (2020), Low Static Shear Modulus Along Foliation and Its Influence on the Elastic and Strength Anisotropy of Poorman Schist Rocks, Homestake Mine, South Dakota, *Rock Mechanics and Rock Engineering*, doi:10.1007/s00603-020-02182-4.

Condon, K. J., H. Sone, H. F. Wang, and EGS Collab Team (2019), Anisotropic Strength and Elastic Properties of Poorman Schist at the EGS Collab Experiment 1 Site, paper presented at 53rd US Rock Mechanics/Geomechanics Symposium, American Rock Mechanics Association, New York, NY, USA, 23–26 June 2019.

Crowe, D., M. Schoenball, and Z. Hao (2019), Support Vector Machine for Near Real-time Identification of Microseismic Events, Lawrence Berkeley Laboratory EGS Collab Project.

Cusini, M., F. Fei, and J. P. Morris (2023), Simulation of Chilled-water Injection at EGS Collab Testbed 2 using the GEOS simulation framework, *LLNL-TR-856009*, Lawrence Livermore National Laboratory.

Daley, T., B. Freifeld, J. Ajo-Franklin, S. Dou, R. Pevzner, V. Shulakova, . . . S. Lueth (2013), Field testing of fiber-optic distributed acoustic sensing (DAS) for subsurface seismic monitoring, *The Leading Edge*, *32*(6), 699-706, doi:10.1190/tle32060699.1.

Daley, T., R. Solbau, J. Ajo-Franklin, and S. Benson (2007), Continuous active-source seismic monitoring of C O2 injection in a brine aquifer, *GEOPHYSICS*, *72*(5), A57-A61, doi:10.1190/1.2754716.

Dobson, P., T. Kneafsey, J. Morris, A. Singh, M. Zoback, W. Roggenthen, . . . EGS Collab Team (2018), The EGS Collab Hydroshear Experiment at the Sanford Underground Research Facility – Siting Criteria and Evaluation of Candidate Sites, paper presented at Geothermal Resources Council 2018 Annual Meeting, Geothermal Resources Council Transactions, Reno, NV.

Doe, T., A. Riahi, P. Fu, B. Damjanac, E. Sonnenthal, A. Finnila, . . . D. Blankenship (2022), Performance evaluation of engineered geothermal systems using discrete fracture network simulations, paper presented at 47th Workshop on Geothermal Reservoir Engineering, Stanford University, Stanford, California, February 7-9, 2022.

Dutler, N., B. t. Valley, V. Gischig, L. Villiger, H. Krietsch, J. Doetsch, . . . F. Amann (2019), Hydraulic fracture propagation in a heterogeneous stress field in a crystalline rock mass, *Solid Earth*, *10*(6), 1877-1904, doi:10.5194/se-10-1877-2019.

Elkhoury, J. E., P. Ameli, and R. L. Detwiler (2013), Dissolution and deformation in fractured carbonates caused by flow of CO2-rich brine under reservoir conditions, *International Journal of Greenhouse Gas Control*, *16, Supplement 1*(0), S203-S215, doi:http://dx.doi.org/10.1016/j.ijggc.2013.02.023.
Elliott, S. J., and J. F. W. Gale (2018), Analysis and Distribution of Proppant Recovered From Fracture Faces in the HFTS Slant Core Drilled Through a Stimulated Reservoir, paper presented at SPE/AAPG/SEG Unconventional Resources Technology Conference, Unconventional Resources Technology Conference, Houston, Texas, USA, 2018/8/9/.
Evans, K. F., A. Genter, and J. Sausse (2005), Permeability creation and damage due to massive fluid injections into granite at 3.5 km at Soultz: 1. Borehole observations, *Journal of Geophysical Research: Solid Earth*, *110*(B4), doi:https://doi.org/10.1029/2004JB003168.
Feng, Z., L. Huang, B. Chi, K. Gao, J. Li, J. Ajo-Franklin, . . . EGS Collab Team (2024), Monitoring spatiotemporal evolution of fractures during hydraulic stimulations at the first EGS collab testbed using anisotropic elastic-waveform inversion, *Geothermics*, *122*, 103076, doi:https://doi.org/10.1016/j.geothermics.2024.103076.
Frash, L. P. (2022), Optimized Enhanced Geothermal Development Strategies with GeoDT and Fracture Caging, paper presented at 47th Workshop on Geothermal Reservoir Engineering, Stanford University, Stanford, California, February 7-9, 2022.
Frash, L. P., K. Arora, Y. Gan, M. Lu, M. Gutierrez, P. Fu, . . . EGS Collab Team (2018a), Laboratory Validation of Fracture Caging for Hydraulic Fracture Control, paper presented at 52nd U.S. Rock Mechanics/Geomechanics Symposium, American Rock Mechanics Association, Seattle, Washington, 2018/8/21.
Frash, L. P., J. W. Carey, N. J. Welch, and EGS Collab Team (2019a), EGS Collab Experiment 1: Geomechanical and Hydrological Properties by Triaxial Direct Shear, paper presented at 44th Workshop on Geothermal Reservoir Engineering, Stanford University, Stanford, California, February 11-13, 2019.
Frash, L. P., P. Fu, J. Morris, and EGS Collab Team (2018b), Fracture Caging: Can We Control the Extent of a Hydraulic Fracture Stimulated Zone?, paper presented at 43rd Workshop on Geothermal Reservoir Engineering, Stanford University, SGP-TR-213.
Frash, L. P., P. Fu, J. Morris, M. Gutierrez, G. Neupane, J. Hampton, . . . T. Kneafsey (2021a), Fracture Caging to Limit Induced Seismicity, *Geophysical Research Letters*, *48*(1), e2020GL090648, doi:https://doi.org/10.1029/2020GL090648.
Frash, L. P., J. C. Hampton, M. S. Gutierrez, and EGS Collab Team (2020), Fracture Caging to Control Induced Seismicity with Inspiration from the EGS Collab Project, paper presented at 45th Workshop on Geothermal Reservoir Engineering, Stanford University, Stanford, California, February 10-12, 2020.
Frash, L. P., W. Li, M. Meng, J. W. Carey, and M. Sweeney (2022), Enhanced Geothermal System Design Using GeoDT and Fracture Caging — EGS Collab Stimulation Prediction Study, paper presented at 56th U.S. Rock Mechanics/Geomechanics Symposium.
Frash, L. P., J. P. Morris, and EGS Collab Team (2019b), Stochastic prediction of multi-well fracture connectivity and application to EGS Collab experiment 2, paper presented at 53rd US Rock Mechanics/Geomechanics Symposium, American Rock Mechanics Association, New York, NY, USA, 23–26 June 2019.
Frash, L. P., N. J. Welch, J. W. Carey, and EGS Collab Team (2019c), Geomechanical evaluation of natural shear fractures in the EGS Collab Experiment 1 test bed, paper presented at 53rd US Rock Mechanics/Geomechanics Symposium, American Rock Mechanics Association, New York, NY, USA.
Frash, L. P., N. J. Welch, M. Meng, W. Li, and J. W. Carey (2021b), A Scaling Relationship for Fracture Permeability After Slip, paper presented at 55th U.S. Rock Mechanics/Geomechanics Symposium.
Fu, P., J. Morris, H. Wu, and X. Yang (2018a), Imaging hydraulic fracture extents and aperture using electrical resistivity tomography, paper presented at Proceedings, 43rd Workshop on Geothermal Reservoir Engineering, Stanford University, Stanford, CA, Feb 12-14, 2018.
Fu, P., M. Schoenball, J. B. Ajo-Franklin, C. Chai, M. Maceira, J. P. Morris, . . . EGS Collab Team (2021a), Close Observation of Hydraulic Fracturing at EGS Collab Experiment 1: Fracture Trajectory, Microseismic Interpretations, and the Role of Natural Fractures, *Journal of Geophysical Research: Solid Earth*, *126*(7), e2020JB020840, doi:https://doi.org/10.1029/2020JB020840.
Fu, P., M. Schoenball, J. Morris, J. Ajo-Franklin, H. Knox, T. Kneafsey, . . . EGS Collab Team (2019), Microseismic Signatures of Hydraulic Fracturing: A Preliminary Interpretation of Intermediate-Scale Data from the EGS Collab Experiment, paper presented at 44th Workshop on Geothermal Reservoir Engineering, Stanford University, Stanford, California, February 11-13, 2019.
Fu, P., M. White, J. Morris, T. Kneafsey, and EGS Collab Team (2018b), Predicting Hydraulic Fracture Trajectory Under the Influence of a Mine Drift in EGS Collab Experiment I, paper presented at 43rd Workshop on Geothermal Reservoir Engineering, Stanford University, Stanford, California, February 12-14, 2018.
Fu, P., H. Wu, X. Ju, and J. Morris (2020), Analyzing Fracture Flow Channel Area in EGS Collab Experiment 1 Testbed, paper presented at 45th Workshop on Geothermal Reservoir Engineering, Stanford University, Stanford, California, February 10-12, 2020.
Fu, P., H. Wu, J. P. Morris, P. C. Schwering, C. Ulrich, J. A. Burghardt, . . . EGS Collab Team (2021b), Simulating Hydraulic Fracture Stimulations at the EGS Collab: Model Validation from Experiments 1 and Design-Phase Simulation for Experiment 2, paper presented at 46th Workshop on Geothermal Reservoir Engineering, Stanford University, Stranford, CA, February 15-17, 2021.

Gale, J. F. W., S. J. Elliott, and S. E. Laubach (2018), Hydraulic Fractures in Core From Stimulated Reservoirs: Core Fracture Description of HFTS Slant Core, Midland Basin, West Texas, paper presented at Proceedings of the 6th Unconventional Resources Technology Conference.
Gale, J. F. W., S. J. Elliott, B. G. Rysak, C. L. Ginn, N. Zhang, R. D. Myers, and S. E. Laubach (2021), Fracture Description of the HFTS-2 Slant Core, Delaware Basin, West Texas, paper presented at SPE/AAPG/SEG Unconventional Resources Technology Conference.
Gao, K., L. Huang, B. Chi, J. Ajo-Franklin, J. Hampton, and EGS Collab Team (2018), Imaging the Fracture Zone Using Continuous Active Source Seismic Monitoring for the EGS Collab Project: A Synthetic Study, paper presented at 43rd Workshop on Geothermal Reservoir Engineering, Stanford University, Stanford, California, February 12-14, 2018.
Gao, K., L. Huang, H. A. Knox, P. C. Schwering, C. R. Hoots, J. Ajo-Franklin, . . . EGS Collab Team (2020), Anisotropic Elastic Properties of the First EGS Collab Testbed Revealed from the Campaign Cross-Borehole Seismic Data, paper presented at 45th Workshop on Geothermal Reservoir Engineering, Stanford University, Stanford, California, February 10-12, 2020.
Gischig, V. S., D. Giardini, F. Amann, M. Hertrich, H. Krietsch, S. Loew, . . . B. Valley (2020), Hydraulic stimulation and fluid circulation experiments in underground laboratories: Stepping up the scale towards engineered geothermal systems, *Geomechanics for Energy and the Environment*, *24*, 100175, doi:https://doi.org/10.1016/j.gete.2019.100175.
Grant, M. A. (2016), Physical performance indicators for HDR/EGS projects, *Geothermics*, *63*(2-4).
Guglielmi, Y., F. Cappa, J.-P. Avouac, P. Henry, and D. Elsworth (2015), Seismicity triggered by fluid injection–induced aseismic slip, *Science*, *348*(6240), 1224.
Guglielmi, Y., F. Cappa, H. Lançon, J. B. Janowczyk, J. Rutqvist, C. F. Tsang, and J. S. Y. Wang (2013), ISRM Suggested Method for Step-Rate Injection Method for Fracture In-Situ Properties (SIMFIP): Using a 3-Components Borehole Deformation Sensor, in *The ISRM Suggested Methods for Rock Characterization, Testing and Monitoring: 2007–2014*, edited by R. Ulusay, Springer-Verlag, Wein, doi:DOI: 10.1007/978-3-319-07713-0.
Guglielmi, Y., P. Cook, F. Soom, P. Dobson, T. Kneafsey, B. Valley, . . . F. Basirat (2021a), Estimating Stress from Three-Dimensional Borehole Displacements Induced by Fluid Injection in Different Types of Fractured or Faulted Rocks, paper presented at 55th US Rock Mechanics/Geomechanics Symposium, Houston, Texas, USA, 20-23 June 2021.
Guglielmi, Y., P. Cook, F. Soom, M. Schoenball, P. Dobson, and T. Kneafsey (2021b), In Situ Continuous Monitoring of Borehole Displacements Induced by Stimulated Hydrofracture Growth, *Geophysical Research Letters*, *48*, e2020GL090782, doi:https://doi.org/10.1029/2020GL090782.
Guglielmi, Y., M. McClure, J. Burghardt, J. P. Morris, T. Doe, P. Fu, . . . EGS Collab Team (2023), Using in-situ strain measurements to evaluate the accuracy of stress estimation procedures from fracture injection/shut-in tests, *International Journal of Rock Mechanics and Mining Sciences*, *170*, 105521, doi:https://doi.org/10.1016/j.ijrmms.2023.105521.
Heise, J. (2015), The Sanford Underground Research Facility at Homestake, *Journal of Physics: Conference Series*, *606*(1), 26.
Hertrich, M., and B. L. team (2021), The Bedretto Underground Laboratory for Geoenergies (BULG) -- a multidisciplinary test-bed, edited, p. 2, American Rock Mechanics Association.
Hopp, C. (2023a), EGS Collab Experiment 2 Distributed temperature (DTS) system, *LBNL-2001515*, Lawrence Berkeley National Laboratory, Berkeley, CA, USA.
Hopp, C. (2023b), EGS Collab Experiment 2: Passive seismic monitoring system, *LBNL-2001514*, Lawrence Berkeley National Laboratory, Berkeley CA, USA.
Huang, H., G. H. Neupane, R. Podgorney, E. Mattson, and EGS Collab Team (2019), Mechanistically Modeling of Hydraulic Fracture Propagation and Interaction with Natural Fractures at EGS-Collab Site, paper presented at 44th Workshop on Geothermal Reservoir Engineering, Stanford University, Stanford, California, February 11-13, 2019.
Huang, H., J. Zhou, E. Mattson, and R. Podgorney (2018), Mechanistically Modeling of Hydraulic Fracture Opening, Closure and Residual Fracture Permeability During Cyclic Flow Injection Tests, paper presented at Geothermal Resources Council 2018 Annual Meeting Geothermal Resources Council Transactions, Reno, NV.
Huang, L., Y. Chen, K. Gao, P. Fu, J. Morris, J. Ajo-Franklin, . . . EGS Collab Team (2017), Numerical Modeling of Seismic and Displacement-Based Monitoring for the EGS Collab Project, paper presented at GRC Transactions, Vol. 41, 2017.
Ingraham, M. D., P. C. Schwering, J. Burghardt, C. Ulrich, T. Doe, W. M. Roggenthen, and C. Reimers (2020), Analysis of Hydraulic Fracturing on the 4100 Level at the Sanford Underground Research Facility, paper presented at 54th U.S. Rock Mechanics/Geomechanics Symposium, American Rock Mechanics Association, 2020/9/18.
Jafarov, E. E., N. Makedonska, S. Karra, R. Pawar, J. Beisman, G. Neupane, . . . EGS Collab Team (2020), Simulations of the 3D Geothermal Heat Flow in Fractured Media, paper presented at 45th Workshop on Geothermal Reservoir Engineering, Stanford University, Stanford, California, February 10-12, 2020.
Jahnke, B., C. Ruplinger, C. E. Bate, M. Trzeciak, H. Sone, and H. F. Wang (2022), Fracture toughness of schist, amphibolite, and rhyolite from the Sanford Underground Research Facility (SURF), Lead, South Dakota, *Scientific Reports*, *12*(1), 15941, doi:10.1038/s41598-022-20031-y.
Jeffrey, R. G., A. P. Bunger, B. Lecampion, X. Zhang, Z. R. Chen, A. van As, . . . M. Mainguy (2009), Measuring Hydraulic Fracture Growth in Naturally Fractured Rock, paper presented at SPE Annual Technical Conference and Exhibition.
Johnson, T., C. Strickland, J. Burghardt, H. Knox, C. Hopp, V. Rodriguez-Tribaldos, . . . T. Pyatina (2022), 3D Electrical Resistivity Characterization and Monitoring at the EGS-Collab Testbed #1: Results and Lessons Learned Applied to Testbed #2, paper presented at 56th U.S. Rock Mechanics/Geomechanics Symposium, Santa Fe, New Mexico, USA, June 26–29, 2022.

Johnson, T., C. Strickland, H. Knox, J. Thomle, V. Vermuel, C. Ulrich, . . . EGS Collab Team (2019a), EGS Collab Project Electrical Resistivity Tomography Characterization and Monitoring Status, paper presented at 44th Workshop on Geothermal Reservoir Engineering, Stanford University, Stanford, California, February 11-13, 2019.
Johnson, T. C., J. Burghardt, C. Strickland, H. Knox, V. Vermeul, M. White, . . . EGS Collab Team (2021), 4D Proxy Imaging of Fracture Dilation and Stress Shadowing Using Electrical Resistivity Tomography During High Pressure Injections Into a Dense Rock Formation, *Journal of Geophysical Research: Solid Earth*, *126*(11), e2021JB022298, doi:https://doi.org/10.1029/2021JB022298.
Johnson, T. C., J. Burghardt, C. Strickland, D. Sirota, V. Vermeul, H. Knox, . . . EGS Collab Team (2024), 4D Electrical Resistivity Imaging of Stress Perturbations Induced During High-Pressure Shear Stimulation Tests, *Geophysical Research Letters*, *51*(10), e2024GL108423, doi:https://doi.org/10.1029/2024GL108423.
Johnson, T. C., C. E. Strickland, H. A. Knox, J. A. Burghardt, V. R. Vermeul, P. Schwering, . . . T. J. Kneafsey (2019b), Geomechanically-Induced Electrical Resistance Responses During High-Pressure Flow Tests in a Stimulated Fracture Zone, paper presented at AGU Fall Meeting 2019, AGU.
Kaiser, P. K., B. t. Valley, M. B. Dusseault, and D. Duff (2013), Hydraulic Fracturing Mine Back Trials — Design Rationale and Project Status, in *Effective and Sustainable Hydraulic Fracturing*, edited by A. P. Bunger, J. McLennan and R. Jeffrey, p. Ch. 44, IntechOpen, Rijeka, doi:10.5772/56260.
Kamali, A., and A. Ghassemi (2018), 3D Analysis of the Proposed "EGS Collab" Circulation Experiments in Sanford Underground Research Facility, SD, paper presented at 52nd US Rock Mechanics/Geomechanics Symposium, American Rock Mechanics Association.
Kneafsey, T., D. Blankenship, J. Burghardt, T. Johnson, P. Dobson, P. C. Schwering, . . . T. E. C. Team (2023), The EGS Collab – Discoveries and Lessons from an Underground Experiment Series, paper presented at 48th Workshop on Geothermal Reservoir Engineering, Stanford University, Stanford, California, February 6-8, 2023.
Kneafsey, T., D. Blankenship, J. Burghardt, T. Johnson, P. Dobson, P. C. Schwering, . . . EGS Collab Team (2022a), The EGS Collab –Experiment 2 Stimulations at 1.25 km Depth, paper presented at Geothermal Rising Conference, Geothermal Rising, Reno, NV, August 28-31, 2022.
Kneafsey, T., D. Blankenship, P. Dobson, J. Burghardt, M. White, J. P. Morris, . . . EGS Collab Team (2022b), The EGS Collab – Initial Results from Experiment 2: Shear Stimulation at 1.25 km depth, paper presented at 47th Workshop on Geothermal Reservoir Engineering, Stanford University, Stanford, California, February 7-9, 2022.
Kneafsey, T., D. Blankenship, P. Dobson, and EGS Collab Team (2019a), EGS Collab SIGMA-V Project: Stimulation Investigations for Geothermal Modeling Analysis and Validation Phase 1 Report. For the period February 2017 – March 2019, 2068 pp, Lawrence Berkeley National Laboratory, Berkeley, CA, USA.
Kneafsey, T., D. Blankenship, P. Dobson, M. White, J. P. Morris, P. Fu, . . . EGS Collab Team (2021a), The EGS Collab Project: Status and Accomplishments, paper presented at 2021 Geothermal Rising Conference, GRC Transactions, Vol. 45, 2021.
Kneafsey, T., D. Blankenship, P. Dobson, M. White, J. P. Morris, P. Fu, . . . EGS Collab Team (2021b), Fracture Stimulation and Chilled-water Circulation Through Deep Crystalline Rock: Characterization, Modeling, Monitoring, and Heat-transfer Assessment, paper presented at 46th Workshop on Geothermal Reservoir Engineering, Stanford University, Stanford, California, February 15-17, 2021.
Kneafsey, T., T. Johnson, J. Burghardt, P. Schwering, L. Frash, W. Roggenthen, . . . EGS Collab Team (2024), The EGS Collab Project – Summaries of Experiments 2 and 3: Experiments at 1.25 km depth at the Sanford Underground Research Facility, *LBNL-2001567, OSTI ID:2280825*, Lawrence Berkeley National Laboratory, Berkeley, CA, USA.
Kneafsey, T., G. Neupane, D. Blankenship, P. Dobson, M. White, J. Morris, . . . EGS Collab Team (2021c), Scientific Findings to Engineering Realities: Coordination across Collab teams and making the connection to FORGE, *LBNL-2001564*, 67 pp, Lawrence Berkeley National Laboratory, Berkeley, CA.
Kneafsey, T. J., D. Blankenship, P. Dobson, M. White, J. P. Morris, P. Fu, . . . EGS Collab Team (2021d), Fracture Stimulation and Chilled-water Circulation Though Deep Crystalline Rock: Characterization, Modeling, Monitoring, and Heat-transfer Assessment, paper presented at 46th Workshop on Geothermal Reservoir Engineering, Stanford University, Stanford, California, Stanford University, Stanford, California, February 15-17, 2021.
Kneafsey, T. J., D. Blankenship, P. F. Dobson, J. P. Morris, M. D. White, P. Fu, . . . EGS Collab Team (2020), The EGS Collab Project: Learnings from Experiment 1, paper presented at 45th Workshop on Geothermal Reservoir Engineering, Stanford University, Stanford, California, February 10-12, 2020.
Kneafsey, T. J., P. F. Dobson, D. Blankenship, P. C. Schwering, J. P. Morris, P. Fu, . . . EGS Collab Team (2021e), Field Experiments and Model Validation: The EGS Collab Project, paper presented at 55th US Rock Mechanics/Geomechanics Symposium, Houston, Texas, USA, 20-23 June 2021.
Kneafsey, T. J., P. F. Dobson, C. Ulrich, C. Hopp, V. Rodríguez-Tribaldos, Y. Guglielmi, . . . EGS Collab Team (2022c), The EGS Collab Project – Stimulations at Two Depths, paper presented at 56th U.S. Rock Mechanics/Geomechanics Symposium.
Kneafsey, T. J., D. P.F., J. B. Ajo-Franklin, Y. Guglielmi, C. A. Valladao, D. A. Blankenship, . . . EGS Collab Team (2019b), EGS Collab Project: Status, Tests, and Data, paper presented at 53rd US Rock Mechanics/Geomechanics Symposium, New York, NY, USA, 23–26 June 2019.
Kutun, K. (2018), Hydraulic Fracture Modeling of an Enhanced Geothermal System (EGS) Experiment, Colorado School of Mines.

Kutun, K., J. L. Miskimins, and K. F. Beckers (2018), Hydraulic Fracture Modeling in Support of EGS Collab Treatment Designs, paper presented at 52nd U.S. Rock Mechanics/Geomechanics Symposium, American Rock Mechanics Association, Seattle, Washington, 2018/8/21.
Lemmon, E. W., I. H. Bell, M. L. Huber, and M. O. McLinden Thermophysical Properties of Fluid Systems, in *NIST Chemistry WebBook, NIST Standard Reference Database Number 69*, edited by P. J. Linstrom and W. G. Mallard, National Institute of Standards and Technology, Gaithersburg MD, 20899.
Li, D., L. Huang, Y. Zheng, Y. Li, M. Schoenball, V. Rodríguez-Tribaldos, . . . EGS Collab Team (2024), Detecting Fractures and Monitoring Hydraulic Fracturing Processes at the first EGS Collab Testbed Using Borehole DAS Ambient Noise, *Geothermics*, *89*(2).
Li, J., L. Huang, Y. Chen, J. Morris, J. Ajo-Franklin, T. Kneafsey, and E. C. Team (2021), Numerical Modeling of Microseismic Monitoring at the Second EGS Collab Testbed, paper presented at 46th Workshop on Geothermal Reservoir Engineering, Stanford University, Stanford, California, February 15-17, 2021.
Lia, J., Y. Qin, L. Huang, P. Fu, M. Schoenball, J. Ajo-Franklin, . . . EGS Collab Team (2023 Submitted), Focal Mechanism Inversion of High-Frequency Microseismic Events Recorded in Multiple Boreholes at the First EGS Collab Testbed, *Geothermics*.
Linneman, D., P. Sprinkle, H. A. Knox, C. E. Strickland, T. C. Johnson, M. D. Ingraham, . . . M. C. Grubelich (2019), Baseline Characterization for Change Detection with Joint Inversion of ERT and Campaign Seismic Data, paper presented at AGU Fall Meeting 2019, AGU.
Lu, J., and A. Ghassemi (2019), Coupled THMS Modeling of Fractured Reservoir Stimulation with Application to EGS Collab, paper presented at 44rd Workshop on Geothermal Reservoir Engineering, Stanford University, Stanford, California, February 11-13, 2019.
Mattson, E., G. Neupane, A. Hawkins, J. Burghardt, M. Ingraham, M. Plummer, and EGS Collab Team (2019a), Fracture Tracer Injection Response to Pressure Perturbations at an Injection Well, paper presented at GRC Transactions.
Mattson, E., M. Plummer, G. Neupane, V. Vermeul, D. Sirota, M. Ingraham, . . . EGS Collab Team (2023), Fluorescein Tracer Testing on the 4100L – A Preliminary Examination of Initial Arrival in Wells and the Drift at the Second EGS Collab Testbed, paper presented at 48th Workshop on Geothermal Reservoir Engineering, Stanford University, Stanford, California, February 6-8, 2023.
Mattson, E., Y. Zhang, A. Hawkins, T. Johnson, J. Ajo-Franklin, G. Neupane, and EGS Collab Team (2019b), Preliminary Collab Fracture Characterization Results from Flow and Tracer Testing Efforts paper presented at 44th Workshop on Geothermal Reservoir Engineering, Stanford University, Stanford, California, February 11-13, 2019.
Mattson, E. D., G. Neupane, M. D. White, M. D. Ingraham, and EGS Collab Team (2021), EGS-Collab Experiment 1 Flow and Tracer Tests at the Stanford Underground Research Facility, paper presented at 55th US Rock Mechanics/Geomechanics Symposium, Houston, Texas, USA, 20-23 June 2021.
McLennan, J., K. England, P. Rose, J. Moore, and B. Barker (2023), Stimulation of a High-Temperature Granitic Reservoir at the Utah FORGE Site, paper presented at SPE Hydraulic Fracturing Technology Conference and Exhibition.
Meng, M., L. P. Frash, W. Li, N. J. Welch, and J. W. Carey (2021), Measurement of Geomechanical and Hydrological Properties of EGS-Collab Geothermal Rocks, paper presented at 55th US Rock Mechanics/Geomechanics Symposium, Houston, Texas, USA, 20-23 June 2021.
Meng, M., L. P. Frash, W. Li, N. J. Welch, J. W. Carey, J. Morris, . . . T. Kneafsey (2022), Hydro-Mechanical Measurements of Sheared Crystalline Rock Fractures With Applications for EGS Collab Experiments 1 and 2, *Journal of Geophysical Research: Solid Earth*, *127*(2), e2021JB023000, doi:https://doi.org/10.1029/2021JB023000.
Moore, J., J. McLennan, R. Allis, K. Pankow, S. Simmons, R. Podgorney, . . . W. Rickard (2019), The Utah Frontier Observatory for Research in Geothermal Energy (FORGE): An International Laboratory for Enhanced Geothermal System Technology Development, paper presented at 44th Workshop on Geothermal Reservoir Engineering, Stanford University, Stanford, California, February 11-13, 2019.
Morris, J. P., P. Dobson, H. Knox, J. Ajo-Franklin, M. D. White, P. Fu, . . . EGS Collab Team (2018a), Experimental Design for Hydrofracturing and Fluid Flow at the DOE Collab Testbed, paper presented at 43rd Workshop on Geothermal Reservoir Engineering, Stanford University, Stanford, California, February 12-14, 2018.
Morris, J. P., P. Fu, P. Dobson, J. Ajo-Franklin, T. J. Kneafsey, H. Knox, . . . EGS Collab Team (2018b), Experimental Design for Hydrofracturing and Fluid Flow at the DOE EGS Collab Testbed, paper presented at 52nd US Rock Mechanics / Geomechanics Symposium, Seattle, Washington, USA, 17–20 June 2018.
Neupane, G., E. Mattson, A. Hawkins, and M. Smith (2019a), EGS Collab Testbed 1: Second Set Tracer Test Results, edited, USDOE Geothermal Data Repository (United States), doi:10.15121/1593283.
Neupane, G., E. D. Mattson, M. A. Plummer, and EGS Collab Team (2020), Results of Multiple Tracer Injections into Fractures in the EGS Collab Testbed-1, paper presented at 45th Workshop on Geothermal Reservoir Engineering, Stanford University, Stanford, California, February 10-12, 2020.
Neupane, G., R. K. Podgorney, H. Huang, E. D. Mattson, T. J. Kneafsey, P. F. Dobson, . . . EGS Collab Team (2019b), EGS Collab Earth Modeling: Integrated 3D Model of the Testbed, paper presented at GRC Transactions, Geothermal Resources Council, Palm Springs, CA.

Oldenburg, C. M., P. F. Dobson, Y. Wu, P. J. Cook, T. J. Kneafsey, S. Nakagawa, . . . J. Heise (2017), Hydraulic fracturing experiments at 1500 m depth in a deep mine: Highlights from the kISMET project, paper presented at 42nd Workshop on Geothermal Reservoir Engineering, Stanford University.
Osburn, M. R., D. E. LaRowe, L. M. Momper, and J. P. Amend (2014), Chemolithotrophy in the continental deep subsurface: Sanford Underground Research Facility (SURF), USA, *Frontiers in Microbiology*, *5*, 610, doi:10.3389/fmicb.2014.00610.
Pan, W., L. Huang, K. Gao, J. Ajo-Franklin, T. J. Kneafsey, and EGS Collab Team (2019), Anisotropic Full-Waveform Inversion and Least-Squares Reverse-Time Migration of CASSM Data for Experiment I of the EGS Collab Project paper presented at 44th Workshop on Geothermal Reservoir Engineering, Stanford University, Stanford, California, February 11-13, 2019.
Pan, W., L. Huang, K. Gao, J. Ajo-Franklin, T. J. Kneafsey, and EGS Collab Team (2020), Anisotropic Elastic-Waveform Inversion and Least-Squares Reverse-Time Migration of CASSM Data for Experiment I of the EGS Collab Project, paper presented at 45th Workshop on Geothermal Reservoir Engineering, Stanford University, Stanford, California, February 11-13, 2019.
Paronish, T. J., P. E. Mackey, R. Schmitt, D. Crandall, J. E. Moore, S. R. Brown, . . . T. J. Kneafsey (2022), Computed Tomography Scanning and Geophysical Measurements of the Enhanced Geothermal Systems (EGS) Collab SURF Core, United States.
Polak, A., D. Elsworth, J. Liu, and A. S. Grader (2004), Spontaneous switching of permeability changes in a limestone fracture with net dissolution, *Water Resour. Res.*, *40*(3), W03502, doi:10.1029/2003wr002717.
Polak, A., D. Elsworth, H. Yasuhara, A. S. Grader, and P. M. Halleck (2003), Permeability reduction of a natural fracture under net dissolution by hydrothermal fluids, *Geophys. Res. Lett.*, *30*(20), 2020, doi:10.1029/2003gl017575.
Qin, Y., J. Li, L. Huang, Z. Feng, K. Gao, D. Li, . . . D. Blankenship (2021), Moment Tensor Inversion of Microearthquakes in Anisotropic Rocks of the EGS Collab Experiment 1 Testbed, paper presented at AGU Fall Meeting 2021, New Orleans, LA, 13-17 December 2021.
Qin, Y., J. Li, L. Huang, M. Schoenball, J. Ajo-Franklin, D. Blankenship, and T. J. Kneafsey (2024), Source mechanism of kHz microseismic events recorded in multiple boreholes at the first EGS Collab testbed, *Geothermics*, *120*, 102994, doi:https://doi.org/10.1016/j.geothermics.2024.102994.
Raterman, K. T., H. E. Farrell, O. S. Mora, A. L. Janssen, G. A. Gomez, S. Busetti, . . . M. Warren (2018), Sampling a Stimulated Rock Volume: An Eagle Ford Example, *SPE Reservoir Evaluation & Engineering*, *21*(04), 927-941, doi:10.2118/191375-PA.
Reinhard, J. (2013), EGS — Goodbye or Back to the Future 95, in *Effective and Sustainable Hydraulic Fracturing*, edited by P. B. Andrew, M. John and J. Rob, p. Ch. 5, IntechOpen, Rijeka, doi:10.5772/56458.
Renner, J., B. Adero, F. Becker, F. Blümle, C. M. Boese, Y. Cheng, . . . T. Wonik (2021), STIMTEC – A mine-scale hydraulic stimulation experiment of anisotropic metamorphic rock with evaluation by mine-back drilling, edited, p. 3, American Rock Mechanics Association.
Rodríguez Tribaldos, V., C. Hopp, A. Pio Rinaldi, K. Tuinstra, F. Lanza, J. Ajo-Franklin, . . . A. Zappone (2024 (in press)), Use of DAS and DSS Technologies for Geomechanical Characterization of Rock Mass Response in Mesoscale Experiments in Underground Laboratories: Lessons Learned, in *Distributed Acoustic Sensing (DAS) in Borehole Geophysics*, edited by Y. Li, R. Mellors and G. Zhan, American Geophysical Union.
Rodríguez Tribaldos, V., M. Schoenball, A.-F. J., and E. C. Team (2021), Low-frequency Distributed Acoustic Sensing (DAS) for monitoring of hydraulic fracturing at the EGS Collab Experiment Testbed, paper presented at SEG-AGU Advances in Distributed Sensing for Geophysics Workshop, Houston, TX, USA, 10 February 2021 - 12 February 2021.
Roggenthen, W., T. Kneafsey, J. Burghardt, T. Doe, C. Hopp, T. Johnson, . . . E. C. Team (2024), Complementary Subsurface Characterization Methods to Develop a Geologic Model for the EGS Collab Experiment, Sanford Underground Research Facility, *LBNL-XXXXX*, 15 pp, Lawrence Berkeley National Laboratory, Berkeley, CA.
Roggenthen, W. M., and T. W. Doe (2018), Natural Fractures and Their Relationship to the EGS Collab Project in the Underground of the Sanford Underground Research Facility (SURF), paper presented at 52nd U.S. Rock Mechanics/Geomechanics Symposium, American Rock Mechanics Association, Seattle, Washington, 2018/8/21.
Roggenthen, W. M., T. C. Johnson, D. M. Crandall, T. J. Paronish, and C. Ulrich (2022), Composition and Structure of the EGS Collab Test Bed 1 Based Upon Electrical Resistivity Tomography, Core Compositions, and Wireline Logging, paper presented at 56th U.S. Rock Mechanics/Geomechanics Symposium.
Schoenball, M., J. Ajo-Franklin, D. Blankenship, P. Cook, P. Dobson, Y. Guglielmi, . . . EGS Collab Team (2019), Microseismic monitoring of meso-scale stimulations for the DOE EGS Collab project at the Sanford Underground Research Facility, paper presented at 44th Workshop on Geothermal Reservoir Engineering, Stanford University, Stanford, California, February 11-13, 2019.
Schoenball, M., J. B. Ajo-Franklin, D. Blankenship, C. Chai, A. Chakravarty, P. Dobson, . . . EGS Collab Team (2020a), Creation of a Mixed-Mode Fracture Network at Mesoscale Through Hydraulic Fracturing and Shear Stimulation, *Journal of Geophysical Research: Solid Earth*, *125*(12), e2020JB019807, doi:https://doi.org/10.1029/2020JB019807.
Schoenball, M., J. B. Ajo-Franklin, T. Wood, M. Robertson, P. Cook, V. Rodriguez-Tribaldos, . . . EGS Collab Team (2020b), Lessons learned from passive seismic monitoring of EGS Collab Experiment 1, paper presented at 45th Workshop on Geothermal Reservoir Engineering, Stanford University, Stanford, California, February 10-12, 2020.
Schoenball, M., Y. Guglielmi, J. B. Ajo-Franklin, P. J. Cook, P. Dobson, C. Hopp, . . . C. Ulrich (2021), In-situ observation of pre-, co-and post-seismic shear slip at 1.5 km depth, *Earth and Space Science Open Archive* doi:10.1002/essoar.10506700.1.

Schwering, P. C., T. W. Doe, W. M. Roggenthen, G. H. Neupane, H. Johnston, P. F. Dobson, . . . EGS Collab Team (2020), Deterministic Discrete Fracture Network (DFN) Model for the EGS Collab Project on the 4850 Level of the Sanford Underground Research Facility (SURF), paper presented at 54th U.S. Rock Mechanics/Geomechanics Symposium, American Rock Mechanics Association, 2020/9/18.
Singh, A. (2021), Stress Layering, Fault Slip and Hydraulic Fracture Propagation: Integrating Field Studies, Laboratory Experiments and Numerical Simulations, Dissertation thesis, 256 pp, Stanford University.
Singh, A., M. Zoback, P. F. Dobson, T. J. Kneafsey, M. Schoenball, Y. Guglielmi, . . . EGS Collab Team (2019), Slip tendency analysis of fracture networks to determine suitability of candidate testbeds for the EGS Collab hydroshear experiment, paper presented at Geothermal Resources Council Transactions.
Sollohub, L., T. Johnson, T. Sugama, and T. Pyatina (2022), High Resistivity Well Cement for Underground Wells Suitable for Sealing Monitoring Equipment, paper presented at 47th Workshop on Geothermal Reservoir Engineering, Stanford University, Stanford, California, February 7-9, 2022.
Sonnenthal, E., W. Pettitt, T. Smith, A. Riahi, D. Siler, M. Kennedy, . . . D. Blankenship (2018), Continuum Thermal-Hydrological-Mechanical Modeling of the Fallon FORGE Site, *GRC Transactions*, *42*.
Templeton, D., J. Morris, M. Schoenball, T. Wood, M. Robertson, P. Cook, . . . EGS Collab Team (2019), Microseismic Correlation and Cluster Analysis of DOE EGS Collab Data, paper presented at 44th Workshop on Geothermal Reservoir Engineering, Stanford University, Stanford, California, February 11-13, 2019.
Ulrich, C., P. F. Dobson, T. J. Kneafsey, W. M. Roggenthen, N. Uzunlar, T. W. Doe, . . . J. A. Burghardt (2022), Characterizing Rock Fractures and Physical Properties for Experiment 2 of the EGS Collab Project, Sanford Underground Research Facility, paper presented at 56th U.S. Rock Mechanics/Geomechanics Symposium.
Ulrich, C., P. F. Dobson, T. J. Kneafsey, W. M. Roggenthen, N. Uzunlar, T. W. Doe, . . . EGS Collab Team (2018), The Distribution, Orientation, and Characteristics of Natural Fractures for Experiment 1 of the EGS Collab Project, Sanford Underground Research Facility, paper presented at 52nd U.S. Rock Mechanics/Geomechanics Symposium, American Rock Mechanics Association, Seattle, Washington, 2018/8/21.
Wang, C., P. Winterfeld, B. Johnston, and Y.-S. Wu (2018), An Embedded 3D Fracture Modeling Approach for Simulating Fracture-Dominated Fluid Flow and Heat Transfer in Geothermal Reservoirs, paper presented at 43rd Workshop on Geothermal Reservoir Engineering, Stanford University, Stanford, California, February 12-14, 2018.
Wang, H. F., M. Y. Lee, T. W. Doe, B. C. Haimson, C. M. Oldenburg, and P. F. Dobson (2017), In-Situ Stress Measurement at 1550-Meters Depth at the kISMET Test Site in Lead, S.D, paper presented at 51st U.S. Rock Mechanics/Geomechanics Symposium, American Rock Mechanics Association, San Francisco, California, USA, 2017/8/28/.
Weers, J., and J. Huggins (2019), Getting Data Out of the Ground: Modern Challenges Facing EGS Collab, the DOE Geothermal Data Repository, and the Geothermal Industry, paper presented at 44th Workshop on Geothermal Reservoir Engineering, Stanford University, Stanford, CA, February 11-13, 2019.
White, M., P. Fu, H. Huang, A. Ghassemi, and EGS Collab Team (2017), The Role of Numerical Simulation in the Design of Stimulation and Circulation Experiments for the EGS Collab Project paper presented at GRC Transactions, Vol. 41, 2017
White, M., T. Johnson, T. Kneafsey, D. Blankenship, P. Fu, H. Wu, . . . EGS Collab Team (2019), The Necessity for Iteration in the Application of Numerical Simulation to EGS: Examples from the EGS Collab Test Bed 1, paper presented at 44th Workshop on Geothermal Reservoir Engineering, Stanford University, Stanford, California, February 11-13, 2019.
White, M. D., J. A. Burghardt, and EGS Collab Team (2021), Modeling the Dynamic Flow Resistance Across the Fracture Network of EGS Collab Experiment 1, paper presented at 46th Workshop on Geothermal Reservoir Engineering, Stanford University, Stanford, California, February 15-17, 2021.
White, M. D., P. Fu, and EGS Collab Team (2020), Application of an Embedded Fracture and Borehole Modeling Approach to the Understanding of EGS Collab Experiment 1, paper presented at 45th Workshop on Geothermal Reservoir Engineering, Stanford University, Stanford, California, February 10-12, 2020.
White, M. D., P. Fu, A. Ghassemi, H. Huang, J. Rutqvist, B. Johnston, and EGS Collab Team (2018), Numerical Simulation Applications in the Design of EGS Collab Experiment 1, paper presented at 43rd Workshop on Geothermal Reservoir Engineering, Stanford University, Stanford, California, February 12-14, 2018.
Williams, C. F., M. J. Reed, R. H. Mariner, J. DeAngelo, and S. P. Galanis Jr. (2008), Assessment of moderate- and high-temperature geothermal resources of the United States, Type United States Geological Survey Fact Sheet 2008–3082, 4 pp.
Winterfeld, P., B. Johnston, K. Beckers, Y.-S. Wu, and EGS Collab Team (2019), Code Modifications for Modeling Chemical Tracers and Embedded Natural Fractures at EGS Collab, paper presented at 44th Workshop on Geothermal Reservoir Engineering, Stanford University, Stanford, California, February 11-13, 2019.
Winterfeld, P. H., and Y.-S. Wu (2020), An Overview of our Coupled Thermal-Hydrological-Mechanical Simulator for Porous and Fractured Media, paper presented at 54th U.S. Rock Mechanics/Geomechanics Symposium.
Wu, H., P. Fu, Z. Frone, M. D. White, J. B. Ajo-Franklin, J. P. Morris, . . . D. A. Blankenship (2021a), Modeling heat transport processes in enhanced geothermal systems: A validation study from EGS Collab Experiment 1, *Geothermics*, *97*, 102254, doi:https://doi.org/10.1016/j.geothermics.2021.102254.
Wu, H., P. Fu, and J. P. Morris (2020a), Predicting thermal responses at the EGS Collab testbed based on tracer test-inferred flow fields, paper presented at 45th Workshop on Geothermal Reservoir Engineering, Stanford University, Stanford, California, February 10-12, 2020.

Wu, H., P. Fu, J. P. Morris, E. D. Mattson, A. J. Hawkins, Y. Zhang, . . . EGS Collab Team (2019a), Characterizing Fracture Flow in EGS Collab Experiment Based on Stochastic Modeling of Tracer Recovery, paper presented at 44th Workshop on Geothermal Reservoir Engineering, Stanford University, Stanford, California, February 11-13, 2019.
Wu, H., P. Fu, J. P. Morris, E. D. Mattson, G. Neupane, M. M. Smith, . . . T. Kneafsey (2021b), Characterization of flow and transport in a fracture network at the EGS Collab field experiment through stochastic modeling of tracer recovery, *Journal of Hydrology*, *593*, 125888, doi:https://doi.org/10.1016/j.jhydrol.2020.125888.
Wu, H., P. Fu, J. P. Morris, R. R. Settgast, F. J. Ryerson, and EGS Collab Team (2019b), A Numerical Scheme to Reduce Numerical Diffusion for Advection-Dispersion Modeling: Validation and Application, paper presented at 44th Workshop on Geothermal Reservoir Engineering, Stanford University, Stanford, California, February 11-13, 2019.
Wu, H., P. Fu, J. P. Morris, R. R. Settgast, F. J. Ryerson, E. D. Mattson, . . . Y. Zhang (2019c), Stochastic modeling of a conservative tracer test for the characterization of fracture flow patterns in EGS Collab Experiment 1, paper presented at 53rd US Rock Mechanics/Geomechanics Symposium, American Rock Mechanics Association, New York, NY, USA, 23–26 June 2019.
Wu, H., P. Fu, X. Yang, J. P. Morris, and EGS Collab Team (2018), Imaging hydraulic fracture extents and aperture using electrical resistivity tomography, paper presented at 43rd Workshop on Geothermal Reservoir Engineering, Stanford University, Stanford, California, February 12-14, 2018.
Wu, H., P. Fu, X. Yang, J. P. Morris, T. C. Johnson, R. R. Settgast, and F. J. Ryerson (2019d), Accurate imaging of hydraulic fractures using templated electrical resistivity tomography, *Geothermics*, *81*, 74-87, doi:https://doi.org/10.1016/j.geothermics.2019.04.004.
Wu, H., P. Fu, J. Zhang, and J. P. Morris (2020b), Interpretation of Tracer Data Using a Markov Chain Monte Carlo Approach for the Characterization of the EGS Collab Testbed, paper presented at 54th U.S. Rock Mechanics/Geomechanics Symposium, American Rock Mechanics Association, 2020/9/18.
Wu, H., J. Zhang, P. Fu, J. P. Morris, and EGS Collab Team (2021c), Inferring fracture aperture distribution at the EGS Collab Experiment 1 testbed through a deep learning accelerated Bayesian approach, paper presented at 46th Workshop on Geothermal Reservoir Engineering, Stanford University, Stanford, California, February 15-17, 2021.
Wu, Y.-S., X. Yu, S. Wang, C. Wang, P. Winterfeld, and EGS Collab Team (2020c), Modeling Thermal-Hydrologic-Mechanical Processes for EGS Collab Thermal Circulation Tests using Embedded Discrete Fracture Model, paper presented at 45th Workshop on Geothermal Reservoir Engineering, Stanford University, Stanford, California, February 10-12, 2020.
Wu, Y. S., X. Yu, S. Wang, and P. H. Winterfeld (2019e), Modeling Thermal-Hydraulic-Mechanical Processes in Enhanced or Engineered Geothermal Systems, paper presented at ARMA-CUPB Geothermal International Conference.
Yasuhara, H., D. Elsworth, and A. Polak (2004), Evolution of permeability in a natural fracture: Significant role of pressure solution, *J. Geophys. Res.*, *109*(B3), B03204, doi:10.1029/2003jb002663.
Ye, Z., A. Ghassemi, and T. Kneafsey (2020), Deformation, Failure and Permeability Evolution of Sealed Fractures/Foliations in EGS Collab Poorman Schist, paper presented at 54th U.S. Rock Mechanics/Geomechanics Symposium, American Rock Mechanics Association, 2020/9/18.
Ye, Z., A. Vachaparampil, X. Zhou, A. Ghassemi, and T. Kneafsey (2019), Failure Behavior of the Poorman Schist and Its Fractures from EGS Collab Stimulation Site, paper presented at 44th Workshop on Geothermal Reservoir Engineering, Stanford University, Stanford, California, February 11-13, 2019.
Yildirim, E. C., K. Im, D. Elsworth, and EGS Collab Team (2018), Co-Evolution of Fracture Permeability and Friction in Rocks From the EGS Collab Experiment 1 Site, paper presented at 52nd U.S. Rock Mechanics/Geomechanics Symposium, American Rock Mechanics Association, Seattle, Washington, 2018/8/21.
Zang, A., O. Stephansson, L. Stenberg, K. Plenkers, S. Specht, C. Milkereit, . . . M. Weber (2017), Hydraulic fracture monitoring in hard rock at 410 m depth with an advanced fluid-injection protocol and extensive sensor array, *Geophysical Journal International*, 790–813, doi:10.1093/gji/ggw430.
Zhang, Y., A. E. Dekas, A. J. Hawkins, A. E. Parada, O. Gorbatenko, K. Li, and R. N. Horne (2020), Microbial Community Composition in Deep-Subsurface Reservoir Fluids Reveals Natural Interwell Connectivity, *Water Resources Research*, *56*(2), e2019WR025916, doi:https://doi.org/10.1029/2019WR025916.
Zhang, Y., C. Doughty, L. Pan, T. Kneafsey, and EGS Collab Team (2018a), What Could We See at the Production Well Before the Thermal Breakthrough?, paper presented at 43rd Workshop on Geothermal Reservoir Engineering, Stanford University, Stanford, California, February 12-14, 2018.
Zhang, Y., R. N. Horne, A. J. Hawkins, J. C. Primo, O. Gorbatenko, and A. E. Dekas (2022), Geological activity shapes the microbiome in deep-subsurface aquifers by advection, *Proceedings of the National Academy of Sciences*, *119*(25), e2113985119, doi:10.1073/pnas.2113985119.
Zhang, Y., Q. Zhou, S. Finsterle, T. Kneafsey, R. Jayne, and EGS Collab Team (2018b), Thermal breakthrough predictions based on multiple flow paths characterized by tracer tests, paper presented at TOUGH Symposium, Lawrence Berkeley National Laboratory. Berkeley, California, October 2018.
Zhou, J., H. Huang, E. Mattson, R. Podgorney, and EGS Collab Team (2018a), Three-Dimensional Quasi-Static Discrete Element Modeling of Hydraulic Fracture Propagation in Crystalline Rock Under Thermal-Mechanical Stress Gradients, paper presented at 2nd International Discrete Fracture Network Engineering Conference, American Rock Mechanics Association, Seattle, Washington, USA, 2018/11/5/.

Zhou, Q., C. M. Oldenburg, T. J. Kneafsey, and EGS Collab Team (2018b), Modeling Transport of Multiple Tracers in Hydraulic Fractures at the EGS Collab Test Site, paper presented at 43rd Workshop on Geothermal Reservoir Engineering, Stanford University, Stanford, California, February 12-14, 2018.
Zhou, Q., C. M. Oldenburg, J. Rutqvist, T. J. Kneafsey, and EGS Collab Team (2018c), Analytical and Numerical Modeling of Heat Transport in Fractured Reservoirs, paper presented at 43rd Workshop on Geothermal Reservoir Engineering, Stanford University, Stanford, California, February 12-14, 2018.
Zimmermann, G., A. Zang, O. Stephansson, G. Klee, and H. Semiková (2019), Permeability Enhancement and Fracture Development of Hydraulic In Situ Experiments in the Äspö Hard Rock Laboratory, Sweden, *Rock Mechanics and Rock Engineering*, *52*(2), 495-515, doi:10.1007/s00603-018-1499-9.

Appendix A

Chai et al. [2022]; *Chai et al.* [2020]; *Chakravarty et al.* [2021]; *Chakravarty and Misra* [2022]; *Chen et al.* [2018; 2019a]; *Chen et al.* [2019b]; *Chi et al.* [2020]; *Crowe et al.* [2019]; *Frash* [2022]; *Frash et al.* [2018a]; *Frash et al.* [2022]; *Frash et al.* [2019b]; *Frash et al.* [2021b]; *Fu et al.* [2021b]; *Gao et al.* [2020]; *Huang et al.* [2019]; *Huang et al.* [2018]; *Huang et al.* [2017]; *Jafarov et al.* [2020]; *Johnson et al.* [2022]; *Johnson et al.* [2019a]; *Johnson et al.* [2021]; *Kamali and Ghassemi* [2018]; *Kutun* [2018]; *Kutun et al.* [2018]; *Li et al.* [2024]; *Li et al.* [2021]; *Lu and Ghassemi* [2019]; *Morris et al.* [2018a]; *Morris et al.* [2018b]; *Neupane et al.* [2019b]; *Pan et al.* [2019]; *Pan et al.* [2020]; *Schwering et al.* [2020]; *Singh* [2021]; *Singh et al.* [2019]; *Templeton et al.* [2019]; *Wang et al.* [2018]; *White et al.* [2017]; *White et al.* [2019]; *White et al.* [2021]; *White et al.* [2020]; *White et al.* [2018]; *Winterfeld et al.* [2019]; *Winterfeld and Wu* [2020]; *Wu et al.* [2021a]; *Wu et al.* [2020a]; *Wu et al.* [2021b]; *Wu et al.* [2019b]; *Wu et al.* [2019c]; *Wu et al.* [2018]; *Wu et al.* [2019d]; *Wu et al.* [2020b]; *Wu et al.* [2021c]; *Wu et al.* [2020c]; *Wu et al.* [2019e]; *Zhang et al.* [2018a]; *Zhang et al.* [2018b]; *Zhou et al.* [2018a]; *Zhou et al.* [2018b]; *Zhou et al.* [2018c]

Tim Kneafsey[1], Pat Dobson[1], Doug Blankenship[2], Paul Schwering,[2] Mark White[3], Joseph Morris[4], Lianjie Huang[5], Tim Johnson[3], Jeff Burghardt[3], Earl Mattson[6], Ghanashyam Neupane[6], Chris Strickland[3], Hunter Knox[3], Vince Vermuel[3], Jonathan Ajo-Franklin[1,7], Pengcheng Fu[4], Bill Roggenthen[8], Tom Doe[9], Martin Schoenball[1,10], Chet Hopp[1], Verónica Rodríguez Tribaldos[1,11], Mathew Ingraham[2], Yves Guglielmi[1], Craig Ulrich[1], Todd Wood[1], Luke Frash[5], Tatiana Pyatina[12], George Vandine[13], Megan Smith[4], Roland Horne[14], Mark McClure[15], Ankush Singh[14, 16], Jon Weers[17], Michelle Robertson[1], and the EGS Collab Team*

Supplemental Information

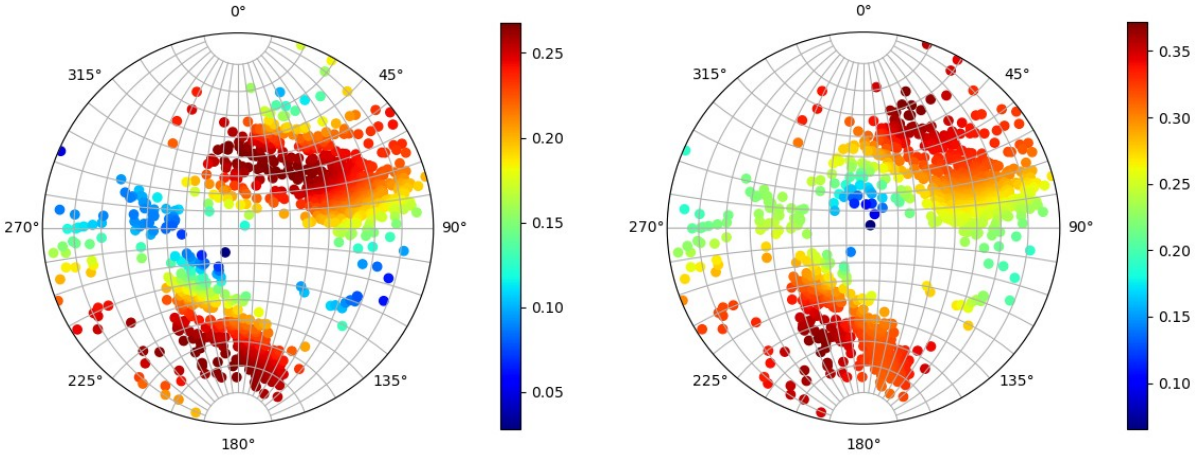

Figure SI-1. E2. Equal angle lower hemisphere projection of poles of identified fractures in E2-TC, colored according to the mean shear-to-normal stress ratio under the hypothesis that the principal stresses are rotated from vertical/horizontal. Left - Stress-driven fracture orientation hypothesis, Right - Rock fabric-driven fracture orientation hypothesis. Plots are colored according to the mean critical shear-to-normal stress ratio (i.e., maximum friction coefficient that permits slip with zero cohesion) (from Burghardt et al. (2022)).

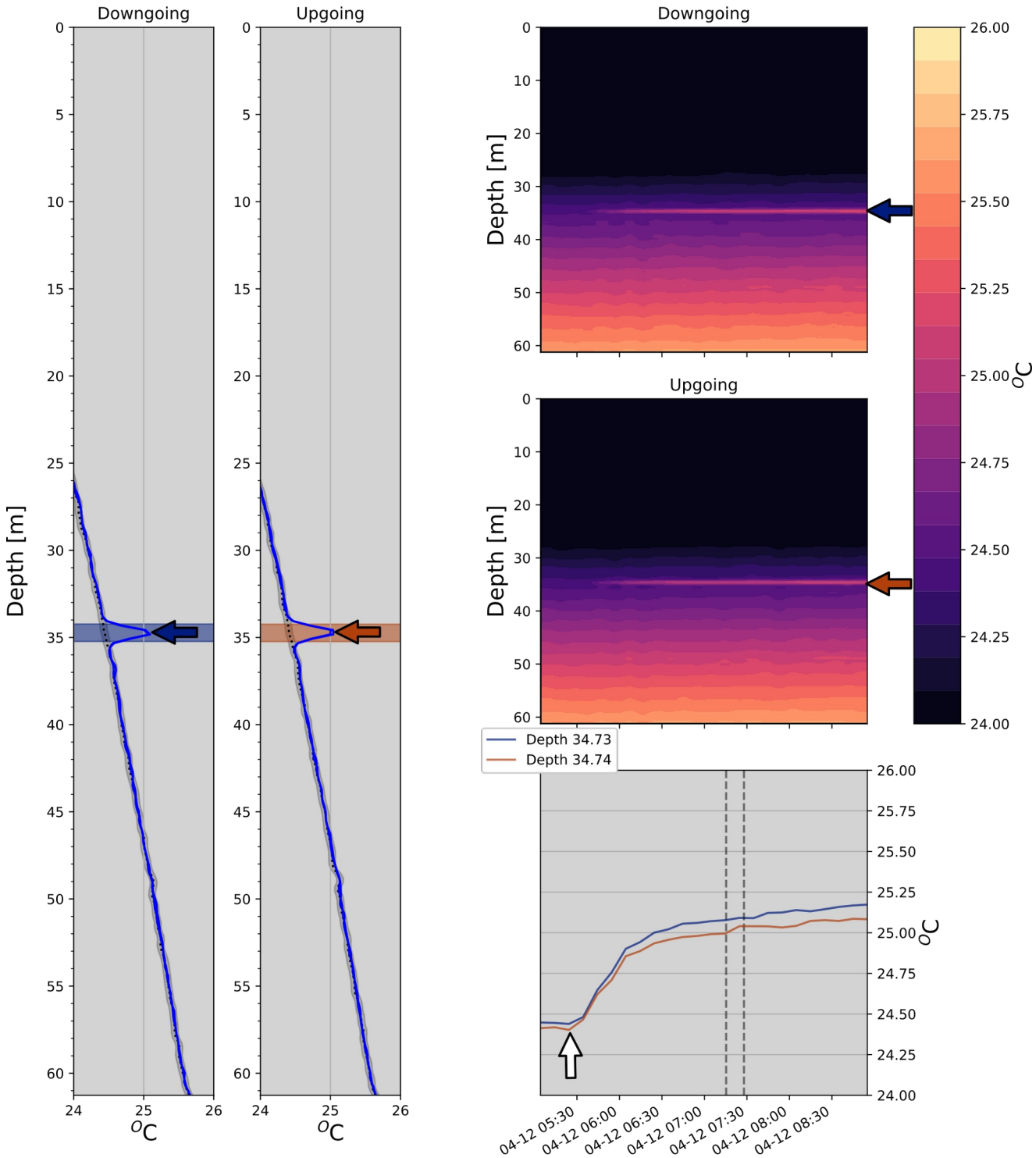

Figure SI-2. E3. Temperature signal from the distributed temperature sensing (DTS) in monitoring well AMU showing a peak

at a depth of about 35 m starting at about 5:30 UTC (white arrow). Blue and red arrows indicate the depth of the fracture on the downgoing and upgoing section of fiber, respectively. These colors correspond to the blue and red timeseries traces shown in the bottom right.

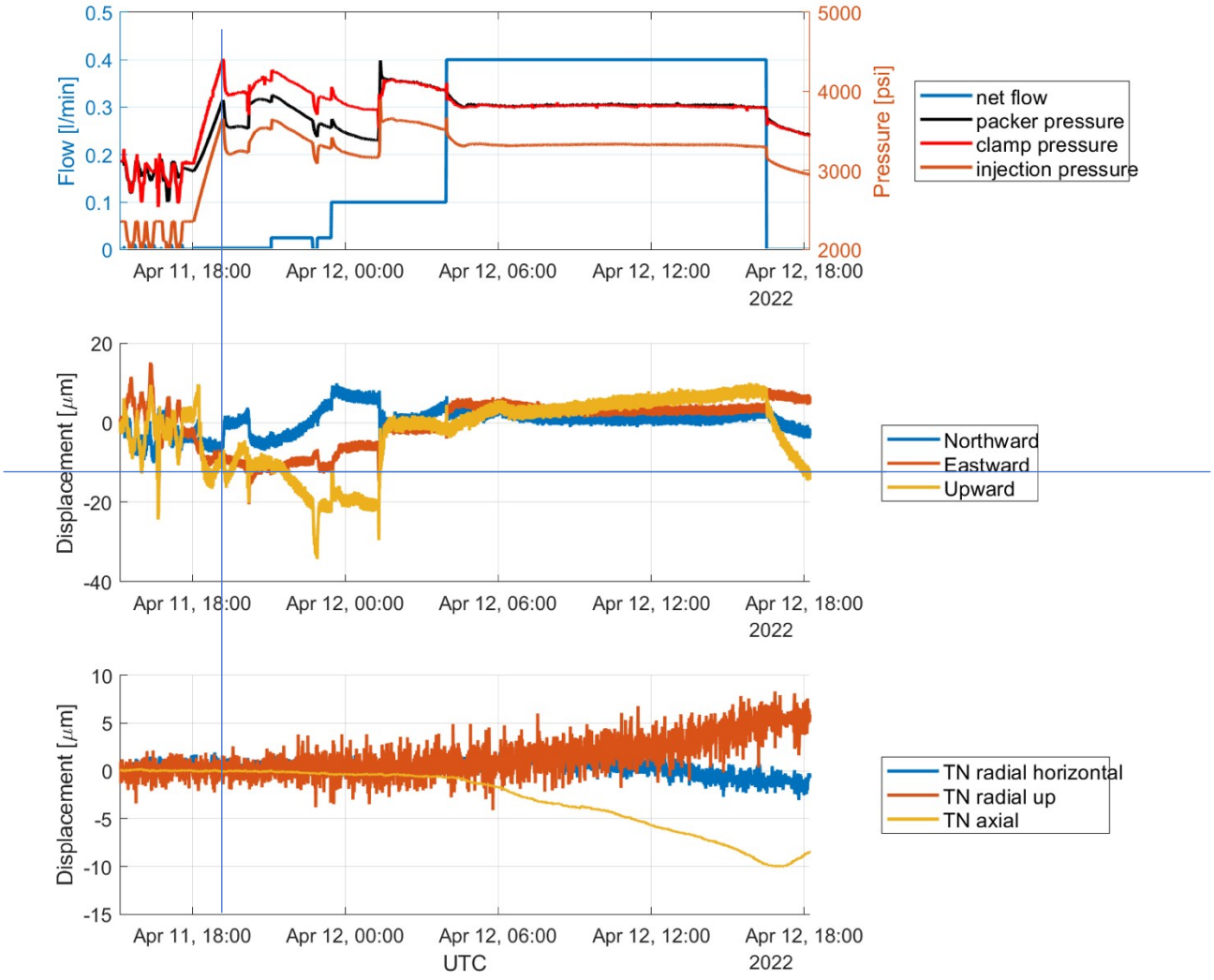

Figure SI-3. E3. Displacements measured by the SIMFIP and DORSA probes during the Zone 7 stimulation. Top: Injection flow rate, pressure, and packer pressures during the test. Center: displacements in borehole TC indicated by the SIMFIP tool. Notable displacements are seen prior to and during stimulation. Bottom: displacements indicated by the DORSA tool in well TN. Note the increases in displacements over the last half of the test. Vertical lines added as visual guides.

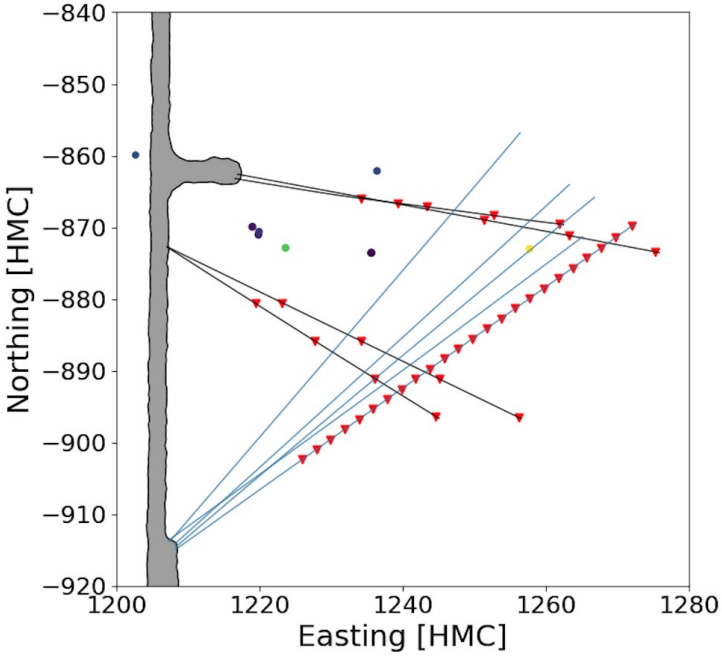
−840
−850
−860
−870
−880
−890
−900
−910
−920
Northing [HMC]
1200
1220
1240
1260
1280
Easting [HMC]

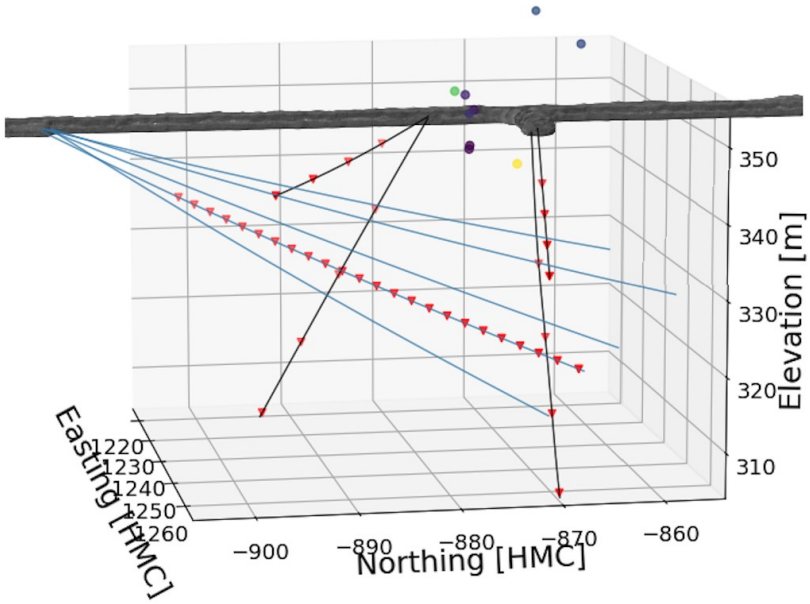
350
340
330
320
310
Elevation [m]
1220
1230
1240
1250
1260
Easting [HMC]
−900
−890
−880
−870
−860
Northing [HMC]

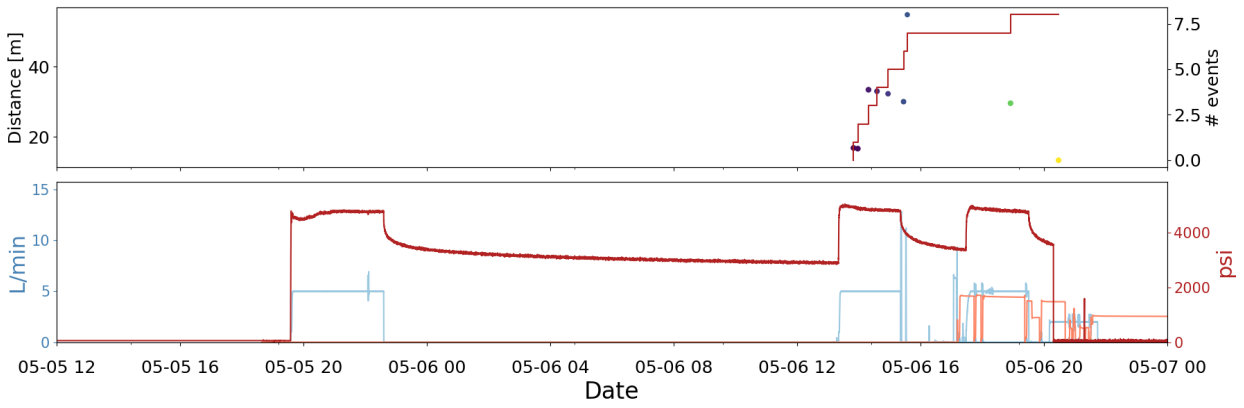

Figure SI-4. E3. Microseismic events detected during stimulation of the 177.4 - 179.6 ft interval of TU. The top two panels show the location of each event. The uppermost timeseries plot shows the cumulative number of events and their distance from the injection point, with dot color changing with time. The bottom timeseries plot shows the injection pressure and flow rate in psi and L/min, respectively. The time axis is in UTC.

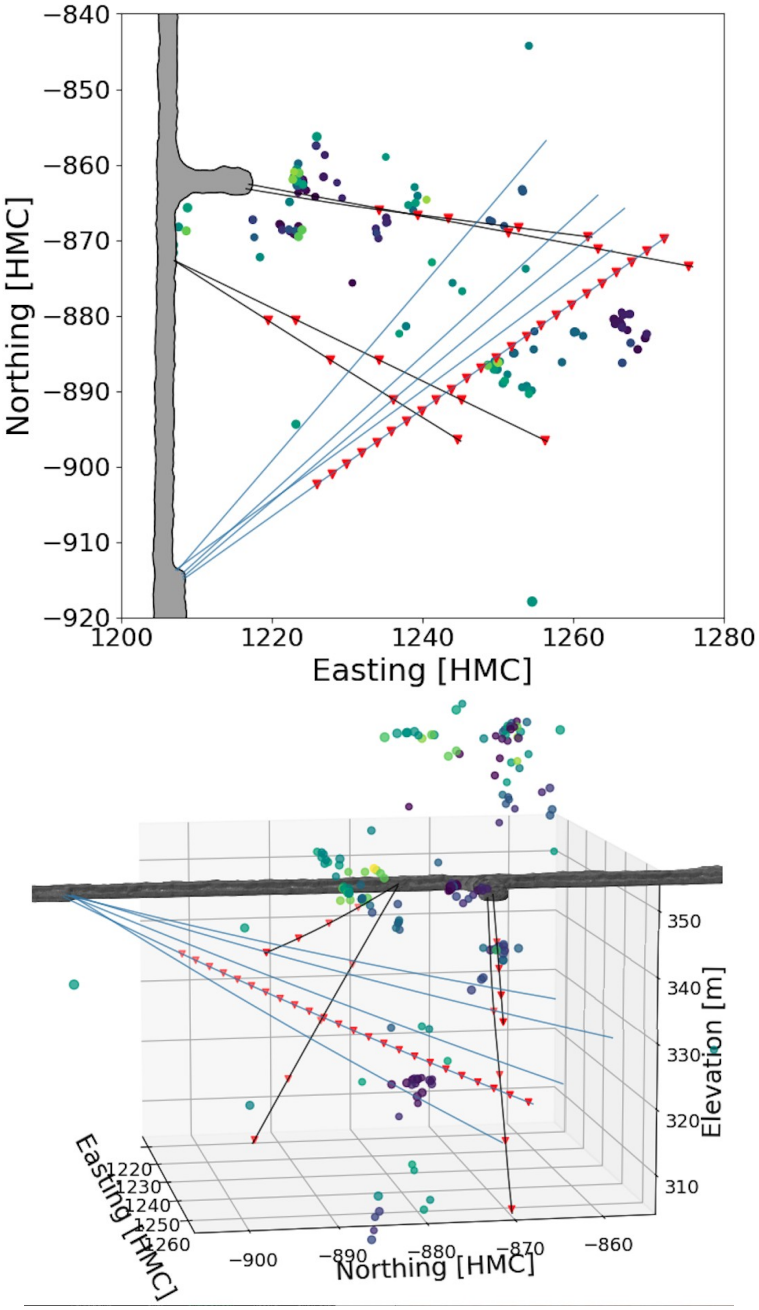
−840
−850
−860
−870
−880
−890
−900
−910
−920
Northing [HMC]
1200
1220
1240
1260
1280
Easting [HMC]
350
340
330
320
310
Elevation [m]
1220
1230
1240
1250
1260
Easting [HMC]
−900
−890
−880
−870
−860
Northing [HMC]

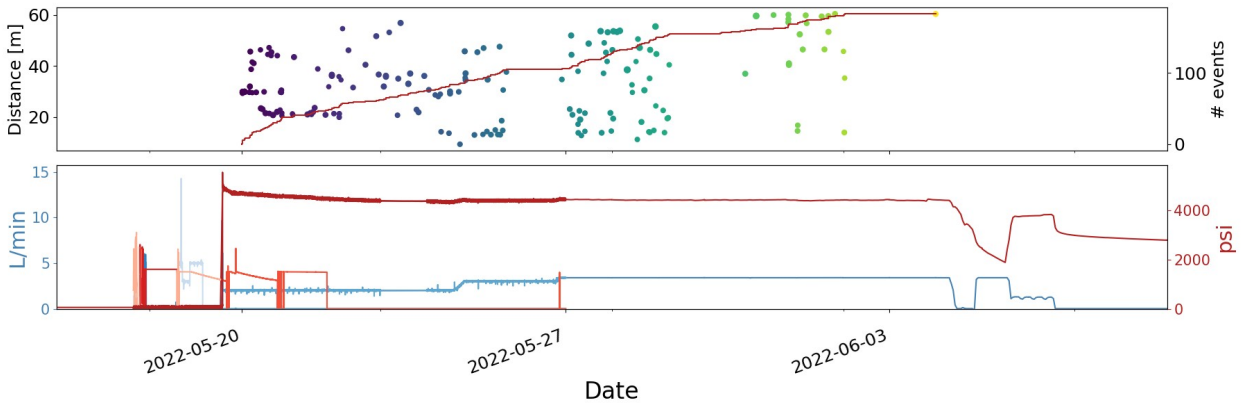

Figure SI-5. E3. Microseismic events detected during flow testing while injecting in the 177.4 - 179.6 ft interval of TU. The top two panels show the location of each event. The uppermost timeseries plot shows the cumulative number of events and their distance from the injection point, with dot color changing with time. The bottom timeseries plot shows the injection pressure and flow rate in psi and L/min, respectively. The time axis is in UTC.

ΔT [°C]
0.2
0.1
0.0
−0.1
−0.2
AMU [m]
AML [m]
DMU [m]
DML [m]
0
25
50
75
100
L/min
psi
4000
2000
0
6
4
2
TU Flow
TN Interval Flow
TU Injection Pressure
TN Interval Pressure
05-19
05-26
06-02
06-09
06-16
06-23
06-30
07-07
07-14
07-21
07-28
08-04
08-11
08-18
08-25
Date [2022]

Figure SI-6. E3. Change in temperature in each grouted borehole during the circulation test in TU. Each borehole is represented by a waterfall plot with red representing temperature increases up to 0.25°C and blue representing decreases from the nominal start. The fiber package is installed as a loop going into and then back out of each borehole, so the y-axes represent distance along the fiber from the point where it enters until the point where it exits each borehole, thus the top half and bottom half of each panel are near mirror images of each other. Sharp local increases in temperature typically indicate fracture hits. Note seasonal warming of the drift is more apparent in DMU and DML where ventilation was greater than the boreholes collared in the alcove (AMU and AML). The injection parameters are shown in the bottom panel for reference.

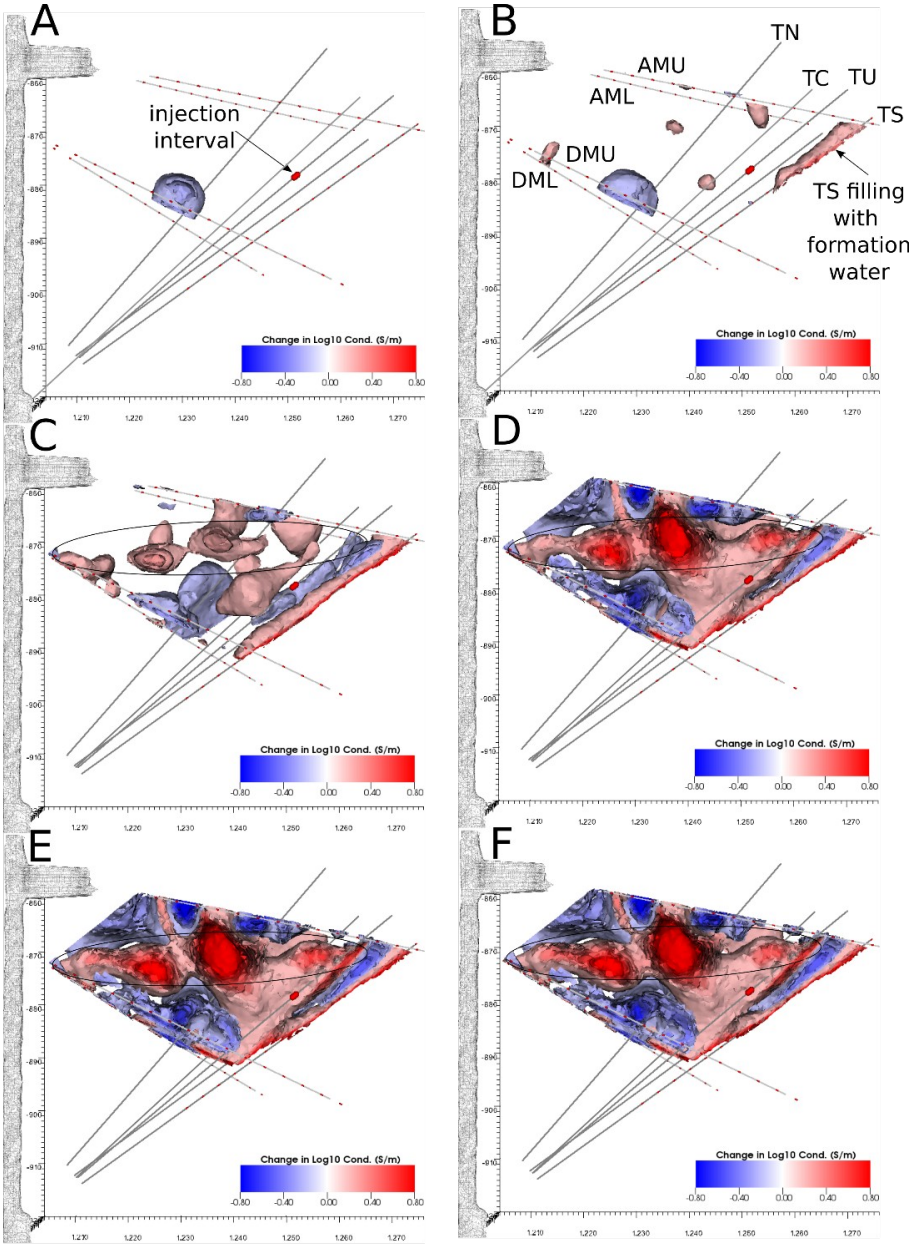
A
injection interval
Change in Log10 Cond. (S/m)
B
TN
AMU
AML
TC
TU
TS
DMU
DML
TS filling with formation water
C
D
E
F

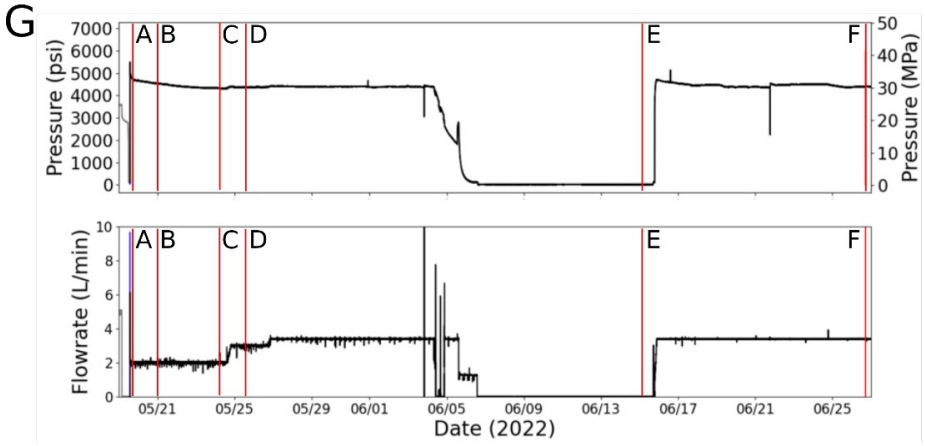
G
Pressure (psi)
Pressure (MPa)
Flowrate (L/min)
A
B
C
D
E
F
05/21
05/25
05/29
06/01
06/05
06/09
06/13
06/17
06/21
06/25
Date (2022)

Figure SI-7. E3. Difference ERT images – subtracting a baseline image from subsequent images highlights changes in the system. ERT imaging sequence showing changes in bulk conductivity during the TU 177.4 - 179.6 ft injection. the baseline ERT for this series is just prior to injection on May 19. These results show the total change in conductivity from the baseline over this duration. A-F show the change in bulk conductivity at the times indicated in panel G. From time A-C, it is apparent that TS is filling with formation water (increasing in conductivity). A large increase in conductivity occurs from times C to D when the flowrate is increased from 2-3 L/ min. Changes during the two-week flow outage are imperceptible (compare D and E), suggesting much of the system remained pressurized during the outage. Note that TS is the only borehole that did not contain a packer: the increases in conductivity around TS are likely caused by infilling of TS with formation water. Negative anomalies adjacent to the positive anomalies are presumably caused by compressive stresses restricting fluid pathways. TC may also be infilling as suggested by the elongated positive anomaly along TC in C-F.

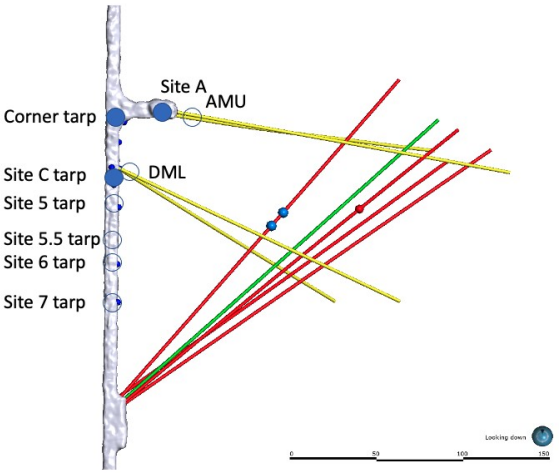

May 24, 2022

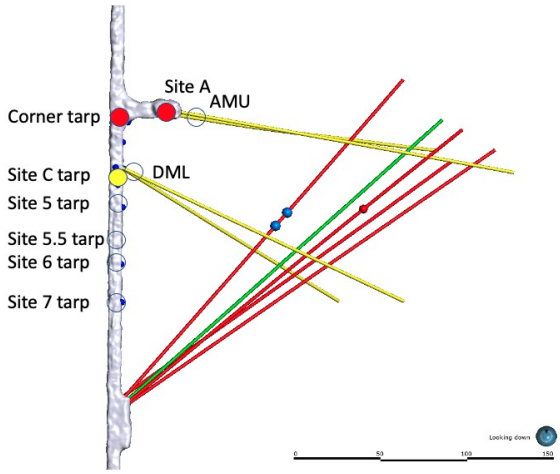

June 1, 2022

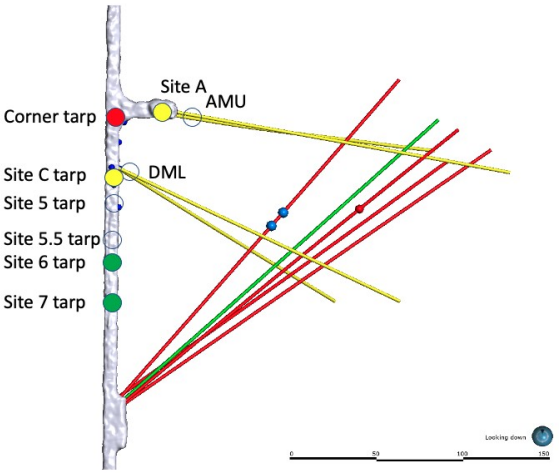

June 22, 2022

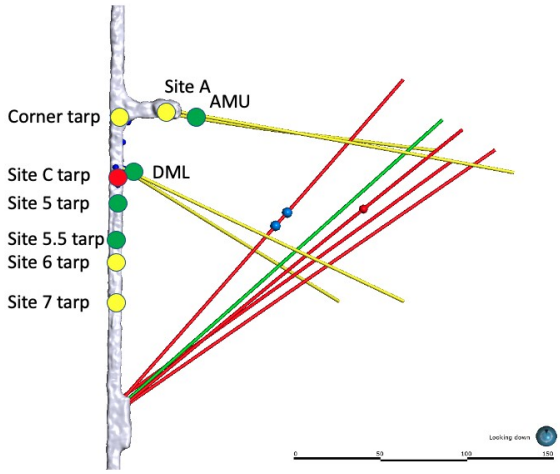

July 5, 2022

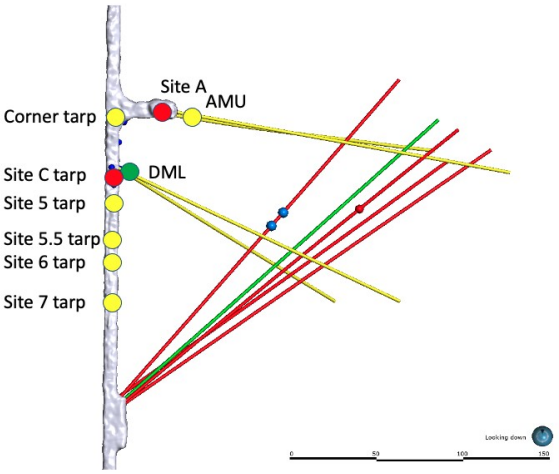

July 26, 2022

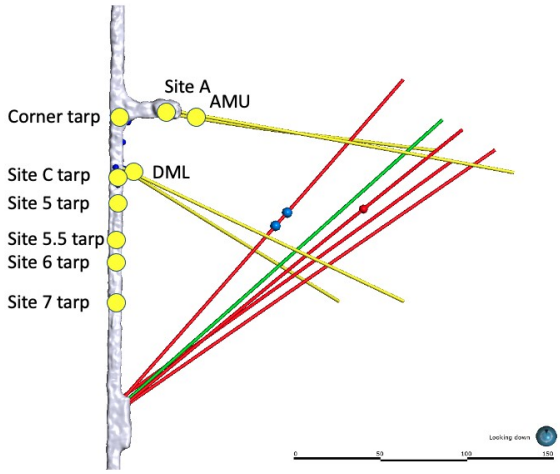

August 15, 2022

Figure SI-8. E3. Subjective observations of dripping from the drift ceiling over time. Empty circles represent nonflowing collection locations, blue dots are initial collection locations, green dots represent increasing discharge over the previous observation, yellow - staying steady, and red - reduced discharge. Note the abundance and relative flow increasing to the south over time.

Geophysical monitoring equipment specifications

Seismicity

Hydrophones had a relatively flat frequency response up to about 35 kHz, accelerometers were specified to have a flat response of 1 V/g up to 5-kHz frequency (±10%) and with a resonance frequency >20 kHz, however upon testing the frequency response became significantly nonlinear above about 5 kHz with several resonance frequencies at about 10 kHz and higher (Schoenball et al., 2020).
Piezoelectric accelerometers had a linear frequency response range of 0.5 Hz to 22 kHz within 3 dB, hydrophones had a flat frequency response from 2 Hz to 2 kHz (Hopp, 2023b).

For Experiment 1 there were three recording systems:

1. Vibbox (passive): 100 kHz sampling rate
2. Geode (CASSM): 48 kHz sampling rate
3. Geores: Passive data was also recorded on a 96 channel OYO Geores system during the 4850 experiment (E1) at 4 kHz. The system recorded all testbed sensors available (hydrophones, accelerometers) as well as several 3C geophones installed in jackleg borings near the drift. Unfortunately, the 4 kHz recording (2 kHz Nyquist) was insufficient to capture the very high frequency microseismic events that were generated in the experiment. The Geores system was not redeployed for the 4100 experiments (E2 and E3).

For Experiment 2, we used only systems 1. and 2. at the same sampling rates.

System geometrical constraints
The network was designed to detect and locate seismicity that occurred along any of the 5-spot boreholes and was also well-situated to detect and locate seismicity along the inferred fracture between TC/TU and the battery alcove. Most seismicity was located *outside* the seismic network. However, the system correctly detected and located the FWS shots in TN, which proves that the system was also sensitive to seismicity inside the network.

CASSM

During the COLLAB 4850 experiment (E1), the CASSM system utilized an array of 17 piezoelectric seismic sources recorded by 2 x 12 channel hydrophone arrays and the 18 3C accelerometers. The sources were operated in pulsed mode (16 stacks/gather) and sequenced between sources to acquire time-lapse epochs every 8-9 minutes continuously. While several 2D profiles provided high ray density (e.g. OT to OB), the 3D volume is

sampled sparsely in space although densely in time, thus allowing tomographic tracking of velocity perturbations during stimulation. Sequential differential traveltime measurements using the CASSM array showed repeatability on the order of 250 ns during quiet periods, thus allowing tomographic resolution of velocity perturbations < 10 m/s.

Fiber Optics

Also see (Hopp, 2023a; Rodríguez Tribaldos et al., 2024 (in press); Rodríguez Tribaldos et al., 2021)

Experiment 1:

- DAS Interrogator: Silixa iDAS v2
  - Sampling frequency: 1 kHz or 10 kHz (we were changing in between with the hope of catching seismicity)
  - Spatial sampling: 1 m
  - Gauge length (which can be understood as spatial resolution): 10 m
- DSS Interrogator: Omnisens DITEST VISION Dual temperature and strain unit
  - Sampling frequency: ~1 min
  - Spatial sampling: 0.41 m
  - Spatial resolution: 1 m

Experiments 2 and 3:

- DAS Interrogator 1: Silixa iDAS v2
  - Sampling frequency: 500 Hz
  - Spatial sampling: 1 m
  - Gauge length (which can be understood as spatial resolution): 10 m
- DAS Interrogator 2: OptaSense ODH3
  - Sampling frequency: 200 Hz
  - Spatial sampling: 1 m
  - Gauge length (which can be understood as spatial resolution): 7 m
- DAS Interrogator 3: Terra15 Treble
  - Sampling frequency: 36 kHz
  - Spatial sampling: 2.45 m
  - Gauge length (which can be understood as spatial resolution): 4.9 m
- DSS Interrogator: Omnisens DITEST VISION Dual temperature and strain unit
  - Sampling frequency: ~4 min
  - Spatial sampling: 0.51 m
  - Spatial resolution: 1 m

In Experiments 2 and 3, the iDAS and the ODH3 interrogators were mostly used to monitor strain (deformation), whereas the Treble interrogator was deployed to monitor seismicity, although it proved challenging. The low-frequency DAS shown in the paper is from the OptaSense ODH3 interrogator. Regarding range and accuracy for DAS, manufacturers claim that they are sensitive down to the picostrain-nanostrain range. For DSS, the sensitivity is in the microstrain range.

Electrical Resistance Tomography
Pertinent ERT settings:
Current injections: Alternating square wave at 1 Hz
Number of stacks: 3
Current magnitudes: 10-150 mA
Voltage applied to current electrodes: 50-170 V
Survey type: Pole-dipole

Table SI-1. Experiment 1 Stimulations

Stimulation	Flow rates (L/ Min) / Injection Volume	Relevant Pressure (MPa)	Notes
Hydraulic Stimulation #1 at 142' Notch May 21, 2018 - May 22, 2018	0.4	Breakdown 31	Breakdown 31 MPa (4500 psi) significantly above the minimum principal stress of 21.7 MPa (3147 psi), probably intersecting an observed natural fracture and leading to water flow returning up the borehole. A total of twelve liters of water were injected in this test. (Kneafsey et al., 2019)
Hydraulic Stimulation #2 at 164' Notch May 22, 2018 - May 24, 2018	0.2 / 2.1 L 0.4 / 23.5 / 80.6	Propagation 25.43, 25.95, 26.88	In the first step, 2.1 L of water was injected at 200 mL/min. The propagation pressure was 25.43 MPa (3688 psi) and the instantaneous shut-in pressure (ISIP) was 25.37 MPa (3679 psi). In the second step, 23.5 L of water was injected at 400 mL/min resulting in slightly higher propagation pressure and ISIP (25.95 and 25.82 MPa respectively, 3763 and 3744 psi). The pressure decay following this step indicated that the hydraulic fracture may have intersected a natural fracture. The third step was performed at 5L/min and had an injection volume of 80.6 L, with a propagation pressure and ISIP of 26.88 and 25.31 MPa (3898 psi and 3670 psi), respectively. (Kneafsey et al., 2019)
Hydraulic Stimulation #3 at 128' Notch Jul. 18, 2018 – Jul. 20, 2018	Day 1 - 0.4 Day 2 - 1.5	Breakdown 27.9	Flow bypassed the top injection packer through fractures, and resulted in a hydraulic fracture connecting to E1-OT. After an overnight shut-in, stimulation treatment continued on 20 July with injection rates up

			to 1.5 L/min and pressure of almost 30 MPa. (Schoenball et al., 2020)
Hydraulic Stimulation #4 at 142' Notch Dec. 7, 2018 - Dec. 20, 2018	Day 1 - 2.5 Day 2 - 5	Day 1 - Fracture opening 32 Day 2 - propagation 32.7	Day 1 pressurized using a flow rate of 2.5 L/min to a pressure of 32 MPa where we observed fracture opening. Less than 2 min after reaching the fracture opening pressure, a packer element burst and we had to cancel the stimulation. After replacing the packer, a third attempt to stimulate the interval began on 21 December 2018. We increased the flow rate up to 5 L/min and observed the maximum pressure of 33.7 MPa, which reduced and stabilized at 32.7 MPa during fracture propagation. (Schoenball et al., 2020) This stimulation extended at least one hydraulic fracture to E1-OB and E1-P, and also connected to all other wells except for E1-PDB. (Kneafsey et al., 2019)

Table SI-2. Summary of Experiment 2 stimulation activities. All simulations were conducted in well TC using SIMFIP. (Schwering et al., 2023)

Start Time (UTC)	End Time (UTC)	Interval Top (m)	Interval Bottom (m)	Notes
3/23/22 14:21	3/23/22 19:28	8.23	10.64	Tensile hydraulic fracture at shallow depth outside of monitoring zone to verify fracture pressure. Hydraulic test was done on 24 March 2022 in the same zone. This test indicated that fracturing may occur between 3500 and 4000 psi (24.13 MPa to 27.6 MPa).
3/23/22 21:38	3/24/22 14:38	58.64 (Zone 7)	61.05	Overnight pressure held at 15.2 MPa (2200 psi).

3/24/22 14:38	3/24/22 17:11	63.46	65.87	60-minute pressure held at 15.2 MPa (2200 psi).
3/24/22 17:12	3/24/22 19:10	53.83	56.24	60-minute pressure held at 15.2 MPa (2200 psi).
3/24/22 19:10	3/24/22 21:04	49.01	51.42	Pressure held at 15.2 MPa (2200 psi). Subsequent injections into TU on 05 May 2022 fractured into this zone and on 06 May 2022 injections were made into the fracture that was created from TU. Additional high-rate injections were made on 18 May 2022. These later injections are documented as part of Experiment 3.
3/24/22 21:04	3/24/22 22:08	44.20	46.61	Pressure held at 15.2 MPa (2200 psi). Subsequent injections in this zone were made on 13 April 2022 and are documented as part of Experiment 3.
3/24/22 22:08	3/24/22 22:42	8.23	10.64	Held pressure at 15.2 MPa (2200 psi) to evaluate post-fracture hydraulic conductivity. The fracture was generated on 23 March 2022 as a tensile fracture.
3/25/22 0:00	3/25/22 0:00	61.05	63.46	Pressure held at 16.1 MPa (2340 psi). Test was shortened to less than 60 minutes due to time constraints.
3/25/22 15:23	3/25/22 17:52	46.60	49.01	Pressure held at 16.1 MPa (2340 psi). There was a Quizix pump communication problem that resulted in a premature depressurization of the interval. The test was resumed but was shortened from the planned 60-minute hold.
3/25/22 17:52	3/25/22 19:21	51.42	53.83	Pressure held at 16.1 MPa (2340 psi). Test was shortened to less than 60 minutes due to time constraints. On 14 April 2022 a stimulation was made in this zone by cycling the injection pressure above/below the fracture opening pressure repeatedly. This later

				injection is documented as part of Experiment 3.
3/25/22 19:23	3/25/22 20:50	56.23	58.64	Pressure held at 16.1 MPa (2340 psi). Test was shortened to less than 60 minutes due to time constraints.
3/25/22 22:08	4/11/22 17:02	58.64 (Zone 7)	61.05	Pressure held at 16.1 MPa (2340 psi) from 25 March 2022 until 11 April 2022 to give as much time as possible for pressure to diffuse into natural fractures and promote shear slip/stimulation. On 11 April 2022, after no indication of shear stimulation had occurred, a constant rate injection at 3 mL/min was started. This is considered as the transition to Experiment 3 since the pressure was intentionally allowed to exceed the least compressive principal stress.

Table SI-3. Summary of Experiment 3 stimulation activities. (Schwering et al., 2023).

Time (UTC)	**Stimulated Well/ Interval**	**Method**	**Volume**	**Connects to/ Interferences**	**Breakdown (psi)**	**Notes**
4/11/22 17:02 - 4/12/22 19:50	TC 58.64 - 61.05 / SIMFIP (Zone 7)	Increasing flow from 0.003 L/min to 0.4 L/min	300 L	TN, TS (dripping), AMU	3650	Constant rate injection at increasing rates, then shut-in when fracture was detected in monitoring well AMU via DTS anomaly and dripping from well head. Subsequent flow test, observed with a downhole camera, was conducted on 20 April 2022.

4/12/22 19:52 - 4/13/22 21:51	TC 44.20 - - 46.61 / SIMFIP (Zone 1)	-	-	-	-	Pressure held at 13.8 MPa (2000 psi) overnight. On 14 April 2022 a high-rate injection was conducted and stopped when outflow was observed in the drift.
4/13/22 21:52 - 4/14/22 15:44	TC 58.64 - - 61.05 / SIMFIP (Zone 7)	1 L/min, 5 L/min	400 L	TN, TL, TS, and TV4100	~3400 psi	Hydraulic test of fracture created with constant-rate injections on 11-12 April 2022.
4/14/22 15:46 - 4/14/22 18:15	TC 44.20 - 46.61 /SIMFIP (Zone 1)	-	-	-	-	Hydraulic test of fracture created on 13 April 2022.
4/14/22 18:16 – 4/14/22 21:30	TC 51.42 - - 53.83 / SIMFIP (Zone 4)	Cyclic (2800 < P < 4500 psi)	40 L	TN, TL, and TS (a little)	Not clear	Cyclical injection above/below fracture pressure until 40 L had been injected and flow from production wells was observed. Following this stimulation, the well was held under 16.1 MPa (2340 psi) constant pressure for several days to observe flowback. Subsequently an injection was made on 21 April 2022 into this zone with the downhole camera deployed in TN and TL to observe outflow locations.
5/5/22	TU	1 L/min,	1200 L	TC,	5500 psi	Initial stimulation

18:39 - 5/7/22 0:00	54.07 - 54.74 26" straddle	5 L/min		TN, and TL		of this zone.
5/17/22 20:45 - 5/18/22 01:45	TC 45.95 – 46.60, 26 “ straddle	5 L/min	1,500 L	TN, TL, DML		Stimulation at 5 L/min in Zone 1. Less than 20% recovery in TL & TN, and DTS indicated intersection with DML. Aborted after 5 hours to try stim/flow of Zone 3. This stim/flow test was accidentally overlooked in the table presented by Schwering et al. (2023).
5/18/22 14:24 - 5/19/22 13:52	TC 50.44 - 51.11 26" straddle	5 L/min	3600L	TL, Battery Alcove, DML	-	Stimulation at 5 L/min. Outflow was mostly from TL with about 20-25% recovery. Weeps in the drift near the Battery Alcove were observed. Flow was stopped on the evening of 19 May 2022 3:44:55 after an intersection with DML was observed with the DTS.
5/19/22 13:42 - 5/19/22 13:52	TU 50.44- - 51.11 26" straddle	-	-	-	-	Stimulation of this zone, leakage observed at DML.

Supplemental Information References

Burghardt, J., Knox, H., Doe, T., Blankenship, D., Schwering, P., Ingraham, M., Kneafsey, T., Dobson, P., Ulrich, C. and Guglielmi, Y., 2022. EGS Stimulation Design with Uncertainty Quantification at the EGS Collab Site, 56th US Rock Mechanics/Geomechanics Symposium. OnePetro.

Hopp, C., 2023a. EGS Collab Experiment 2 Distributed temperature (DTS) system. LBNL-2001515, Lawrence Berkeley National Laboratory, Berkeley, CA, USA.

Hopp, C., 2023b. EGS Collab Experiment 2: Passive seismic monitoring system. LBNL-2001514, Lawrence Berkeley National Laboratory, Berkeley CA, USA.

Kneafsey, T.J., Blankenship, D., Knox, H.A., Johnson, T.C., Ajo-Franklin, J.B., Schwering, P.C., Dobson, P.F., Morris, J.P., White, M.D., Fu, P., Podgorney, R., Huang, L., Johnston, B., Roggenthen, W., Doe, T., Mattson, E., Ghassemi, A., Valladao, C. and EGS Collab Team, 2019. EGS Collab Project: Status and Progress, 44th Workshop on Geothermal Reservoir Engineering, Stanford University, Stanford, California.

Rodríguez Tribaldos, V., Hopp, C., Pio Rinaldi, A., Tuinstra, K., Lanza, F., Ajo-Franklin, J., Kneafsey, T., Robertson, M., Guglielmi, Y. and Zappone, A., 2024 (in press). Use of DAS and DSS Technologies for Geomechanical Characterization of Rock Mass Response in Mesoscale Experiments in Underground Laboratories: Lessons Learned. In: Y. Li, R. Mellors and G. Zhan (Editors), Distributed Acoustic Sensing (DAS) in Borehole Geophysics. Geophysical Monograph Series. American Geophysical Union.

Rodríguez Tribaldos, V., Schoenball, M., J., A.-F. and Team, E.C., 2021. Low-frequency Distributed Acoustic Sensing (DAS) for monitoring of hydraulic fracturing at the EGS Collab Experiment Testbed, SEG-AGU Advances in Distributed Sensing for Geophysics Workshop, Houston, TX, USA.

Schoenball, M., Ajo-Franklin, J.B., Blankenship, D., Chai, C., Chakravarty, A., Dobson, P., Hopp, C., Kneafsey, T., Knox, H.A., Maceira, M., Robertson, M.C., Sprinkle, P., Strickland, C., Templeton, D., Schwering, P.C., Ulrich, C., Wood, T. and EGS Collab Team, 2020. Creation of a Mixed-Mode Fracture Network at Mesoscale Through Hydraulic Fracturing and Shear Stimulation. Journal of Geophysical Research: Solid Earth, 125(12): e2020JB019807.

Schwering, P., Ingraham, M., Vermeul, V., Burghardt, J., Johnson, T., Strickland, C., White, M., Hopp, C., Tribaldos, V.R., Kneafsey, T., Artz, T., Mattson, E., Doe, T. and Team*, E.C., 2023. Shut-In Testing on the 4100L - Implications on the State of Stress, Fractures, and Wellbores in the Second EGS Collab Testbed, 48th Workshop on Geothermal Reservoir Engineering, Stanford University, Stanford, California.